Highly Oriented Thin Films and Porous Thin Films of $Pb(Zr_xTi_{1-x})O_3$

Charnwit Ruangchalermwong

A Thesis Submitted in Fulfillment of the Requirements

for the Degree of Doctor of Philosophy in Physics

Prince of Songkla University

2009

Copyright of Prince of Songkla University

Thesis Title	Highly Oriented Thin Films and Porous Thin Films of $Pb(Zr_xTi_{1-x})O_3$
Author	Mr. Charnwit Ruangchalermwong
Major Program	Physics

Major Advisor	**Examining Committee:**
……..…	……...……Chairperson
(Assoc. Prof. Dr. Supasarote Muensit)	(Assoc. Prof. Dr. Tripob Bhongsuwan)
	……..…
Co-advisor	(Assoc. Prof. Dr. Supasarote Muensit)
……..…	……..…
(Dr. Paradorn Pakdeevanich)	(Dr. Paradorn Pakdeevanich)
	……..…
	(Assoc. Prof. Dr. Sumpun Wongnawa)
	……..…
	(Dr. Sutiporn Chewasatn)

The Graduate School, Prince of Songkla University, has approved this thesis as fulfillment of the requirements for the Doctor of Philosophy Degree in Physics

……..……..……..……
(Assoc. Prof. Dr. Krerkchai Thongnoo)
Dean of Graduate School

ชื่อวิทยานิพนธ์ ฟิล์มบางที่มีการจัดตัวสูงและฟิล์มบางพรุนของ $Pb(Zr_xTi_{1-x})O_3$

ผู้เขียน นายชาญวิทย์ เรืองเฉลิมวงศ์

สาขาวิชา ฟิสิกส์

ปีการศึกษา 2551

บทคัดย่อ

วิทยานิพนธ์นี้มุ่งสนใจวัสดุเลดเซอร์โคเนตไทเทเนตหรือพีแซดทีเนื่องจากความโดดเด่นของสมบัติเฟร์โรอิเล็กตริก สมบัติไดอิเล็กตริก และสมบัติไพอิโซอิเล็กตริกในรูปของฟิล์มบางที่เตรียมขึ้นโดยวิธีโซลเจลบนฐานรอง $Pt(111)/TiO_2/SiO_2/Si(100)$ สารละลายพีแซดทีเตรียมจากสารประกอบโลหะอัลคอกไซด์และฟิล์มบางพีแซดทีได้ถูกนำไปศึกษาเชิงระบบสำหรับสมบัติทางไฟฟ้าและการตรวจสอบเชิงผลึก

ส่วนประกอบที่เปลี่ยนแปลงสัมพันธ์กับสัดส่วนเซอร์โคเนียมต่อไทเทเนียมมีค่าระหว่าง 20/80 ถึง 80/20 โดยคร่อมขอบเขตเฟสมอร์โฟโทรปิกหรือเอ็มพีบีของสารแบบก้อน และถูกศึกษาร่วมกับการดัดแปลงเชิงเคมีโดยเจือไนโอเบียมในฟิล์มบางพีแซดทีหรือพีเอ็นแซดทีซึ่งฟิล์มบางจะมีการบังคับให้เกิดการเรียงระนาบผลึก (100) และ (111) ภายใต้อิทธิพลของชั้นเมล็ดชั้นเมล็ดของตะกั่วออกไซด์เฟสเบต้าบนรอยต่อระหว่างฟิล์มพีเอ็นซีทีและฐานรองทำให้เกิดการก่อตัวของฟิล์มบางพีเอ็นซีทีแบบโครงผลึกแบบเพอรอฟสไกท์เชิงเดี่ยวและระนาบผลึกเรียงตัวเด่นแบบ (100) สูง ในทำนองเดียวกันการบังคับระนาบผลึกฟิล์มบางพีเอ็นซีทีเด่นแบบ (111) ถูกทำให้เกิดขึ้นโดยการเหนี่ยวนำของชั้นเมล็ดของไทเทเนียมไดออกไซด์เฟสรูไทล์บนรอยต่อ การตรวจสอบเลี้ยวเบนรังสีเอ็กซ์หรือเอ็กซ์อาร์ดีถูกนำมาตรวจสอบความเป็นผลึกของฟิล์ม ฟิล์มบางพีเอ็นซีทีระนาบเด่นแบบ (100) แสดงการเปลี่ยนเฟสของผลึกแบบเตตระโกนอลที่สัดส่วนไทเทเนียมมากไปยังเฟสของผลึกแบบรอมโบฮีดรอลที่สัดส่วนเซอร์โคเนียมมาก บริเวณเอ็มพีบีแสดงค่าตรงรอยต่อใกล้เคียงกับค่า 52/48 ในการตรวจสอบเชิงความเป็นฟิล์มเฟร์โรอิเล็กตริกและฟิล์มไพอิโซอิเล็กตริกสัดส่วนเซอร์โคเนียมต่อไทเทเนียมมีความสัมพันธ์อย่างมากกับค่าโพลาไรเซชันตกค้าง ค่าคงที่ไดอิเล็กตริก และค่าสัมประสิทธิ์ไพอิโซอิเล็กตริก ในกรณีระนาบผลึกเด่นแบบ (100) ค่าโพลาไรเซชันตกค้างและค่าสัมประสิทธิ์ไพอิโซอิเล็กตริกมีค่าที่ดีที่สุดเท่ากับ 75 $\mu C/cm^2$ และ 161 pm/V ตามลำดับ ณ สัดส่วนเซอร์โคเนียมต่อไทเทเนียมเข้าใกล้เอ็มพีบี ส่วนฟิล์มระนาบผลึกเด่นแบบ (111) มีโพลาไรเซชันตกค้างเท่ากับ 80 $\mu C/cm^2$ และค่าคงที่ไดอิเล็กตริกเท่ากับ 1550 ค่าสมบัติทางไฟฟ้าเหล่านี้มีค่ามากกว่าฟิล์มบางพีซีทีที่ไม่ได้เจือไนโอเบียม

ฟิล์มบางพีเอ็นซีทีที่สัดส่วน 30/70 ระนาบผลึกแบบ (100) และ (111) สูง และฟิล์มบางระนาบผลึกแบบสุ่มโดยเตรียมฟิล์มบนฐานรองซิลิคอนแพลตินัม ถูกนำไปศึกษาความสัมพันธ์เชิงความหนาของฟิล์มกับสมบัติทางไฟฟ้า ความหนาฟิล์มพีเอ็นซีทีเปลี่ยนแปลงจาก 80 ถึง 400 นาโนเมตร ผลการตรวจสอบเอ็กซ์อาร์ดีแสดงว่าฟิล์มบางควบแน่นผลึกเป็นโครงสร้างแบบเพอรอฟสไกท์เฟสเตตระโกนอล ฟิล์มบางพีเอ็นซีทีมีระนาบผลึกต่างๆแสดงสมบัติผ่านทางเฟร์โรอิเล็กตริกฮิสเทอรีซิสคล้ายกัน และเมื่อความหนาของฟิล์มบางเพิ่มขึ้นค่าโพลาไรเซชันตกค้างเพิ่มและลดค่าสนามไฟฟ้าบังคับ ฟิล์มบางระนาบผลึกเด่นแบบ (111) ที่ความหนา 400 นาโนเมตรให้ค่าโพลาไรเซชันตกค้างดีที่สุดเท่ากับ 108 $\mu C/cm^2$

ท่อนาโนคาร์บอนชนิดผนังหลายชั้นที่ปริมาณสัดส่วนอัตราร้อยละโดยน้ำหนักเท่ากับ 0.4 และ 0.6 ถูกเติมลงในสารละลายตั้งต้นเพื่อทำฟิล์มบางก่อนการเคลือบฟิล์มแบบหมุนปั่นเพื่อการพัฒนาโครงสร้างแบบพรุนในฟิล์มบางพีซีทีที่สัดส่วน 52/48 ฟิล์มที่เตรียมได้ถูกวิเคราะห์โดยการตรวจสอบเอ็กซ์อาร์ดีแสดงโครงสร้างผลึกแบบเพอรอฟสไกท์ร่วมกับผลึกฟลูออไรต์และเรียงตัวแบบสุ่มทั้งกรณีฟิล์มแน่นและฟิล์มพรุนหลังเผาแอนนีลที่อุณหภูมิ 650 องศาเซลเซียส โครงสร้างจุลภาคของฟิล์มแน่นแสดงเกรนแบบแท่งและฟิล์มพรุนแสดงเกรนแบบก้อนกลม การเปลี่ยนแปลงอย่างมีนัยสำคัญของค่าคงที่ไดอิเล็กตริกที่ลดลงปรากฏในฟิล์มพรุนพีซีทีที่เติมท่อนาโนคาร์บอนชนิดผนังหลายชั้น นอกจากนี้ฟิล์มพรุนทั้งหมดแสดงวงเฟร์โรอิเล็กตริกฮิสเทอรีซิสที่ไม่สมมาตรและบิดเบี้ยว ดังนั้นการเติมท่อนาโนคาร์บอนชนิดผนังหลายชั้นสามารถเหนี่ยวนำทำให้เกิดการเปลี่ยนแปลงสมบัติของฟิล์มเฟร์โรอิเล็กตริก

Thesis Title	Highly Oriented Thin Films and Porous Thin Films of $Pb(Zr_xTi_{1-x})O_3$
Author	Mr. Charnwit Ruangchalermwong
Major Program	Physics
Academic Year	2008

ABSTRACT

This thesis mainly focused on the lead zirconate titanate (PZT) materials for their outstanding ferroelectric, dielectric and piezoelectric properties. All of PZT ferroelectric thin films were prepared by a sol-gel method on a conventional $Pt(111)/TiO_2/SiO_2/Si(100)$ substrate, in which metal alkoxides were used as the raw materials. These thin films were systematically investigated for the electrical properties and the crystallographic characterizations.

The compositional variation in relation with Zr/Ti ratio ranging from 20/80 to 80/20 across the morphotropic phase boundary (MPB) of bulk materials was studied for niobium-modified PZT (PNZT) thin films with two types of textured films: [100] and [111] orientations under the influence of seeding layer. The β-PbO thin seeding layer on the interface of the PNZT film and the substrate resulted in the formation of single-phase perovskite and highly [100]-textured PNZT films. Similarly, [111]-textured PNZT thin films were carried out by introducing rutile-TiO_2 thin seeding layer to the interface. X-ray diffraction (XRD) was used to examine the crystallization of the films and examination results showed that there was distinct phase transition only for the PNZT(100) films from titanium-rich tetragonal to zirconium-rich rhombohedral when the Zr/Ti ratio varied across the MPB close to 52/48. Strong dependence on the Zr/Ti ratio was investigated to develop both ferroelectric and piezoelectric films with remanent polarization, dielectric constant and piezoelectric coefficient. For the [100] orientation, enhanced remanent polarization and improved piezoelectric coefficient, whose best values reached 75 $\mu C/cm^2$ and 161 pm/V, respectively, were measured at the composition close to MPB. This was consistent with the largest remanent polarization of 80 $\mu C/cm^2$ and the

corresponding high dielectric constant of 1550 for 52/48 PNZT(111) film. All these values were superior to those of undoped PZT films.

Highly oriented [100], [111] and randomly oriented films of 30/70 PNZT were deposited on the platinized silicon substrate to study thickness dependency on electrical properties. The thickness of the PNZT films was varied from 80 to 400 nm. The XRD data showed that the materials crystallized into a tetragonal perovskite phase. The PNZT thin films with preferred orientation exhibited a similar characteristic of the ferroelectric hysteresis loop. The films with increasing thickness possessed the higher remanent polarization with a lower coercive field. The highest remanent polarization of 108 $\mu C/cm^2$ was obtained from [111]-oriented PZNT thin film with its thickness of 400 nm.

Addition of different amounts (0.4 and 0.6 wt%) of multiwalled carbon nanotubes in the precursor solution prior to spin coating proved to be an excellent method for developing porous structure in sol-gel derived $Pb(Zr_{0.52}Ti_{0.48})O_3$ thin films. The crystal structure of as deposited films, which were analyzed by XRD, revealed that the perovksite phase with secondary fluorite phase took place to randomly orient for dense and porous films after annealing at 650 °C. The microstructure of the dense film showed columnar grain structure but globular one for porous films. Significant changes in lowered dielectric constant of the PZT/MWNT porous films were observed. In addition, all the porous films had asymmetric and slightly distorted ferroelectric hysteresis loops. The presence of small amount of the MWNTs induced changes of the properties of the ferroelectric films.

ACKNOWLEDGEMENTS

I wish to express my sincere and deepest gratitude to my academic advisor Assoc. Prof. Dr. Supasarote Muensit for her endless help, inspiring guidance, constant suggestion and encouragement given during entire research at Prince of Songkla University (PSU). I am grateful to her for providing fund and support during the writing of this thesis.

I would like to express my sincere appreciation to foreign co-advisor Prof. Dr. Jing-Feng Li who always supported and advised me while I was at Tsinghua University (TU), P.R. China. He also gave me an invaluable opportunity as a member in his laboratory unit for providing new compromising topic of thesis and remarks in his already heavy loads of responsibility. Thank you for all the discussions concerned in publications.

I also would like to express my sincere appreciation to Prof. Dr. Hai-Yan Zhang at Guangdong University and Technology (GDUT), P.R. China, who gave me the opportunity for research in CNTs; however, the topic concerned was not completed as one in this thesis. I also express my greatest thank to thesis committee members Assoc. Prof. Dr. Tripob Bhongsuwan, Dr. Paradorn Pakdeevanich, Assoc. Prof. Dr. Sumpun Wongnawa and Dr. Sutiporn Chewasatn for providing invaluable suggestions. I dedicate this small achievement to my parents.

I want to acknowledge Mr. Zhi-Xiang Zhu who became one of my best friends. He was an assistant and an educator during the learning how to prepare good PZT thin film. I was indebted to Mrs. Yu-Hua Zhen, now became Dr. Yu-Hua Zhen, for her friendship before and after coming to Beijing and all time in Prof. Li's laboratory. My life both in Guangzhou and Beijing City was full of fun due to all the members of research group at GDUT and TU. My sincere thanks go to many friends in PSU whom always encouraged me.

This work was financially supported by PSU Grant and the Thailand Research Fund through the Royal Golden Jubilee Ph.D. Program under Grant No. PHD/0105/2548.

Charnwit Ruangchalermwong

CONTENTS

		Page
CONTENTS		viii
LIST OF TABLES		xi
LIST OF FIGURES		xii
LIST OF ABBREVIATIONS AND SYMBOLS		xvii
CHAPTER 1:	**INTRODUCTION**	1
1.1 Statement of the problem……..		1
1.2 Thesis outline……...		3
1.3 Objectives of research……..		3
CHAPTER 2:	**BACKGROUND ON FERROELECTRIC MATERIALS**	5
2.1 Introduction to the perovskite materials……..……...		5
2.1.1 Ferroelectricity……..……...		5
2.1.2 Piezoelectricity: constitutive equations and PFM measurement....		9
2.1.3 Pyroelectric effect ……...……...		14
2.1.4 Ferroelectric domains ……...……		15
2.1.5 Possible polarization vectors in ferroelectric film ……...…..		17
2.1.6 Ferroelectric film applications ……....…..		19
2.2 Ferroelectric materials …….…….		22
2.2.1 Lead Zirconate Titanate (PZT)……..….....		22
2.2.2 Chemical modification …….……		25
2.2.3 Other alternative ferroelectric materials …….……..…….		26
2.3 PZT film fabrication……..……..……..		29
2.3.1 Possible preparations of PZT films ……...……..…..		29
2.3.2 Chemical solution deposition ……...……		29
2.3.3 Sol-Gel precursor solution……..		32

CONTENTS (Continued)

		Page
CHAPTER 3:	**HIGHLY ORIENTED AND NIOBIUM-MODIFIED PZT THIN FILMS**	36
3.1 Introduction……...		36
3.2 Review of previous works……..…...		37
3.3 Materials and methods…….…..		40
3.3.1 Preparation of PNZT solutions……...		40
3.3.2 Preparation of metal containing organic solution……...		42
3.3.3 PNZT thin film deposition……..		42
3.3.4 Thin film characterization……..		44
3.4 Results and discussions…….……..……..		45
3.4.1 Crystallographic and structural analysis of PbO seeding and PNZT(100) thin films……...……		45
3.4.2 Crystallographic and structural analysis of TiO_2 seeding and PNZT(111) thin films…….		55
3.4.3 Electrical properties of PNZT(100) thin films……...		60
3.4.4 Electrical properties of PNZT(111) thin films……...		65
3.4.5 Role of niobium modification on electrical properties……...		71
3.5 Conclusions…….……..		73
CHAPTER 4:	**TEXTURE AND THICKNESS DEPENDENT NIOBIUM MODIFIED PNZT THIN FILMS**	74
4.1 Introduction……..…		74
4.2 Review of previous works……..……...		75
4.3 Materials and methods…….……..		76
4.4 Results and discussions……		77
4.4.1 X-ray characterization for different thicknesses and orientations..		77
4.4.2 Electrical characterization for different thicknesses and orientations…….....…...…….....		81

CONTENTS (Continued)

	Page
4.5 Conclusions……..…….	87
CHAPTER 5: THIN POROUS PZT FILMS	88
5.1 Introduction……..…….	88
5.2 Review of related works……...…….	89
5.3 Materials and methods…….……..	91
5.4 Results and discussions……	92
5.4.1 Thermo gravimetric analysis of PZT dried gels ……...…….	92
5.4.2 X-ray characterization of the dense and porous PZT films…...…	93
5.4.3 Electrical characterization of dense and porous PZT films…….....	97
5.5 Conclusions……...	102
CHAPTER 6: CONCLUSIONS AND FUTURE WORKS	103
6.1 Main conclusions…….……..	103
6.2 Future works…….…….	104
REFERENCES	106
VITAE	126

LIST OF TABLES

Table		Page
2.1	Dielectric and piezoelectric properties of lead-free perovskite piezos “past and present”.	28
3.1	The piezoelectric coefficient of oriented PNZT(100) films compared with randomly oriented PZT films without Nb doping.	65
3.2	The dielectric constant of oriented PNZT(111) films compared with highly and randomly oriented PZT films without Nb doping.	68
3.3	The remanent polarization of oriented PNZT films compared with randomly oriented PZT films without Nb doping.	71

LIST OF FIGURES

Figure		Page
2.1	A typical ferroelectric hysteresis loop.	6
2.2	ABO_3 perovskite unit cell under an applied electric field.	7
2.3	The conventional method of assigning Cartesian coordinate axes for a piezofilm which has been uniaxially drawn and poled.	10
2.4	Schematics of the vertical (a) and lateral (b) PFM signal detection.	14
2.5	Ferroelectric domain types and structures in tetragonal phase. Up to six domain orientations with the spontaneous polarization oriented parallel (*a* domain) or normal (*c* domain) to the sample surface can be found. Different domain orientations can be observed to form quite complex domain patterns with mixing 90° and 180° domain.	16
2.6	Possible orientations of the polarization vector in textured ABO_3 films: (a) (111)- and (b) (100)-rhombohedral films, (c) (111)- and (d) (100)-tetragonal films.	19
2.7	Overview of typical ferroelectric thin-film applications.	20
2.8	PZT phase diagram. In the middle, the standard phase diagram is shown. The diagram around the MPB showing the monoclinic phase between the tetragonal and rhombohedral phases is shown at the upper right. F_M stands for ferroelectric monoclinic in the inset.	24
2.9	Layer perovskite structure.	27
3.1	Flow chart of the preparation of PNZT solution.	42
3.2	Flow chart for the PNZT(100) deposition by sol-gel method.	43
3.3	SEM surface morphology of the PbO seeding layer.	45
3.4	XRD pattern of the PbO seeding layer compared with standard PDF card No. 65-2809.	46
3.5	XRD patterns of PNZT(100) thin films with different Zr/Ti ratios on PbO seeding layers.	47

LIST OF FIGURES (Continued)

Figure		Page
3.6	XRD patterns of PNZT(100) thin thin films with different Zr/Ti ratios for step scanning of (002)/(200) peaks. The inset shows the magnification by log scale of (002)/(200) peaks for Ti-rich composition.	48
3.7	Orientation degree summarized for the PbO seeded PNZT thin films.	49
3.8	Calculated *a*-axis lattice parameters as a function of Zr content for PNZT(100) films.	51
3.9	FE-SEM cross-sectional image of the PNZT thin film with PbO seeding. The sample contained a Zr/Ti ratio of 52/48.	52
3.10	FE-SEM planar image of the PNZT thin film with PbO seeding. The sample contained a Zr/Ti ratio of 52/48.	52
3.11	Compositional depth profile of PNZT thin films with Zr/Ti= 52/48 on PbO seeding layers……..	54
3.12	Compositional depth profile of PNZT thin films with Zr/Ti= 70/30 on PbO seeding layers……..	54
3.13	SEM surface morphology of the TiO_2 seeding layer.	55
3.14	XRD pattern of the TiO_2 seeding layer compared with standard PDF card No. 73-1232.	56
3.15	XRD patterns of PNZT(111) thin films with different Zr/Ti ratios on TiO_2 seeding layers; (a) overall patterns and (b) step scanning.	57
3.16	Orientation degree summarized for the TiO_2 seeded PNZT thin films.	58
3.17	FE-SEM planar image of the PNZT thin film with TiO_2 seeding. The sample contained a Zr/Ti ratio of 52/48.	59
3.18	FE-SEM cross-sectional image of the PNZT thin film with TiO_2 seeding. The sample contained a Zr/Ti ratio of 52/48.	60

LIST OF FIGURES (Continued)

Figure		Page
3.19	*P–E* hysteresis loops of PNZT thin films with different Zr/Ti ratios on PbO seeding layers for Zr/Ti= 20/80, 30/70, 40/60 and 52/48.	61
3.20	*P–E* hysteresis loops of PNZT thin films with different Zr/Ti ratios on PbO seeding layers for Zr/Ti = 53/47, 60/40, 70/30 and 80/20.	61
3.21	Remanent polarization and coercive field of PNZT(100) thin films as a function of Zr content.	63
3.22	Piezoelectric coefficient of PNZT(100) thin films as a function of Zr content. The inset is a typical *Z-V* curve of PNZT film with Zr/Ti = 52/48.	65
3.23	Dielectric constant–voltage curves of PNZT(111) thin films with different Zr/Ti ratios. The inset shows loss factor at Zr/Ti = 52/48.	66
3.24	Dielectric constant of PNZT(111) films as a function of Zr content.	67
3.25	*P-E* hysteresis loops for PNZT(111) thin films with Zr-rich composition.	69
3.26	*P-E* hysteresis loops for PNZT(111) thin films with Ti-rich composition.	69
3.27	Remanent polarization and coercive field as a function of Zr content for PNZT(111) thin films.	70
4.1	XRD patterns of different thicknesses in PNZT films with [100]-preferred orientation.	78
4.2	XRD patterns of different thicknesses in PNZT films with [111]-preferred orientation.	79
4.3	XRD patterns of different thicknesses in PNZT films with random orientation.	79
4.4	Orientation ratio as a function of film thickness. Films posses (a) [100]-preferred, (b) [111]-preferred and (c) random orientation.	81
4.5	Leakage current density of [100]-preferentially oriented PNZT films with different thicknesses.	82

LIST OF FIGURES (Continued)

Figure		Page
4.6	Dielectric constant–voltage curves for [100]-, [111]- and randomly oriented PNZT films with film thickness of 160 nm.	83
4.7	Dielectric constant–voltage curves for [100]-, [111]- and randomly oriented PNZT films with film thickness of 400 nm.	83
4.8	*P-E* hysteresis loops of different thicknesses in PNZT films with [100]-preferred orientation.	84
4.9	*P-E* hysteresis loops of different thicknesses in PNZT films with [111]-preferred orientation.	85
4.10	*P-E* hysteresis loops of different thicknesses in PNZT films with random orientation.	85
4.11	Dependence of remanent polarization (solid line) and coercive field (dotted line) on film thickness with (■) [100]-preferred, (●) [111]-preferred and (▲) random orientation.	87
5.1	Flow chart of the MWNT mixed PZT film deposition.	92
5.2	TGA curves of MWNTs and PZT dried gels with and without additional MWNTs.	93
5.3	XRD patterns of PZT films with and without additional MWNTs.	94
5.4	SEM planar image of PZT dense film.	95
5.5	SEM planar image of the PZT porous film with 0.4 wt% MWNTs.	95
5.6	SEM planar image of the PZT porous film with 0.6 wt% MWNTs.	96
5.7	SEM cross sectional image of PZT dense film.	96
5.8	SEM cross sectional image of PZT porous film with 0.4 wt% MWNTs.	97
5.9	SEM cross sectional image of PZT porous film with 0.6 wt% MWNTs.	97
5.10	Ferroelectric hysteresis loops of PZT dense film.	98
5.11	Ferroelectric hysteresis loops of PZT porous film with 0.4 wt% MWNTs.	99

LIST OF FIGURES (Continued)

Figure		Page
5.12	Ferroelectric hysteresis loops of PZT porous film with 0.6 wt% MWNTs.	99
5.13	Frequency-dependent dielectric constant of PZT dense film.	100
5.14	Frequency-dependent dielectric constant of PZT porous film with 0.4 wt% MWNTs.	101
5.15	Frequency-dependent dielectric constant of PZT porous film with 0.6 wt% MWNTs.	101

LIST OF ABBREVIATIONS AND SYMBOLS

α	= rhombohedral angle	p	= pyroelectric coefficient
$\alpha_{(hkl)}$	= orientation degree	P	= polarization
ε_r	= dielectric constant	P_r	= remanent polarization
$tan\ \delta$	= loss factor, loss tangent	P_s	= spontaneous polarization
A	= electrode area	P_{sat}	= saturation polarization
D	= dielectric displacement	Q	= charge
c	= specific heat	S	= strain
d_{ij}	= piezoelectric stress coefficient	T	= stress
E	= electric field	T_c	= Curie temperature
E_c	= coercive field	T_o	= Curie-Weiss temperature
f	= frequency	T	= temperature
F_d	= detectivity figure of merit	V	= voltage
F_v	= voltage figure of merit	Z	= thickness
k	= coupling factor		

2-ME	= 2-methoxyethanol
AES	= Auger electron spectroscopy
AFM	= atomic force microscopy
BST	= $Ba_xSr_{1-x}TiO_3$
CNT	= carbon nanotube
CSD	= chemical solution deposition
CVD	= chemical vapor deposition
DRAM	= dynamic random access memory
EXAFS	= extended X-ray absortion fine structure
FeRam	= ferroelectric random access memory
FE-SEM	= field emission electron microscope
MEM	= microelectromechanical system
MOCVD	= metalorganic chemical vacuum deposition
MOD	= metalorganic deposition

LIST OF ABBREVIATIONS AND SYMBOLS (Continued)

MPB = morphotropic phase boundary

MWNT = multiwalled carbon nanotube

NBT = $Na_{1/2}Bi_{1/2}TiO_3$

PFM = piezoresponse force microscope

PLAD = pulsed laser ablation deposition

PLZT = La doped $Pb(Zr_xTi_{1-x})O_3$

PNZT = Nb-modified $Pb(Zr_xTi_{1-x})O_3$, Nb-doped $Pb(Zr_xTi_{1-x})O_3$

PVD = physical vapor deposition

PVDF = polyvinylidenfluoride

PZT = $Pb(Zr_xTi_{1-x})O_3$

SEM = scanning electron microscope

SPM = scanning probe microscopy

TGA = thermogravimetric analysis

XRD = X-ray diffraction

CHAPTER 1

INTRODUCTION

1.1 Statement of the problem

Ferroelectric thin films have evolved into several areas of scientific and technical interest for high potential applications such as non-volatile ferroelectric random access memories, microelectromechanical systems (MEMs) device, infrared device, optical switch and surface acoustic wave (Verardi *et al.*, 1998; Oh and Jang, 2000). Most experimental studies have been carried out to emphasize a promising ferro-, and piezoelectric $Pb(Zr_xTi_{1-x})O_3$ (PZT) owing to simpler crystal structure and advantageous combination of properties including ferroelectric and piezoelectric properties at the so-called morphotropic phase boundary (MPB) region (Gong *et al.*, 2004). Typically, the low processing temperature in the range 500-700 °C are used for the deposition, thus allowing incorporation of PZT ceramic layers into a standard IC technology (Pérez *et al.*, 2007).

Much works have been made to develop high-performance PZT films on platinized silicon substrates. However, polycrystalline PZT thin films deposited on silicon substrates show high energy loss and low electrical properties compared with bulk PZT materials (Zeng *et al.*, 1999). One effective approach to tailor this problem is to fabricate thin films with a preferential crystallographic orientation. In view of the texture of PZT thin films, the largest piezoelectric coefficient was found in [100]-textured films (Gong *et al.*, 2004). Experimental and theoretical results demonstrated that the [100] orientation was more suitable for the MEMs sensor and actuation applications (Taylor and Damjanovic, 2000; Du *et al.*, 1998). It is well known that the crystal symmetry changes from tetragonal to rhombohedral with an increasing x of about 0.5 for MPB together with a change in polar axis from [001] for the tetragonal to [111] direction for the rhombohedral (Oikawa *et al.*, 2004). This suggests that the oriented film is expected to have superior properties to randomly oriented ones. It is also found that [100]-oriented PZT thin films in both crystal symmetries show a better

fatigue characteristic than those with [111]-oriented ones (Wu *et al.*, 2007). Therefore, the orientation control of the PZT films is also important in order to obtain good electrical properties. However, compositional optimization for PZT films is also indispensable because the substrate constraint may affect the phase structure and hence the location of MPB (Oh and Jang, 2001). In fact, the MPB of epitaxial PZT films on single crystal substrate, i.e. $SrTiO_3$ substrates, is not observed at the well-known composition close to Zr/Ti = 52/48 (Zhu *et al.*, 2007).

However, PZT is especially attractive for material property designing. Chemical modification is almost always used with a foreign ions substitution part of host atoms (Pb, Zr and Ti) to improve and optimize the basic properties of PZT films for specific applications. For instance, Nb ion substituting B-site (Zr and/or Ti) expected to act as a donor was compensated by negatively charged defects originated from Pb vacancies (Matsuzaki and Funakubo, 1999), so that the leakage of the film decreased. Donor doping, on the other hand, introduces immobile defect dipoles which should result in a decrease of the mobile defect dipole concentration and hence in a reduction of imprint and fatigue (Grossmann *et al.*, 2002). In addition, ceramics produced with this additive is characterized to reduce oxygen vacancies, resulting to an improvement of dielectric constant, piezoelectric response, pyroelectric coefficient and remanent polarization (Kwok *et al.*, 2004; Haccart, Remiens and Cattan, 2003).

In recent years, pyroelectric materials have been largely used as point detector or arrays in many applications, e.g. intruder alarm, air condition control, gas analysis and thermal imaging which are based on advantages such as lower system cost, room-temperature operation, fast and wide spectral response with high sensitivity (Li *et al.*, 2004). The materials of choice for such applications mostly rely on PZT either in bulk ceramic or thin film formation due to their enhanced pyroelectric coefficient but (Es-Souni *et al.*, 2005), however, the quality is based on their figure of merit in which it is necessary to maximize the pyroelectric coefficient and/or lower the permittivity (Stancu *et al.*, 2007). Porous films with reduced permittivity are carried out to overcome this challenge by forming a matrix-void composite. Some issues related to thermal annealing (Seifert, Muralt and Setter, 1998) or adding a polymer (Stancu *et al.*, 2007) in PZT precursor but porosity by carbon nanotubes seems to be lacking.

1.2 Thesis outline

This thesis consists of six chapters. In chapter 1, the statement of the problem is presented with additional objectives of research.

In chapter 2, a general introduction of physics in ferroelectric material is described. An overview of PZT material focusing on single composition with alternative chemical dopings is introduced. Various techniques for the fabrication of PZT thin films are presented.

Chapter 3 presents a study on the preparation and characterization of niobium-modified and highly oriented PZT thin films focusing on single-composition. Understanding the role of composition on phase transition and electrical properties of both [100]- and [111]-orientation is discussed.

In chapter 4, a study on microstructure, crystallographic texture and ferroelectric property of thickness dependent PNZT thin films under highly preferential and random orientation.

Chapter 5 presents the fabrication and characterization of CNT incorporated PZT thin films for the influence of pore formation on ferroelectric and dielectric properties.

In chapter 6, a main conclusion is provided for each stated one in previous chapters and recommendations for future works are given.

1.3 Objectives of research

The objectives of this work are the following:

1. To fabricate Nb-modified PZT or PNZT thin films of two types: [100]- and [111]-oriented films under the control of metal oxide seeding layer using a two-step sol-gel processing.
2. To investigate the effect of Zr/Ti ratio on the crystallographic structure and electrical properties of both types of highly oriented PNZT films and find out the location of MPB.
3. To prepare PNZT thin films with various thicknesses and to observe their effect on the ferroelectric property.

4. To fabricate carbon nanotube incorporated PZT thin porous films by sol-gel processing for characterizing the microstructure and ferroelectric properties.

CHAPTER 2

BACKGROUND ON FERROELECTRIC MATERIALS

This chapter is to provide an overview of physical phenomenon in ferroelectric materials through ferroelectricity, piezoelectricity, pyroelectricity and their state-of-the-art applications. The subject of interest is the lead-zirconate-titanate based thin films together with the alternative chemical doping. Other materials of ferroelectric perovskite are introduced for selective choices. The processing methods of ferroelectric thin film are reviewed as well.

2.1 Introduction to the perovskite materials

2.1.1 Ferroelectricity

Ferroelectricity was found first in 1921 by Valasek in Rochelle salt for medical purpose (Cross and Newham, 1987). Although the term is analogous to ferromagnetism, in which a material exhibits a permanent magnetic moment, the prefix “ferro” meaning iron, is to describe the property despite the fact that most ferroelectric materials do not consist of iron in their unit cell. In 1940, the discovery of ferroelectric ceramic is remarkable breakthrough by the introduction of ceramic perovskite dielectrics such as barium titanate (Jaffe, Cook and Jaffe, 1971). Because of the anomalously high dielectrics in capacitors, these materials raise strong interest. The discovery of ferroelectric switching in 1945 showed the existence of ferroelectricity in simple oxide materials for the first time (Haertling, 1999). This leads to the discovery of a large number of ferroelectric materials and furthermore a lot of important phenomenological and theoretical work in the field of ferroelectrics.

At first, ferroelectricity was found in crystalline materials which are linked to the crystal symmetry. The ferroelectric crystals are classified as a subset of pyroelectric crystals in up to 10 of the 32 symmetry point groups. Pyroelectric crystals are a subset of piezoelectric crystals and show a spontaneous polarization at zero external field. Because of the hierarchy, the ferroelectric crystals show both

piezoelectric (section 2.1.2) and pyroelectric (section 2.1.3) properties. Meanwhile, ferroelectricity has also been found in a variety of other material classes. Liquid crystals reveal ferroelectric properties in certain phase if the molecules provide a net electric dipole moment (Xu, 1991). There are even ferroelectric polymers, such as polyvinylidenfluoride (PVDF) (Bauer, 1996).

Ferroelectrics materials are dielectric materials characterized by a spontaneous electrical polarization that is switchable by an external electric field. This polarization is present even in the absence of an external electric field. Ferroelectricity is established if the spontaneous can be switched between at least two equilibrium states of orientation by the external electric field of practicable magnitude. The switching behavior is highly non-linear and exhibits a hysteresis loop (*P*-*E* loop) in terms of the ferroelectric polarization as a function of the external electric field as shown in Fig. 2.1. Unit cell of a ABO_3-perovskite ferroelectric material is illustrated in Fig. 2.2., in which it is intended that: A is cation with valence +1, +2 or +3 and B cation with +3, +4, +5 or +6. The A cations occupy the corner sites of a cubic cell, whereas the oxygen anions are located at the face-centers of the cubic cell forming a BO_6-octahedron with the B ions arranged in the centers of the cubes.

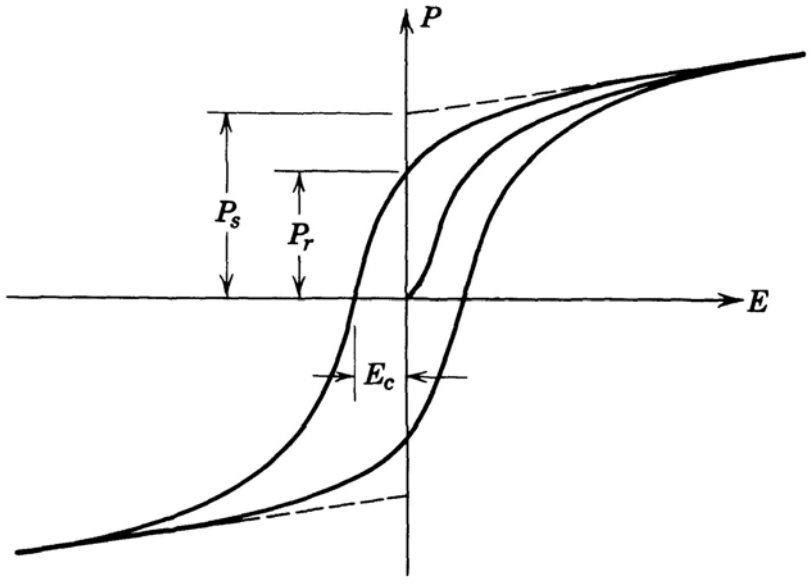

Figure 2.1 A typical ferroelectric hysteresis loop (Jona, 1993).

When an electric field is applied, the B-site ion, which has two thermodynamically stable positions inside oxygen octahedral, is displaced relative to the oxygen upward or downward, depending on the polarity of the electric field. The spontaneous polarization is generated from noncentrosymmetric arrangement of these ions in unit cell, which produces an electric dipole moment align in the direction of an external electric field. Adjacent unit cells are inclined to polarize in the same direction and form regions called ferroelectric domains, separated by domain walls.

In ferroelectric materials, the domain walls are extremely narrow, often not more than one or two lattice layers. Basically, in the absence of an electric field, the domains are randomly oriented, leading to a net polarization. In an electric field, the domain initiates to align in the field direction by movement of the domain walls and rotation of the dipoles, and the polarization reaches the maximum of saturation polarization P_{sat}. When the electric field reduces to zero or no applied electric field, domains cannot return to their original states, yielding a non-zero polarization or remanent polarization P_r. Of interest also is the spontaneous polarization P_s obtained by extrapolating the polarization at high fields P_{sat} back to zero field along a tangent. P_s is somewhat higher than P_r in ceramics, but is virtually equal to P_r in crystals. In order to reverse the direction of polarization, we need to apply a coercive electric field E_c.

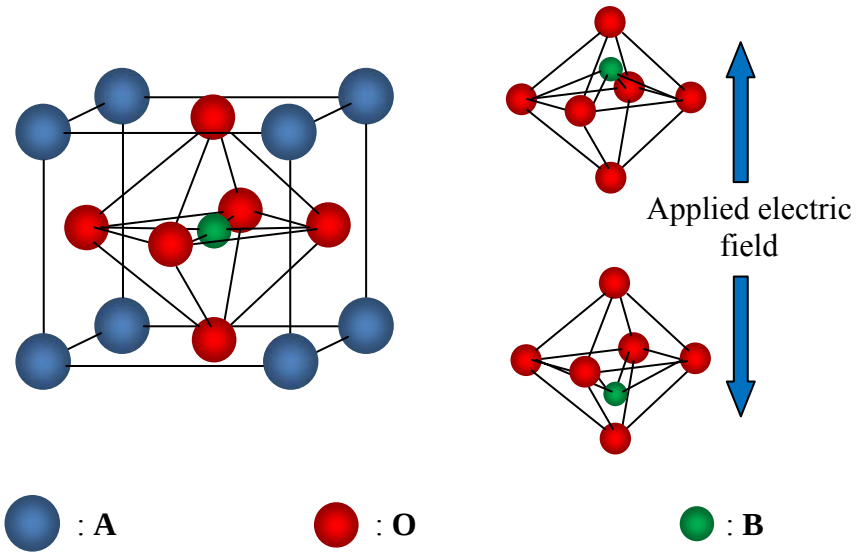

Figure 2.2 ABO_3 perovskite unit cell under an applied electric field.

The occurrence of ferroelectricity is typically limited to certain phases of the material. Above a critical temperature called the Curie temperature T_c, these materials become a centrosymmetric structure and hence loss all spontaneous polarization. In this state, the material is termed paraelectric. As the temperature is lowered through the Curie point, a phase transformation takes place from paraelectric state to ferroelectric state and therefore a lot of material property, i.e. dielectric constant ε, shows a remarkable temperature dependence, especially close to this phase transition. In paraelectric state, the relationship between ε and the temperature follows the Curie-Weiss law through (Jaffe, Cook and Jaffe, 1971):

$$\varepsilon \cong \frac{C}{T - T_0}, \tag{2.1}$$

where C is the Curie constant and T_0 the Curie-Weiss temperature, which in most cases equal to or slightly different from T_c. Generally, the center ion displaces from its body-center and the cubic unit cell further deforms to assume one of the noncentrosymmetric structures dependent on their crystallographic structure such as tetragonal, rhombohedral and monoclinic (or orthorhombric) structures.

Ferroelectric materials are classified into two groups according to their size and dimension. One is bulk ceramic and the other is ceramic film. A ferroelectric ceramic is a polycrystalline material in which the grains are randomly oriented. The bulk ceramics has been of interest in wide range of applications. Recently, the production of ferroelectric film has been developed in the form of thick film (1-20 μm) and thin film (less than 1 μm) on a substrate (Araujo, Scott and Taylor, 1996) with an advantage of low processing temperature. However, the properties of ceramic films are poorer than those of bulk ceramics, due to their high porosity and the clamping effects of the substrate (Sung-Gap *et al.*, 2008). In addition, the availability of film ferroelectric opens to integration of ferroelectrics with semiconductor circuits (Muralt, 2008). Along with the rapid development of microelectromechanical system (MEMS) technology, ceramic films have attracted much attention because of their excellent properties such as high piezoelectric constant and high electromechanical coupling coefficient. Another trend is that of the downscaling of ferroelectrics to new generation of nanotechnology based devices (Setter, 2001).

2.1.2 Piezoelectricity: constitutive equations and PFM measurement

Since the discovery in 1880, the experimental work on asymmetric crystal shows an additional creation of an electric charge produced by the applied stress (direct piezoelectric effect). Mathematical prediction of a converse effect (i.e. that a crystal becomes strained when in an electric field) in 1881 from basic thermodynamic principles was successively verified. Intensive research from the first technically relevant application of the piezoelectric effect was aimed to lead the development of materials with enhanced electromechanical properties. In current applications, the most used materials are polycrystalline ferroelectric ceramics, e.g. PZT and piezoelectric polymers, e.g. PVDF. However, PZTs pose a stronger electromechanical coupling.

Tensor of the piezoelectric coefficients

The piezoelectric effect can be explained in relation with a vector quantity (field E or displacement D) to a second rank tensor (strain S or stress T). In general, the piezoelectric coefficients are tensors of rank three with 27 components represented as d_{ijk} where each subscript corresponds to the Cartesian axis but, indeed, posses 18 independent components due to a symmetric type of the stress tensor. Using the contracted notation, the piezoelectric coefficient can be written with two subscripts, one representing the direction of the electric variable (i = 1-3), while the other represents the mechanical variable (j = 1-6). The fundamental piezoelectric relations can be expressed in constitutive matrix as shown in Eqs. 2.2 and 2.3 for the direct and converse effect, respectively (Nye, 1985).

$$\begin{pmatrix} S_1 \\ S_2 \\ S_3 \\ S_4 \\ S_5 \\ S_6 \end{pmatrix} = \begin{pmatrix} d_{11} & d_{21} & d_{31} \\ d_{12} & d_{22} & d_{32} \\ d_{13} & d_{23} & d_{33} \\ d_{14} & d_{24} & d_{34} \\ d_{15} & d_{25} & d_{35} \\ d_{16} & d_{26} & d_{36} \end{pmatrix} \begin{pmatrix} E_1 & E_2 & E_3 \end{pmatrix} \tag{2.2}$$

$$\begin{pmatrix} D_1 \\ D_2 \\ D_3 \end{pmatrix} = \begin{pmatrix} d_{11} & d_{12} & d_{13} & d_{14} & d_{15} & d_{16} \\ d_{21} & d_{22} & d_{23} & d_{24} & d_{25} & d_{26} \\ d_{31} & d_{32} & d_{33} & d_{34} & d_{35} & d_{36} \end{pmatrix} \begin{pmatrix} T_1 \\ T_2 \\ T_3 \\ T_4 \\ T_5 \\ T_6 \end{pmatrix} \tag{2.3}$$

In the case of the piezoelectric films, the convention for assigning axes is shown in Fig. 2.3.

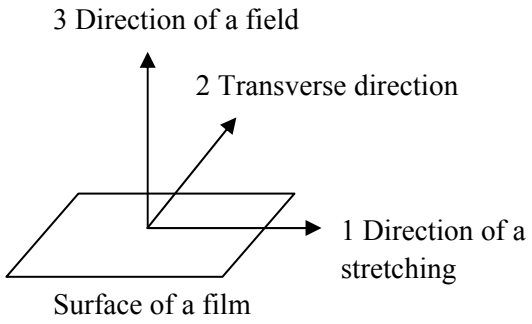

Figure 2.3 The conventional method of assigning Cartesian coordinate axes for a piezofilm which has been uniaxially drawn and poled.

The 3 direction is always associated with the film thickness, and this is invariably the direction of the applied field. If the film has been oriented by stretching, then the 1 direction is associated with the stretch and the 2 direction is perpendicular to 1 and 3. For un-oriented films, the directions of the 1 and 2 axes are arbitrary. In the twenty piezoelectric crystal classes, various symmetries lead to particular piezoelectric coefficients being zero, or being equal to other coefficients. For a poled ceramic film which has not been oriented by stretching, the matrix of piezoelectric coefficients is (Nye, 1985):

$$d_{ij} = \begin{pmatrix} 0 & 0 & 0 & 0 & d_{15} & 0 \\ 0 & 0 & 0 & d_{24} & 0 & 0 \\ d_{31} & d_{32} & d_{33} & 0 & 0 & 0 \end{pmatrix}. \tag{2.4}$$

For a uniaxially stretching film, which has been poled, the component d_{24} will change to d_{15}.

For the method using the converse effect, piezoelectric thin films deposited on a substrate always suffers clamping by substrate so that the ratio strain/field (or displacement/stress) does not represent the coefficient d_{33} of the free sample. For the inverse piezoelectric (ip) effect where a voltage is applied to induce a strain which is measured, this effective piezoelectric coefficient d_{33}(ip) can be calculated based on the assumption of the opposite extreme condition, i.e. in-plane strain is zero due to the extremely strong lateral constraint through (Lefki and Dormans, 1994):

$$d_{33}(\text{ip}) = d_{33} - \frac{2d_{31}S_{13}}{S_{11} + S_{12}}, \tag{2.5}$$

where S_{13}, S_{12} and S_{11} are the mechanical compliances of the piezoelectric film and d_{31} the transverse piezoelectric coefficient. It is expected that d_{33}(ip) gives an underestimation of the real d_{33}.

Piezoelectric measurements: Classification

Techniques for piezoelectric measurement of thin films classified into two groups: direct measurement and indirect measurement. One relies on a direct probe of either the displacement induced by applied electric field or charge amount produced by imposing a load, from which d_{33} can be extracted. The measurement considers the intrinsic linkage between the mechanical properties (stress and strain) and the electrical ones (voltage and charge), utilizing piezoelectric effects such as bulk or surface acoustic wave. An incomplete list of those is given as follows (Liu *et al.*, 2002):

(1) Piezoelectric effect (classified as direct techniques), e.g. normal load, periodic compression force, cantilever,

(2) Reverse piezoelectric effect (classified as direct techniques), e.g. single-beam optical interferometry, double-beam optical interferometry,

(3) Other indirect techniques, e.g. bulk acoustic wave, surface acoustic wave, impedance and return loss, composite resonance.

Piezoresponse force microscopy

The rapid emergence of thin-film ferroelectric materials resulted in considerable interest to piezoresponse force microscopy (PFM) as a key tool for ferroelectric characterization on local electromechanical properties which result in rapid development of this technique in the ferroelectric community. Along with the local measurements of piezoelectric coefficients and domain visualization, this technique allows for a direct matching of local properties to the microstructural-nanoscale details, since both are imaged simultaneously. In addition, because of PFM technique employed to carry out piezoelectric measurement, some of PFM principles are briefly discussed later.

The linear coupling between the piezoelectric and ferroelectric parameter infers that the domain polarity can be determined from the sign of the field-induced strain. Application of the uniform electric field along the polar direction results in the elongation of the domain with polarization parallel to the applied field and in the contraction of the domain with opposite polarization. The field-induced strain in this case can be written as:

$$S = \frac{\Delta Z}{Z} = \pm d_{33} E, \tag{2.6}$$

where ΔZ is the sample deformation and Z is the sample thickness. Eq. 2.6 can be written as:

$$\Delta Z = \pm d_{33} V, \tag{2.7}$$

where V is an applied voltage. The ± sign reflects the piezoelectric coefficient of opposite sign for antiparallel domains. Thus, opposite domains can be visualized by monitoring their voltage-induced surface displacement.

However, domain imaging based on detection of static piezoelectric deformation is difficult to implement unless a sample has a very smooth surface. The reason is that the static cantilever deflection due to the piezoelectric deformation will be superimposed on the deflection signal due to the surface roughness, which renders static piezoresponse domain imaging in samples with rough surfaces highly problematical.

Based on Eq. 2.7 one may conclude that the electrically induced topographic contrast between opposite domains can be infinitely enhanced by increasing the imaging voltage. However, there is a strict limitation imposed on this parameter to perform nondestructive visualization of domain structure. The imaging voltage should be kept below the coercive voltage of the ferroelectric sample. In addition, a high imaging voltage will lead to an increased contribution of the electrostatic signal to the tip-sample interaction, which in some cases can obscure the domain image.

A problem of low sensitivity of a static piezoresponse mode has been circumvented by employing a dynamic piezoresponse imaging method based on the voltage modulation approach, which allowed sensitivity to be increased by three orders of magnitude (Guthner and Dransfeld, 1992; Gruverman *et al.*, 1997). In this approach, an ac modulation (imaging) voltage $V = V_0 \cos \omega t$ is applied to the ferroelectric sample and surface displacement is measured using a standard lock-in technique by detecting the vertical vibration of the cantilever (Fig. 2.4(a)), which follows sample surface oscillation. A domain can be mapped by scanning the surface while detecting the first harmonic component of the normal surface vibration (vertical piezoresponse, or VPFM):

$$\Delta Z = \Delta Z_0 \cos(\omega t + \varphi), \tag{2.8}$$

where $\Delta Z_0 = d_v V_0$ is a vibration amplitude, d_v is effective piezoelectric constant and φ is a phase difference between the imaging voltage and piezoresponse, which provides information on the polarization direction. With the modulation voltage applied to the probing tip, positive domains (polarization vector oriented downward) will vibrate in phase with the applied voltage so that $\varphi(+) = 0$C, while vibration of negative domains (polarization vector oriented upward) will occur in counter phase: $\varphi(-) = 180°$ Note that while Eq. 2.8 is rigorous for a uniform field case, the field below the SPM tip is highly nonuniform. The rigorous solution has been given by Kalinin, Karapetian and Kachanov (2004) and it was shown that for transversally isotropic materials (e.g. *c*-domains in tetragonal perovskite ferroelectrics, poled polymers, etc.) $d_v \approx d_{33}$, recovering the early assumptions in PFM data interpretation (Gruverman *et al.*, 1997).

In lateral PFM (LPFM) (Eng *et al.*, 1998), *a*-domains are visualized by detecting the torsional vibration of the cantilever (Fig. 2.4(b)). Application of the modulation voltage across the sample generates sample vibration in the direction parallel to its surface due to the piezoelectric shear deformation. This surface vibration, translated via the friction forces to the torsional movement of the cantilever, can be detected in the same way as the normal cantilever oscillation in vertical PFM. For the uniform field for *a* domain, the amplitude of the in-plane oscillation is given by:

$$\Delta X_0 = d_{15} V_0, \tag{2.9}$$

while polarization direction can be determined from the phase signal since oscillation phases of opposite *a*-domains differ by 180°. It should be noted, however, that quantification of the shear piezoelectric coefficients in LPFM is a challenging problem that is complicated by the tip-surface tribology, inhomogeneous field distribution and mechanical clamping effects.

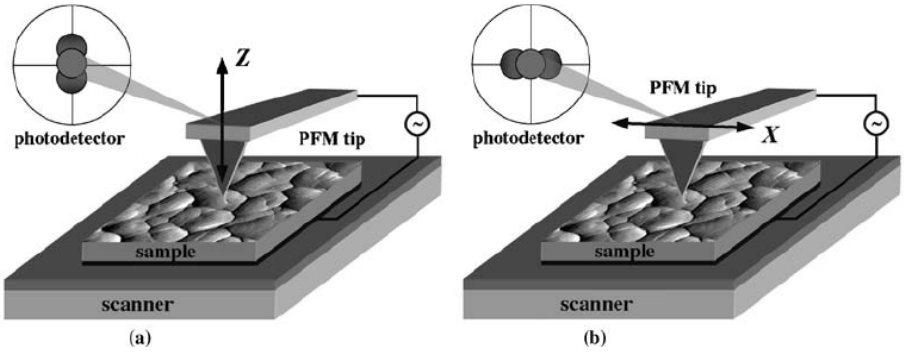

Figure 2.4 Schematics of the vertical (a) and lateral (b) PFM signal detection (Gruverman and Kalinin, 2006).

2.1.3 Pyroelectric effect

Pyroelectricity refers to the change of the ferroelectric polarization resulted from fluctuation of temperature in crystalline materials. A change in temperature will alter the ionic and electronic force within the crystal cell leading to change the dipole moments in polar materials. Over a range of temperature below the

Curie point and excluding other phase transitions the temperature variation of this ferroelectric polarization is reversible and maybe defined by a pyroelectric coefficient:

$$p = \frac{\Delta P}{\Delta T} = \frac{\Delta Q}{A \Delta T}, \tag{2.10}$$

where p: pyroelectric coefficient, ΔP: change in polarization, ΔT: change in temperature and ΔQ: change in pyroelectric charge over the cross-area A. Since the unit cells of the crystal are aligned, a net change in crystal polarization occurs and results changing the surface bound charge density. The additional bound charges will compensated by free surrounding ones when the materials are left for long time. If the change of temperature is fast enough then there is no time for charge compensation to occur. The result is that a pyroelectric current will flow in circuit with external load. The quantity p can be related to the figures of merit, which are (Stancu *et al.*, 2007)

$$F_v = p / \varepsilon_r \tag{2.11}$$

for voltage responsivity, where ε_r: relative dielectric constant and

$$F_d = p / c\sqrt{(\varepsilon_r \tan\delta)} \tag{2.12}$$

for current responsivity, where c: specific heat of the materials and tan δ: loss factor.

2.1.4 Ferroelectric domains

Ferroelectric crystals are not uniformly polarized in general. More typical is the formation of domains characterized by different orientations of the spontaneous polarization. The number of possible domain orientation depends on the perovskite phase. There are uniaxial ferroelectrics that have only two antiparallel states of orientation like for instance triglycinsulfate or lithium niobate, while there exist also multiaxial ferroelectrics that have more than two states. It is believed that PZT showed up to six and eight equivalent polar directions in the <100> directions of the spontaneous polarization in its tetragonal phase and in the <111> directions for rhombohedral phase, respectively, and the monoclinic [110] phase with 12 directions.

Thereby, the tetragonal-rhombohedral coexisting phase will result up to 26 possible different directions of alignment. For the simplest instance, if we assume that the sample surface is parallel to one of the tetragonal unit-cell faces, then these states can be divided into two groups. Four states correspond to the *a* domain orientation with the spontaneous polarization being parallel to the sample surface, while for the remaining two *c* domain states the spontaneous polarization is oriented normal to the sample surface. Quite complex domain structures can be illustrated in Fig. 2.5.

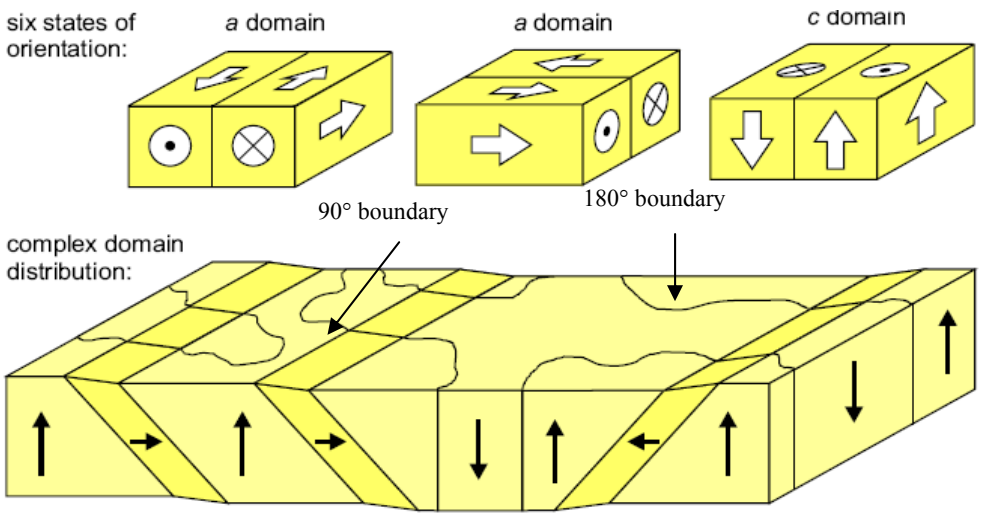

Figure 2.5 Ferroelectric domain types and structures in tetragonal phase. Up to six domain orientations with the spontaneous polarization oriented parallel (*a* domain) or normal (*c* domain) to the sample surface can be found. Different domain orientations can be observed to form quite complex domain patterns with mixing 90° and 180° domain (Moulson and Herbert, 1990).

An equilibrium domain configuration is established only if sufficient time is allowed for domain wall mobility. The pattern generated will depend on the electrical and mechanical stress conditions (Arlt, 1990). The electrostatic conditions defining the domain pattern change when an external field is applied and may result in displacement of the domain walls. The surface energy of the domain wall will be increased when it is set in motion because of the inertia of the ions which change position slightly as their dipole moment changes direction on passage of the domain wall. The vibration motion of the domain wall as an extrinsic contribution to

polarization response of ferroelectric materials was a subject of many theoretical and experimental studies. However, clamping by adjacent grains hinders the formation of any domain configuration. As the tetragonal structure is anisotropic a change of domain direction by 90° will require a change in shape. This is different to magnetic domains that are not related to crystal structure but to the electron configuration.

Concerning the formation of domain structure, also the thickness of a single domain wall is of interest, since it determines the lower limit of the domain size. In ferroelectrics, no long-range ordering is present and therefore very narrow domain walls with width in the order of the lattice constant are expected (Lines and Glass, 2001). Nevertheless, a complete understanding is still lacking due to limited experimental data and little theoretical work. The thickness of a 180° domain wall is assumed to be in the order of 5-20 Å (Wadhawan, 2000; Padilla, Zhong and Vanderbilt, 1996).

Note that surface grains will twin differently compared to bulk grains due to reduced clamping stresses. An un-poled piezoelectric will have randomly orientated domains that produces no overall polarization. Poling requires the alignment of 180° domains and rotation of 90° domains (Sayer *et al*., 1981). The intention of poling is to cause as many domains as possible to be aligned in the poling direction. Domains can be switched (90° domain rotated while 180° domains reversed) by electrical fields due to the ferroelectric properties of the material (Ogawa, 2000). Application of mechanical stresses can only produce 90° domain rotation due to crystal dimension anisotropy (Zhu and Yang, 1997).

2.1.5 Possible polarization vectors in ferroelectric film

The main introduction of this section is to review the nature of polarization reorientation or rotation behavior in each crystal phase of each orientation. For simplification, the complicated domain structures are assumed to depend on their crystallographic structure and texture (Taylor and Damjanovic, 2000). The magnitude of polarization and piezoelectric response is not only affected by clamping of the film by the substrate, but also by domain structure as well as the mobility of the domain walls. For the rhombohedral structure, one can consider possible orientations of domains for two crystallographic orientations in a [111]-

oriented film. There is one possible orientation normal to the film substrate and three canted an angle of approximately 71° or 109° with the normal to the film given in Fig. 2.6(a). As an adequate electric field is applied on, all the domains tend to rotate (or switch). That is all polarization orientations are the same normal to the film/substrate interface. The origin of the domain rotation lies in the reorientation of the displacement vector of B-site ions in the oxygen octahedron without induced strain.

In contrast, the domains in the [100]-texture film display four equivalent orientations, which cant at an angle of about 54.7 to the normal of the film shown in Fig. 2.6(b). However, the ultimate polarization orientation of the domains is perpendicular to the film as the poling treatment is accomplished. Therefore, the rotation of domains is associated with the lattice distortion, leading to remarkable local stress in the grains, which is the origin of the depolarization. In the case of tetragonal, the spontaneous polarization is align with [001] direction which is the fourfold axis of the oxygen octahedron for pseudoperovskite structure as shown in Figs. 2.6(c) and 2.6(d). Therefore, as the film is [100]-textured, the domain orientations are parallel with the surface of the film. The domain rotations caused by an electric field applied in out-plane direction result in significant stress. Finally, the domain structure not only depends on PZT texture and composition, but also or defects, internal and external stress, and so forth.

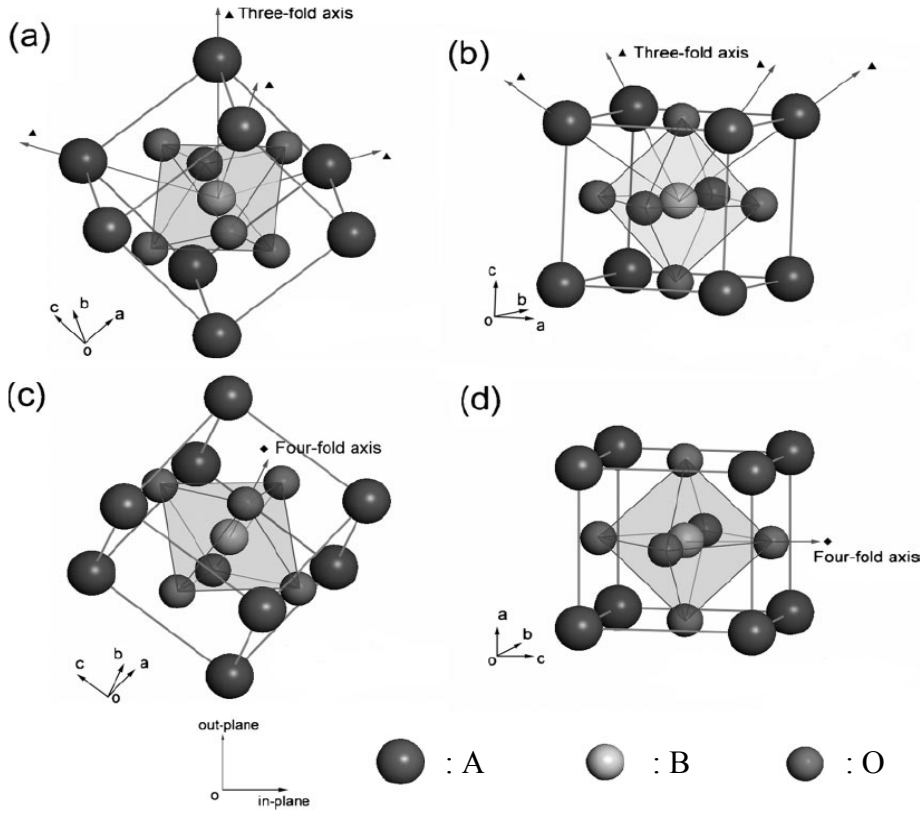

Figure 2.6 Possible orientations of the polarization vector in textured ABO_3 films: (a) (111)- and (b) (100)-rhombohedral films, (c) (111)- and (d) (100)-tetragonal films (Gong *et al.*, 2004).

2.1.6 Ferroelectric film applications

As ferroelectric materials have a special nature and posses a unique combination of properties, a broad spectrum of potential applications in commercial devices can be developed with these materials. Figure 2.7 gives a schematic overview of these applications and some of them are detailed later. Though the largest number of applications with ferroelectrics is still associated with bulk materials, important applications are under development for ferroelectric films. This is because the feasibility of practical applications is still dependent on the status of the film preparation, processing and integration technologies. Each application has different requirements which might be fulfills certain requirements and not others. In addition, the ferroelectric film properties can differ largely from the bulk ones.

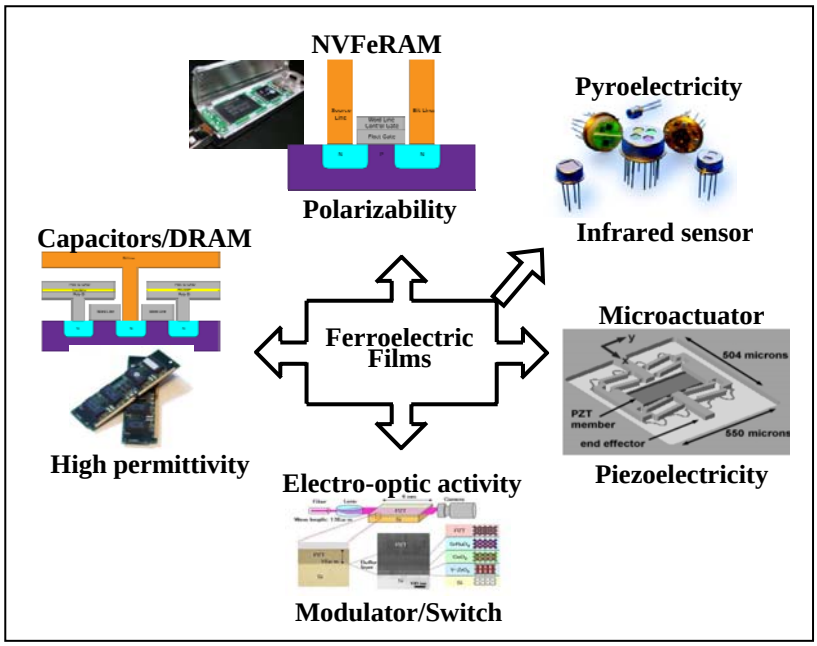

Figure 2.7 Overview of typical ferroelectric thin-film applications (Auciello, Scott and Ramesh, 1998).

Memories

Ferroelectric films have attracted a lot of attention especially for their use in memories. The largest emphasis is probably on NVRAM (Nonvolatile Random Access Memory) (Larsen *et al.*, 1994; Ramesh, 1997). The application is based on the hysteresis properties of ferroelectrics. States of negative and positive remanent polarization can be used as binary of 1 and 0 in data storage. This is due to low fatigue with low operation driven voltage in SBT and more ease of integration with higher polarization value in PZT (Nagel *et al.*, 2001).

Ferroelectrics are also being considered for other types of memories: DRAM (Dynamic Random Access Memories), which are volatile (the information is required power supply to retain its state). These are based on transistors tandemed with capacitors (Ramesh, 1997). Increasing miniaturization requires higher capacitance for smaller feature size.

Microelectromechanical systems (MEMs)

The MEMs technology is the integration of mechanical elements and electronics on a same substrate, usually silicon. Micromachining and microelectronics are brought together to obtain a complete system on one chip. By adding sensors and actuators to MEMs, the aim is to transform MEMs into smart structures, which can sense and react to environment or stimuli. Therefore, ferroelectrics are studied for their piezoelectric properties to be used as sensors and actuators in these type of systems. As an order of magnitude, an average value for piezoelectric coefficient of a ferroelectric material bulk is 100 pC/N. The converse piezoelectric effect would lead to a displacement of 100 Å for V =100 V. A piezoelectric coefficient (d_{31}) of 65 pC/N was measured on a 200 nm thick MOCVD PZT layer grown for this study (Rossinger and Misat, 2000).

Electro-optic application

By varying the ferroelectric polarization with an electric field, one produces a change in the optical properties of the ferroelectrics. Ferroelectric films can be used in nonlinear optic applications to convert light to different wavelength (Fork, Armani-Leplingard and Kingston, 1996), or in electro-optic modulators (Buchal and Siegert, 1999). The advantage of films is twofold. Wave guide electro-optic modulators require relatively low driven power in comparison to bulk modulators, because of the optical confinement in the film. Additionally, thin films produced on heterostructure substrates used in the semiconductor industry are more readily integrated than bulk hybrid technologies. Efforts are always directed to implement new technologies on Si wafers to integrate optical devices in existing silicon technology on a large scale. There are several thin film candidates for electro-optic technology. These include $LiTaO_3$ (Buchal and Siegert, 1999), $BaTiO_3$ (Wessels, 1998), PLZT (Dogheche *et al.*, 1995) as well as electro-optic polymers. All of these are highly transmissive at the infrared wavelengths used in optical communication networks. Additionally, the polymers can be deposited onto a wide variety of substrate (Steier *et al.*, 1999).

Infrared sensors

Uncooled infrared image sensors are increasingly demanded for many applications such as automobile, biomedical, plant monitoring and security system. IR sensors can be classified into two major types including photon sensors and thermal sensors. Photon sensors are based on the photovoltaic, photoconductive or photoelectric effect. They are wavelength selective. Photon sensors are often cooled to cryogenic temperature to obtain a better performance. Thermal type IR sensors, such as bolometer, thermopile and pyroelectric sensors, can be operated at room temperature (uncooled) with little wavelength dependence of the response over a wide infrared range. IR sensors using pyroelectric material have the highest sensitivity in thermal type IR sensors. To realize uncooled pyroelectric IR image sensors, an integration of pyroelectric material and circuitry using silicon devices is required. A change of pyroelectric current perpendicular to the polar axis on the crystal faces with a change of temperature was considered in ferroelectric materials. Si integrated pyroelectric IR sensors using PVDF thin films have been reported, however that pyroelectric film is lower sensitivity compared to the pyroelectric ceramics (Fujitsuka *et al.*, 1988). On the other hand, high sensitive pyroelectric sensors using $PbTiO_3$ films on MgO single crystalline substrates have been reported (Iijima *et al.*, 1986).

2.2 Ferroelectric materials

2.2.1 Lead Zirconate Titanate (PZT)

Lead titanate ($PbTiO_3$) was reported to be ferroelectric in 1950 on the basis of its structural analogy with $BaTiO_3$ and the discovery of a high temperature transition around 500 °C (Shirane, Hoshino and Suzuki, 1950). Substitution of Zr^{+4} for Ti^{+4} in $PbTiO_3$ reduces the tetragonal distortion of *P4mm* symmetry and ultimately causes the appearance of another ferroelectric phase of rhombohedral *R3m* symmetry. In $Pb(Zr,Ti)O_3$ (PZT) crystals, lead and oxygen atoms appear at the corners and face centers, respectively. Octahedrally co-ordinated titanium or zirconium ions are located at the center of the unit cell. Solid solutions form with their boundary nearly independent of temperature (morphotropic). More amount of Zr^{+4} cause the appearance of the orthorhombic antiferroelectric phase with a small field of stability

of a tetragonal antiferroelectric phase near the Curie point. Curie temperature variations from 220 °C to 490 °C are dependent of the compositional PZT (Newham, 1997; Jaffe *et al.*, 1971). When Zr/Ti is within a region of $0.9 < x < 1$, antiferroelectric and rhombic phase exists at the normal conditions, however, in some application the antiferroelectric to ferroelectric phase transitions induced by external electric field are used in applications. Ceramics based on these compositions are promising for shape memory applications due to relatively high coefficients of electroelasticity. The deformation of these ceramics can be controlled by various domain configurations and structures (Cross, 1995). Additional applications of these ceramics are relation to fabrications of elements with high electron emission obtained during ferroelectric-antiferroelectric phase transition controlled by external electric field and mechanical stress (Okuyama, Asano and Hamaka, 1995). There are two rhombohedral phases at Zr/Ti within $0.6 < x < 0.9$. The ferroelectric phase transition from the low-temperature to the high-temperature phase is accompanied by the loss of oxygen octahedron tilt angle and corresponding superstructure (Glazer, Mabud and Clarke, 1978). These ceramic are characterized by relatively low spontaneous deformations and low range of dielectric constants and are used in electromechanical transducers and surface acoustic wave devices. Another feature of this compositional range with dopant is the experimentally observed states of metastable polarization which is typical for relaxor (Dalington, 1988; Cross, 1995).

The phase diagram originally established by Jaffe *et al.* (1971) in Fig. 2.8 shows the morphotropic phase boundary (MPB) which separates the rhombohedral and tetragonal structure at about 45 mole percent $PbTiO_3$. The investigation of the piezoelectric property in this solid solution showed the coupling factor and dielectric constant to be the highest near the MPB (Jaffe and Roth, 1954). Since the boundary in nearly morphotropic, the temperature dependence of the electromechanical properties is practically free of polymorphic irregularities in contrast with $BaTiO_3$. Compositional rich in $PbTiO_3$ were not successfully poled, but a significant piezoelectric effect existed throughout the rhombohedral range. It is believed that the proximity to such a phase boundary between ferroelectric phases favors strong piezoelectric effects in a ceramic because of the increased ease of reorientation during poling. In addition, in such compositional range ($0.4 < x < 0$),

tetragonal crystal structure possess relatively high anisotropy of piezoelectric coefficient d_{33} and d_{31} and corresponding electromechanical coupling factors k_t and k_p (Turik and Topolov, 1997; Tashiro *et al.*, 1987). Other features of these compositions are relatively high coercive field and high spontaneous deformations. Some applications of these materials include filters and frequency stabilizers.

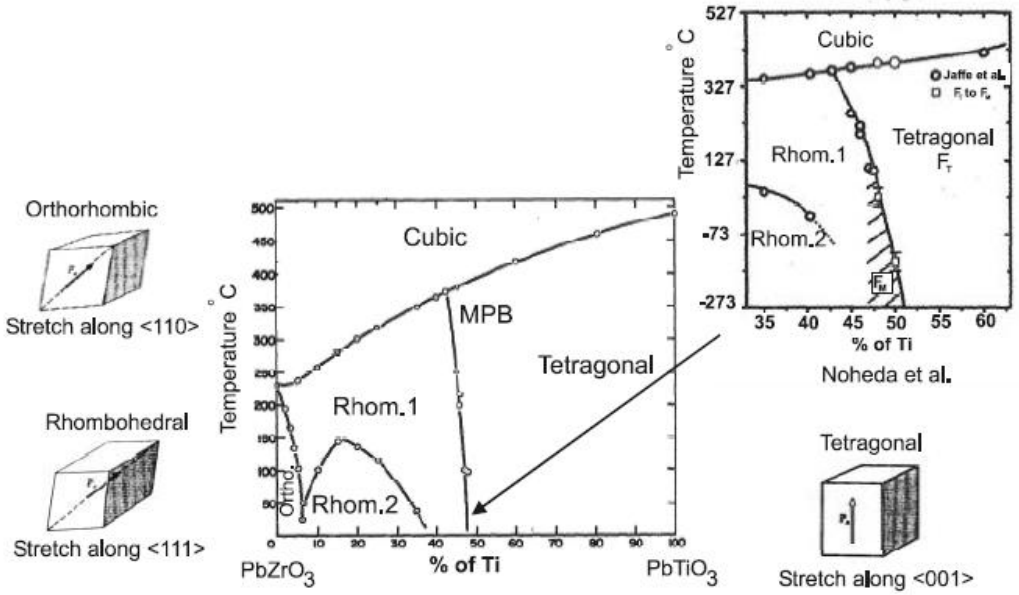

Figure 2.8 PZT phase diagram. In the middle, the standard phase diagram is shown (Jaffe, Cook and Jaffe, 1971). The diagram around the MPB showing the monoclinic phase between the tetragonal and rhombohedral phases is shown at the upper right (Noheda *et al.*, 2000). F_M stands for ferroelectric monoclinic in the inset.

Recently, the discovery of a new intermediate monoclinic phase is within a narrow region of $0.45 < x < 0.52$ for bulk PZT around the MPB (Noheda *et al.*, 1999; Noheda *et al.*, 2000). The very high electromechanical response seems to be directly related to the existence of the low symmetry monoclinic phase (Noheda, 2002). Since the monoclinic structure can be constructed from the tetragonal structure by shifts of the Pb and Zr/Ti atoms along a tetragonal [110] axis, the monoclinic structure can also be considered as a "bridge" between the tetragonal and rhombohedral phase in PZT. Therefore the authors suggested that this is not a really morphotropic phase boundary, but rather a morphotropic phase connecting the

tetragonal and rhombohedral phases of PZT. Glazer *et al.* (2004) also discussed the local structures of the tetragonal, rhombohedral and monoclinic phases across the MPB of PZT. They argued that on an appropriate length scale all three phases may be considered to be monoclinic at the local level and there is no need to invoke any discrete phase boundaries across the MPB. A new intermediate monoclinic phase with a composition close to the MPB of bulk ceramics was also theoretically predicted for epitaxial PZT films in Ref. (Pertsev *et al.*, 2003). This phase is strain induced and similar to the monoclinic phase of PZT bulk ceramics with x = 0.48. However, for PZT films the monoclinic phase is not confined to a composition close to the bulk MPB, but it rather exists for all studied compositions (x = 0.4-0.9) depending on the misfit strain. However, the direct transformation of the paraelectric phase into the monoclinic phase can only be observed during cooling in PZT films with $x < 0.7$ for film-substrate systems with no lattice mismatch. If a misfit strain exists in the films, the paraelectric phase transforms either into the tetragonal phase (for $\Delta a/a < 0$) or into the orthorhombic phase (for $\Delta a/a > 0$) and, at still lower temperatures, into the monoclinic phase.

2.2.2 Chemical modification

PZT is especially attractive for material properties designing. Wide range of physical can be obtained by variation of Zr/Ti ratio, particularly in so-called MPB region. In addition, to meet stringent requirements of applications, ferroelectric ceramics have been modified in various ways. PZT ceramics are almost always used with a dopant or a modifier to improve and optimize their basic properties for specific applications (Jaffe and Berlincourt, 1965; Haertling, 1986). The donors, such as Nb^{5+} replacing B-site cations (Zr^{4+},Ti^{4+}), are compensated either by A-site vacancies or by electrons. The donors are usually compensated by A-site vacancies. These additives in combination with corresponding vacancies appear to enhance domain orientation with respect to undoped material. Ceramics produced with these additives are characterized by square hysteresis loops, high dielectric loss, high mechanical compliance, advanced piezoelectric properties, reducing ageing and easy depoling. This type of ceramics is called Soft PZT (Jaffe, Cook and Jaffe, 1971; Gerson, 1960).

Acceptors like Fe^{3+} replacing B-site cations are compensated by oxygen vacancies and usually have only limited solubility in the lattice. These additives lead to opposite effect to those of donors. Domain reorientation is limited, and, hence, ceramics with acceptor additive are characterized by poorly developed hysteresis loops, lower dielectric constant, low dielectric losses, low piezoelectric properties, low compliances, higher aging rate and ceramics are more difficult to depole. These ceramics are called Hard PZT (Jaffe, Cook and Jaffe, 1971).

Isovalent additives, such as Ba^{2+} or Sr^{2+} replacing Pb^{2+} or Sn^{4+} replacing Zr^{4+} or Ti^{4+} in which the substituting ion is of the same valency and approximately the same size as the replaced ion, usually lead to inhibited domain orientation and poorly developed hysteresis loops. Other properties include lower dielectric loss, low compliance, and higher aging rates. For some applications the isovalent modifiers are used to change Curie temperature, for example, the transition temperature of Sr-modified PZT ceramics decreases about 9.5 °C per each atomic percent of Sr concentration (Ikeda, 1959).

2.2.3 Other alternative ferroelectric materials

Promising lead-free ferro- and piezoelectric materials with perovskite structure which could be alternative to PZT are $Na_{1/2}Bi_{1/2}TiO_3$ (NBT) (Chiang, Garrey and Soukhojak, 1998) and textured $(K_{0.44}Na_{0.52}Li_{0.04})(Nb_{0.86}Ta_{0.1}Sb_{0.04})O_3$ (LF4T) (Saito *et al.*, 2004). While LF4T is an alkaline niobate-bated solid solution at the MPB, NBT is a chemical compound, in which one half of the A cation sites are occupied by Na^+ ions, the remaining by Bi^{3+} ions.

Bismuth layer structured ferroelectrics (BLSF) such as $Bi_4Ti_3O_{12}$ (BiT), SBT and their related compounds exhibit ferroelectric properties, which are indeed slightly inferior to those of PZT, but they show no fatigue effect which is of interest in NvFRAM cells (Auciello and Foster, 1998; Kingon, 1999; Park *et al.*, 1999). For this reason they were extensively investigated in the last decade. A family of layered Aurivilius family such as $SrBi_2Ta_2O_9$, $SrBi_2NbTaO_9$ and $SrBi_2Ti_4O_{15}$ has been of interest (Jona, 1993; Auciello, Scott and Ramesh, 1998). Their general chemical formulas are represented as $(Bi_2O_2)^{2+}(A_{m-1}B_mO_{3m+1})^{2-}$ where A is a large mono di- or trivalent metal cation such as Na, K, Ca, Bi, Sr, Ba or Pb, and B is a small cation with

high electric charge of tetra-, penta- or hexavalent like Ti, Nb, Ta, Mo or W (Paz de Araujo *et al.*, 1995; Aurivillius, 1949; Irie, Miyayama and Kudo, 2001). *m* is an integer from 1 to 8 and denotes the perovskite-like units ($A_{m-1}B_mO_{3m+1}$) along the c-axis between two bismuth oxide layers $(Bi_2O_2)^{2+}$. The layered structured structure of this kind of material is given in Fig. 2.9. These materials yield a high endurance during electrical cycling with excellent improved fatigue-free properties. This good fatigue behavior is believed due to the oxygen-rich bismuth layer preventing degradation of the polarization. Other materials are based on $BaTiO_3$ and its chemical modification. For example $Ba_xSr_{1-x}TiO_3$ or abbreviated BST is currently being investigated as a dielectric material for tunable microwave-device applications and decoupling capacitors due to its large field-dependent permittivity, high dielectric constant, and relatively low-loss tangent.

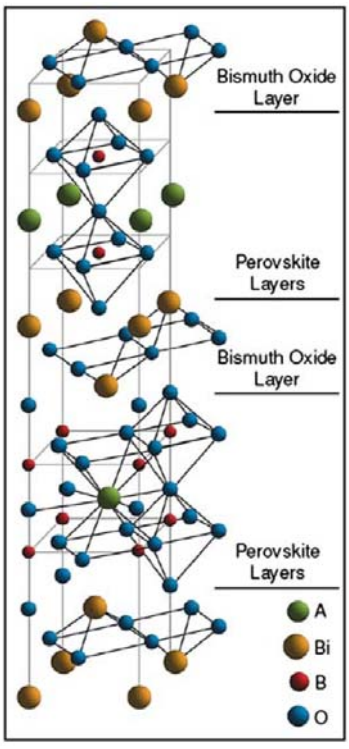

Figure 2.9 Layer perovskite structure (Auciello, Scott and Ramesh, 1998).

Ferroelectric material such as NBT based composition has received much attention for electromechanical applications like MEMS, actuators, micro-machines, and pressure sensors due to their often superior piezoelectric properties

compared to the more traditional materials like ZnO and quartz (Damjanovic, Muralt and Setter, 2001; Uhlmann *et al.*, 2000; Chiang *et al.*, 1998). Ferroelectrics with electro-optic activity like $KNbO_3$ (Chow *et al.*, 1994) and $LiNbO_3$ (Sakashita and Segawa, 1995; Yamaguchi *et al.*, 1998) are applied in color filter devices or computer displays. The thickness of the oxide films depends on the application: while for piezoelectric and IR sensing devices the thickness should be in the region of 0.1-1 mm, the typical thickness needed for actuators is about 10-50 mm (Whatmore *et al.*, 2003) and for ferroelectric memory cells 100 nm or less. Room temperature values of the dielectric, piezoelectric, and electromechanical properties have been complied and tabulated in Table 2.1. As a major concern compared to lead based materials, these discussed materials do not contain toxic, which is an important environmental aspect.

Table 2.1 Dielectric and piezoelectric properties of lead-free perovskite piezos "past and present" (Zhang, Xia and Shrout, 2007).

Material	ε_r	loss	d_{33} (pC/N)	k_p	k_{33}	T_c (°C)
$BaTiO_3$	1,700	0.01	190	0.36	0.5	115
$BaTiO_3$-$CaTiO_3$-Co	1,420	0.005	150	0.31	0.46	105
$(K_{0.5}Na_{0.5})NbO_3$ (HP)	500	0.2	127	0.46	0.6?	420
$(K_{0.5}Na_{0.5})NbO_3$	290	0.4	80	0.35	0.51	420
KNN-Li (7%)	950	0.084	240	0.45	0.64	460
KNN-Li3%; Ta20%	920	0.024	190	0.46	0.615	310
KNN-LF4*	1,570	/	410	0.61	/	253
KNN-SrTiO3 (5%)	950	/	200	0.37	/	277
KNN-LiTaO3 (5%)	570	0.04	200	0.36	/	430
KNN-LiNbO3 (6%)	500	0.04	235	0.42	0.61	460
KNN-LiSbO3 (5%)	1,288	0.019	283	0.5	/	392
NBT-KBT-LBT	1,550	0.034	216	0.401	/	350
NBT-KBT-BT	820	0.03	145	0.162	0.519	302
NBT-KBT-BT (MPB)	730	0.02	173	0.33	0.59	290
SBT-KBT90	870	0.04	110	0.15	0.507	296
SBT-KBT85	1,000	0.05	120	0.16	0.491	250
BBT-KBT90	837	0.05	140	0.23	0.538	297
BBT-KBT80	630	0.04	95	0.15	0.361	290
$Sr_2NaNb_5O_5$*	1,100	/	120	/	/	280

*Textured; HP: Hot Pressed; NBT: $(Na_{0.5}Bi_{0.5})TiO_3$; KBT: $(K_{0.5}Bi_{0.5})TiO_3$

LBT: $(Li_{0.5}Bi_{0.5})TiO_3$; BT: $BaTiO_3$; SBT: $(Sr_{0.7}Bi_{0.2})TiO_3$; BBT: $(Ba_{0.7}Bi_{0.2})TiO_3$

2.3 PZT film fabrication

2.3.1 Possible preparations of PZT films

The PZT films have been fabricated using several techniques, each of which has to satisfy different requirements:

(1) device compatibility, ease of oriented control or single-crystalline films and heterostructure with specific properties like resistance to fatigue effect, long polarization retention time and no imprint behavior,

(2) integration with metallic or conductive oxide substrate,

(3) ability to produce patterned, multilayered or superlattice structure,

(4) relatively low processing temperature to avoid a harmfully undesired structure and unintentional diffusion,

(5) good film quality (conformity and uniformity),

(6) high reproducibility,

(7) simple, inexpensive and environmental-friendly fabrication process.

The preparation processes in PZT films can be classified into three groups:

(1) physical vapor deposition (PVD) e.g. sputtering deposition and pulsed laser ablation deposition (PLAD),

(2) chemical vapor deposition (CVD) e.g. metalorganic chemical vacuum deposition (MOCVD),

(3) chemical solution deposition (CSD) e.g. sol-gel method and metalorganic deposition (MOD).

However, one of the methods that were far more popular to employ in the past few years is the sol-gel method which gives several advantages of stoichiometric control including the addition of dopants which is very important for multicomponent systems, ease of process integration with standard one-IC-chip technology and low-cost consumption.

2.3.2 Chemical solution deposition

During the 1980s, the experimental results based on CSD of PZT films were carried out (Budd, Dey and Payne, 1985; Fukushima, Kodaira and Matsushita,

1984) and some examples of systems suitable for growing perovskite film with the same properties as bulk ceramics were provided. The CSD as well as sol-gel method is very versatile and offer many advantages but, however, it suffers from several drawbacks such as for instance the difficult deposition of epitaxial and ultra-thin films (thickness < 30 nm). Furthermore, conformal coating of 3D structures with a high aspect ratio represents a problem (Schwartz, Schneller and Waser, 2004). Chelating in metal compound allows the formation of crack-free films that they can block the condensation reaction sites, offering structural flexibility of gel films and suppressing crack formation (Schmidt *et al.*, 1988). Fabrication of the sol-gel method composed of four basic steps (Schwartz, Schneller and Waser, 2004; Schwartz, 1997):

(i) synthesis of the precursor solution,

(ii) deposition by spin, spray or dip coating, where drying processes usually begin depending on the solvent,

(iii) low-temperature heat treatment (300-450 °C depending on the oxide material) in air or oxygen for drying, pyrolysis of organic species and formation of an amorphous film,

(iv) higher temperature heat treatment (typically 500-700 °C) in air or oxygen atmosphere for densification and crystallization of the coating into the desired perovskite phase.

Often influences of the heat treatment scenario including the atmosphere also play the important role on the texture selection of the perovskite phase evolution which transfers from amorphous phase to a pyrochlore-lie (or fluorite) intermediate phase independent of the precursor system (Chen and Chen, 1998). In addition to the two-step heat treatment described above, there is also a single-step process described elsewhere (Schwartz, Schneller and Waser, 2004; Tuttle and Schwartz, 1996) by rapid heat treatment (omitting step (iii)) to the crystallization temperature which results in both organic pyrolysis and crystallization. The purpose is to enhance film densification by delaying the onset of crystallization to higher temperature, thus resulting that the film texture is promoted to grow a preferred [111] orientation (Jiang *et al.*, 2006). In accordance with the reports (Reaney *et al.*, 1994; Brooks *et al.*, 1994), the pyrolysis of the as-deposited films at temperature above ~400 °C leads to a preferred [100] oriented growth while in the range between 350 °C

and ~400 °C a preferred [111] textured film is obtained after the final crystallization step. Liu and Phule (1996) hypothesize that a layer of "seed nuclei", which is only formed if a 400 °C pyrolysis step is applied, is responsible for the development of [111] oriented film during the final crystallization at 700 °C. Schwartz *et al.* (1997) explain the differences in the microstructure and texture evolution of various chemically different CSD routes to PZT films with a thermodynamic model deduced from the standard nucleation and growth theory. They propose that changes in the film pyrolysis temperature cause changes in the crystallization temperature, which in turn alter the driving force governing the transformation from the amorphous to the crystalline phase. These changes in the pyrolysis temperature are induced by the precursor chemistry. All such variations in the driving force cause a change in the thermodynamic barriers that define the active nucleation mechanism, and thereby the microstructure or texture development. The typical film thickness of one deposition cycle is in the range of 50-100 nm (Scott, 2000; Wright *et al.*, 2002) except for thicker film which inevitably concerns step (ii) and (iii) through repeated several times for the desired thickness.

The microstructure of the ferroelectric perovskite phase is determined by solution chemistry, stoichiometry and the underlying substrate as well as the substrate treatment (Tuttle and Schwartz, 1996). The substrate can be altered in various ways in order to control the nucleation of the perovskite crystallites at the electrode-film interface. The influence of a very thin seeding or buffer layer was intentionally introduced to control the overlaid film texture. Thereby the nucleation activation energy may be reduced. Because of the abundance of nucleation sites, fine grains and more uniform microstructures are formed. A thin Ti or TiO_2 film on a Pt/Si electrode can induce a strong [111] texture (Muralt *et al.*, 1998), while pre-depositing a thin [100] oriented layer of $PbTiO_3$ (Hiboux and Muralt, 2004) or PbO (Gong *et al.*, 2004) on Pt/Si can lead to a strong [100] texture in the PZT films. In addition, when film and substrate have different structures or large lattice mismatches, highly oriented texture is achieved through a two-step process where first a polycrystalline film is deposited and then heated to cause it to break up into isolated grains (seeds) that posses a low interfacial energy. The isolated islands may then act as nucleation sites for the subsequent growth of a highly oriented film. The use of Ag or Au as

alloying elements to expand the lattice parameter of the Pt electrode produces a closer lattice match to PZT which improves the degree of film orientation (Whatmore *et al.*, 2003). Norga *et al.* (2004) described the dependence of the orientation of polycrystalline PZT films on pyrolysis conditions. For oxygen-rich conditions, a quasi-amorphous intermediate phase occurred resulting in a [100] preferred orientation due to its minimum surface energy in perovskite structure. If in reverse a reduced oxygen partial pressure was used during pyrolysis a homogeneous crystalline fluorite developed as intermediate phase. The fluorite grains were believed to be [111] textured leading to [111] oriented perovskite PZT grains after crystallization.

The most important part in the sol-gel process would be the synthesis of an appropriate precursor solution. The microstructure and physical properties of sol-gel derived PZT films can be greatly influenced by their precursor solution. Solution preparation generally involves the use of one or more metal-organic compounds which are dissolved in a common solvent. The sol-gel reaction in the precursor solution is not known in more detail, but it is considered that this reaction proceeds in three steps: stabilization of metal complex, partial hydrolysis and condensation (Kwon *et al.*, 1999). The chemical properties of sol-gel solutions can be altered by modifying the organic ligands from the metal complexes or using different stabilizer and/or solvent systems. In turn, the modified solutions affect the physical properties of the resultant PZT films since the thermal decomposition of sol-gel precursors and the formation of nuclei and grains are not mutually independent procedures.

2.3.3 Sol-Gel precursor solution

The raw starting materials will be selected by their solubility, reactivity considerations and the type of solution precursor species desired, all of which are typically metal alkoxide compounds $M(OR)_x$ (where M is a metal and R is an alkyl group), metal carboxylates $M(OOCR)_x$ and metal β-diketonates $MO_x(CH_3\text{-}COCHCOCH_3)_x$. The most common used sol-gel approaches are:

(1) sol-gel processes which use 2-methoxyethanol (or namely ethylene monoethylether) as reactant and solvent,

(2) chelate or hybrid processes which use modifying ligands such as acetic acid or acetyl acetone or both,

(3) metal-organic decomposition route which uses water-sensitive metal carboxylate compounds.

In step (2) and sometimes towards to step (3), the reactivity of the reagents is high and the structure of the species in solution can bear little resemblance to the starting compounds and contains more than one type of cation. In contrast, for the long-chain carboxylate compounds the reactivity is low and chemical interactions between the different precursor compounds are minimal (Schwartz, Schneller and Waser, 2004).

The common choices of precursors when making sol-gel are metal alkoxides because they provide a convenient source for inorganic network, or oligomers, which in most cases are soluble in common solvents. Another advantage of using the alkoxides is the possibility to control the reaction rate by controlling hydrolysis and condensation, which are the most critical processes in sol-gel technique (Banno, 1995).

There are several routes based on a solvent to prepare precursor in sol-gel processing, such as 2-methoxyethanol (Kwon *et al.*, 1999; Budd, Dey and Payne, 1985), acetic acid (Kwon *et al.*, 1999) and 1,3 propanediol (Tu *et al.*, 1996). Although 2-methoxyethanol is toxic and unfriendly for use because of its carcinogenic and teratogenic properties (Zhang, Whatmore and Vickers, 1999) which lead to a greater emphasis on the use of other simple solvents, processes based on 2-methoxyethanol has been most appropriately considered sol-gel processes for pure perovskite phase at lower pyrolysis temperature (600 °C or below) (Budd, Dey and Payne, 1985). The reaction can be described as a hydrolysis of the precursor which leads to the formation of M-O-M bonds, followed by a polycondensation process with the departure of a water molecule or an alcohol molecule (Calzada *et al.*, 1995). In general, the course of the sol-gel process can be described through (Bruncková *et al.*, 2004):

Hydrolysis

$$M(OR)_x + mH_2O \rightarrow M(OR)_{x-m}(OH)_m + mROH, \quad (2.13)$$

Water condensation

$$2M(OR)_{x-m}(OH)_m \rightarrow (RO)_{x-m}(OH)_{m-1}M\text{-}O\text{-}M(OR)_{x-m}(OH)_{m-1} + H_2O, \quad (2.14)$$

Alcohol condensation

$$2M(OR)_{x-m}(OH)_m \rightarrow (RO)_{x-m}(OH)_{m-1}M\text{-}O\text{-}M(OR)_{x-m-1}(OH)_m + ROH\ . \quad (2.15)$$

Prehydrolysis of less reactive alkoxides may also be used to improve solution compositional uniformity. However, the use of complex alcohol gives the alcohol-exchange reaction that results in a decrease in the hydrolysis sensitivity of metal-alkoxides through:

Alcohol exchange

$$M(OR)_x + xR'OH \rightarrow M(OR')_x + ROH, \quad (2.16)$$

where OR is a reactive alkoxy group and OR′ is the less reactive methoxyethoxy group. Due to instability and limited commercial availability, lead carboxylate as well as lead acetate was often chosen in 2-methoxyethanol route. This is because one of the acetate groups in lead acetae is replaced for the formation of the soluble lead precursor, $Pb(OOCCH_3)(OCH_2CH_2OCH_3)\mathbf{.}0.5H_2O$.

The precursor chemistry has an important influence. Malic *et al.* (2005) concluded from an extended X-ray absorption fine structure (EXAFS) study on chemically differently modified precursors that the distributions of constituent metal atoms in the sols can be homogenized by the tailored addition of acetic acid. Residual organics such acetates in the pyrolyzed film result in a strongly [111] oriented film and that films with large densities of OH bonds prior crystallization exhibit a mixed [111]/[100] orientation. A study of the reactivity of the starting compound lead(II) acetate with the transition metal *n*-propoxides and *n*-butoxides shows differences in the amount of released ester (Kosec and Malic, 1998). The resulting precursor structures are supposed to affect the microstructure of PZT due to a lack of homogeneity in the solution-precursor caused by zirconium. Coffman *et al.* (1996) studied the structural evolution of precursor solutions prepared by two different synthetic schemes from the 2-methoxy ethoxides of titanium, zirconium and lead. The residual acetate alkoxy and carbonate groups as well as the hydrolysis conditions influence the pyrolysis behavior of the gels and the resulting film microstructure. The effect of chelating acetylacetone (Hacac) on the crystallization behavior and the

resulting physical properties of PZT films by the inverted mixing order route have been investigated (Schwartz *et al.*, 1995). The result showed that upon addition of two or three moles Hacac/mol PZT to aged precursor solutions the ferroelectric response and the optical scattering losses could be significantly improved.

The particle size and shape (branched or linear) as a result of hydrolysis conditions and aging of sol-gel precursor are key factors that influence film orientation. Zhang *et al.* (1999) found linear particle size in the range of 5-16 nm. With the increase of the particle size, the intensity of [111] orientation decreased and the non-ferroelectric pyrochlore phase seemed to appear more significantly which in turn resulted in a failure of the ferroelectric properties. Besides that, weakly branched precursor species allow for a better interpenetration and rearrangement during the deposition process than highly branched ones (Chen, Ryder and Spurgeon, 1989). As an important factor which governs the shape of the particles the type of applied hydrolysis catalyst (acid or base) has been considered (Coffman *et al.*, 1996; Dey, Budd and Payne, 1987; Livage, Henry and Sanchez, 1988). Due to different mechanisms, acid catalyst such as nitric or acetic acid lead to more linear and less cross-linked species, whereas base catalysts such as ammonia yield stronger cross-linked structure (Jacobs and Salamanca-Riba, 2003).

CHAPTER 3

HIGHLY ORIENTED AND NIOBIUM-MODIFIED PZT THIN FILMS

This chapter presents in details the properties and characterization of the niobium-doped PZT thin film of [100]- and [111]-orientation. The process used is based on 2-methoxyethanol with chelate or hybrid process as introduced in chapter 2. The PNZT thin films derived from the same route discussed on texture and thickness dependent properties were presented separately in chapter 4.

3.1 Introduction

PZT thin films have received much attention for their practical or potential applications in various fields, e.g. ferroelectric nonvolatile random access memories, infrared sensors, piezoelectric micro-actuators and microelectromechanical systems (MEMS) (Wang, Kokawa and Maeda, 2005; Akai, 2005). Platinized silicon is a conventional substrate for the microfabrication of MEMS devices, and much work has been done to develop high-performance PZT films on silicon substrates. However, the PZT films deposited on platinized silicon substrate tend to crystallize polycrystalline films with complicated grain orientations and exhibit weak spontaneous and piezoelectric response which leads to difficulties in yielding the desired properties (Guo *et al.*, 2007). One effective approach to resolving this problem is to fabricate thin films with a preferential crystallographic. In literatures (Gong *et al.*, 2004; Kalpat and Uchino, 2001), most feasible attempts were taken to tailor crystal alignment. Several studies also found that the PZT thin films posing the [111] orientation have better ferroelectric and dielectric properties and the [100] orientation for enhanced piezoelectric response both of which these properties are great than those of the randomly oriented ones (Gong *et al.*, 2004; Ruanghchalermwong *et al.*, 2008; Du *et al.*, 1998).

The main objective of the present study was to develop the PZT-based thin films with high ferroelectric, dielectric and piezoelectric properties. For this

purpose, highly textured PZT films were fabricated and characterized. Although the properties of the PZT material were well acceptable for ABO_3 ferroelectric, they need to dope elements either on B(Ti, Zr)-, A(Pb)-sites or both for improving not only the ferroelectric but also the piezoelectric properties. The Nb doping was always reported an optimal one for the improvement of dielectric constant, remanent polarization and piezoelectric coefficient (Haccart, Rémiens and Cattan, 2003; Remiens *et al.*, 2003; Kwok *et al.*, 2004). Then, the properties of the niobium doped PZT films are of great interest for device fabrication. Because it is well known that the composition near the morphotropic phase boundary (MPB) region has its optimal values in the spontaneous polarization and the reorientation of domains under the maximum of an external electric field (Khaenamkaew *et al.*, 2007), the phase structure and electrical properties of the present Nb-doped PZT films were investigated systematically as a function of Zr/Ti ratios to find out the existence of MPB for high orientation and its location. The relationship between electrical property and composition was also discussed as well with an emphasis placed on the effect of MPB.

3.2 Review of previous works

The work of highly oriented PZT film has received much attention at the beginning of film fabrication each of which [100]- or [111]-orientation is appropriate for different kinds of device operation, i.e. [100] for MEMs (Taylor and Damjanovic, 2000) and [111] for FeRAM (Ruangchalermwong *et al.*, 2008). The orientation control in thin film technology has been carried out both by solution technique and physical vapor deposition as well as MOCVD. In general, for a reliable investigation of the solely orientation-related effects of these films, crystal orientation can be controlled through three ways (Kalpat and Uchino, 2001): (1) control of the growth parameters during the in situ crystallization; (2) control of the parameters during the post deposition annealing; (3) change of buffer layer or use of single crystalline substrate.

For the PZT films deposited on silicon substrate, the growth parameter under the use of buffer layer/single crystalline substrate is the simplest one. Furthermore, platinum deposited on silicon substrate is usually used as a bottom

electrode, because it has reasonably good thermal stability and chemically inert in the oxidizing conditions. However, it was discussed by Aoki *et al.* (1995) that Pt(111) is not the ideal substrate to induce the perovskite nucleation of PZT films due to a low nucleation density and consequently high leakage current. The same authors recognized that a few nanometer-thick Ti play a key role in the nucleation of the perovskite phase. As suggested by Muralt *et al.* (1998), Ti film works as a seed layer for [111] oriented growth of PZT. The same behavior for nanometer thick was confirmed by TiO_2 (Gong *et al.*, 2004) and TiO_x (Millon, Malhaire and Barbier, 2004). In growing the [100] textured PZT films, there were reports of using PbO (Gong *et al.* 2004; Fu *et al.*, 2002) and PbO_x (Wu *et al.*, 2007).

In addition to buffer layer as the metal oxide of which its ingredient elements relate mainly in PZT films, [100]- and [111]-orientations have been reported through Pt(100) and Pt(111), respectively (Kim *et al.*, 2002). The comparison of such a study found that [111]-oriented tetragonal PZT films exhibited highly square polarization hysteresis loops with a slightly better fatigue endurance than the [100]-oriented films but, however, the measured d_{33} values of [100]-oriented films were somewhat higher than those of [111]-oriented films. Another orientation control has been carried out under the use of [110]-oriented $LaNiO_3$ buffered silicon substrate which leads to [110] preferred PZT films with good pyroelectric and well satisfied ferroelectric properties although [110] orientation is often preferred in randomly oriented PZT films (Guo *et al.*, 2007). Regarding PZT, it has been found that it also grows epitaxially with various degree of epitaxy and orientation control of [100], [110] and [111] on a lot of systems including $SrTiO_3$ (Yokoyama *et al.*, 2005), MgO (Wakiya *et al.*, 1999), LASCO (Ramesh *et al.*, 1992), YbCO (Boikov *et al.*, 1992) and Al_2O_3 (Adachi *et al.*, 1991).

Many studies concerned with phase transition and electrical properties of the PZT thin film with controlling composition. With respect to thin films, PZT's properties are greatly different from those of bulk ceramics due to fine grains, extrinsic stress, and substrate effects (Gong *et al.*, 2004). The effect of Zr content on properties of randomly oriented PZT films was reported by Khaenamkaew *et al.* (2007). It was found that among investigated films, the PZT films at Zr/Ti = 52/48 exhibited the highest remanent polarization and excellent dielectric constant of 24

$\mu C/cm^2$ and 1200, respectively. Phenomenological calculation for the composition near MPB found that, for a tetragonal PZT, the effective d_{33} along the perovskite [001] direction was much larger than those along the spontaneous polarization [111] and similar behavior was found for a rhombohedral PZT (Du *et al.*, 1998). However, the distinct peak in d_{33} at the MPB found in bulk PZT ceramics was not observed in [111]-textured thin film PZTs (Kim *et al.*, 2003). Similarly, compositional studies were carried out though [100]- and [111]- textured PZT films but narrow variation of Zr/Ti ratio (Gong *et al.*, 2004). The employment of epitaxial growth of PZT thick films was suggested to compositional study on [100], [110] and [111] oriented films (Yokoyama *et al.*, 2005). Although the effects of the Zr/Ti ratio had on the crystal structure, dielectric and ferroelectric properties, and piezoelectric response with different crystal orientations, the existence of MPB was not confirmed in agreement with each other orientation and polycrystalline bulk ceramics. As reviewed above, some studies show that no distinct phase transition was observed from tetragonal to rhombohedral in the film form when the Zr/Ti ratio was varied across the MPB of the PZT system, indicating the complexity of the PZT films relative to bulk ceramics.

Many aliovalent compositional alternations to PZT have been studied either with higher valence substitutions (donors), either with lower valence ions (acceptors). However, some of the critical properties of PZT were optimized by the addition of donor dopant ions. Pereira, Peixoto and Gomes (2001) found that the solubility limit of Nb in PZT bulk ceramics (perovskite structure) is about 7 mol%. Above this concentration, a secondary pyrochlore phase is formed. The addition of Nb decreases the dielectric constant maximum and the Curie point. In addition, grain size and porosity decrease as the Nb concentration increase and texture becomes more intense with increasing Nb concentration (Durruthy, 1999). Although the niobium modification relates with PZT film in the range of small level 1-4 mol%, the XRD patterns reveal the same resultant diffraction peaks with pure PZT films (Han *et al.*, 2008). This is consistent with another report of similar doping level but the XRD results were found that an annealing temperature for perovskite phase transformation rises to higher crystallized temperature, i.e. from 600 to 700 °C at doping level of 7 mol% (Kurchania and Milne, 2003). This is because the amount of a secondary fluorite phase increases with increasing niobium content (Pintilie *et al.*, 2004). In

addition, crystallographic orientation has been reported independent to niobium level (Haccart, Remiens and Cattan, 2003). The microstructures obtained for the niobium doped PZT films are considerably finer than those obtained with non-doped PZT which indicates that Nb doping affects the morphology of the crystallized grains (Es-Souni *et al.*, 2001). The electrical properties of Nb-modified PZT ceramics have been generally studied in thin film form. Kwok *et al.* (2004) optimize the Nb level for improving the piezoelectric and pyroelectric properties at about 2 mol%. The observed d_{33}, P_r and p values were about 95 pm/V, 30 μC/cm^2 and 350 μC/m^{2}K, respectively. The optimum level of 2 at% Nb concentration was also confirmed by authors (Remiens *et al.*, 2003; Klissurka *et al.*, 1997; Tuttle *et al.*, 1992) for the best electrical properties measured. Nowadays, the publication of Nb-modified PZT films are taken into account for enhanced ferroelectric, pyroelectric and piezoelectric device operations.

Therefore, to obtain the desired better electrical properties, chemical doping is necessary to accompany with orientation control. Besides, the compositional Zr/Ti ratio plays a key role to tailor the electrical properties of PZT films (Khaenamkaew *et al.*, 2007).

3.3 Materials and methods

3.3.1 Preparation of the PNZT solutions

As introduced in chapter 2, lead zirconate titanate solution can be prepared by the most frequent approaches which are grouped into three categories. In this work, the procedure of the preparation of precursor solution was based on chelate or hybrid process proposed by authors (Takahashi et al., 1990; Yi and Sayer, 1991; Schwartz, Assink and Headley, 1992). By the same way, the process of precursor solution was also used for PNZT and PZT solution in chapter 3 and 4, respectively. The sol-gel method was used to prepare the films on the platinized silicon substrates. The precursor solution was obtained from lead acetate trihydrate [$Pb(CH_3COO)_2.3H_2O$, Alfa-Aesar, 99% purity], zirconium *n*-propoxide [$Zr(OCH(CH_3)_2)_4$), Alfa-Aesar, 70% purity], titanium iso-propoxide [$Ti(OCH(CH_3)_2)_4$), Alfa-Aesar, 97% purity] and niobium ethoxide [$Nb(OC_2H_5)_5$,

Alfa-Aesar, 99.999% purity] as raw materials and 2-methoxyethanol (2-ME) ($CH_3OCH_2CH_2OH$, 95% purity) as a solvent. The purity of raw materials and solvents would influence to the properties of the PNZT films. Therefore, chemical materials were kept by consistent purity in this work. The process preparation of the precursor solution was described as follows: lead acetate trihydrate including Pb excess of 8 mol% for PNZT(100) films and 20 mol% for PNZT(111) films was dissolved in the mixing solvent between 20 mL 2-ME and 1mL acetylacetone ($C_5H_8O_2$, 95% purity), and then refluxed for 3 hours at 128 °C. This stage is to remove the water contaminated in the lead acetate powder and to avoid the formation of titanium hydroxide later. Acetylacetone also chelate with lead acetate to stabilize the lead containing organic solution and to prevent the precipitation in the final PNZT solution. Before an addition of titanium, acetylacetone was added to stabilize the titanium iso-propoxide in order to reduce the hydrolysis speed at molar ratio 1:1 and not to be sensitive to moisture when exposed to air (Sun, Tan and Zhu, 2006). Then, titanium iso-propoxide, zirconium *n*-propoxide, and niobium ethoxide were added into anhydrate lead acetate solution at the same time and the PNZT solution was continuously refluxed for 3 hours at the same temperature. Each PNZT solution was doped with Nb at 2 at% according to the formula $Pb(Zr_x,Ti_{1-x})_{0.98}Nb_{0.02}O_3$. The desired compositional solutions were x= 0.2, 0.3, 0.4, 0.52, 0.53, 0.6, 0.7 and 0.8. 1 mL formamide ($HCONH_2$, 99.3% purity) was also added to prevent the films from cracking. The preparation of PNZT solution concerns with refluxing at temperature of about 128° for 3 hours because this condition of temperature used was optimal for the best quality of PNZT film surface without surface defect. In addition, 1 mL acetic acid (CH_3CO_2H, 99.5% purity) was added to stabilize the final solution in order to avoid lead oxide precipitation. The procedure of the preparation was summarized in Fig. 3.1. The precursor solutions were diluted to 0.5 M and aged for 24 hours or more.

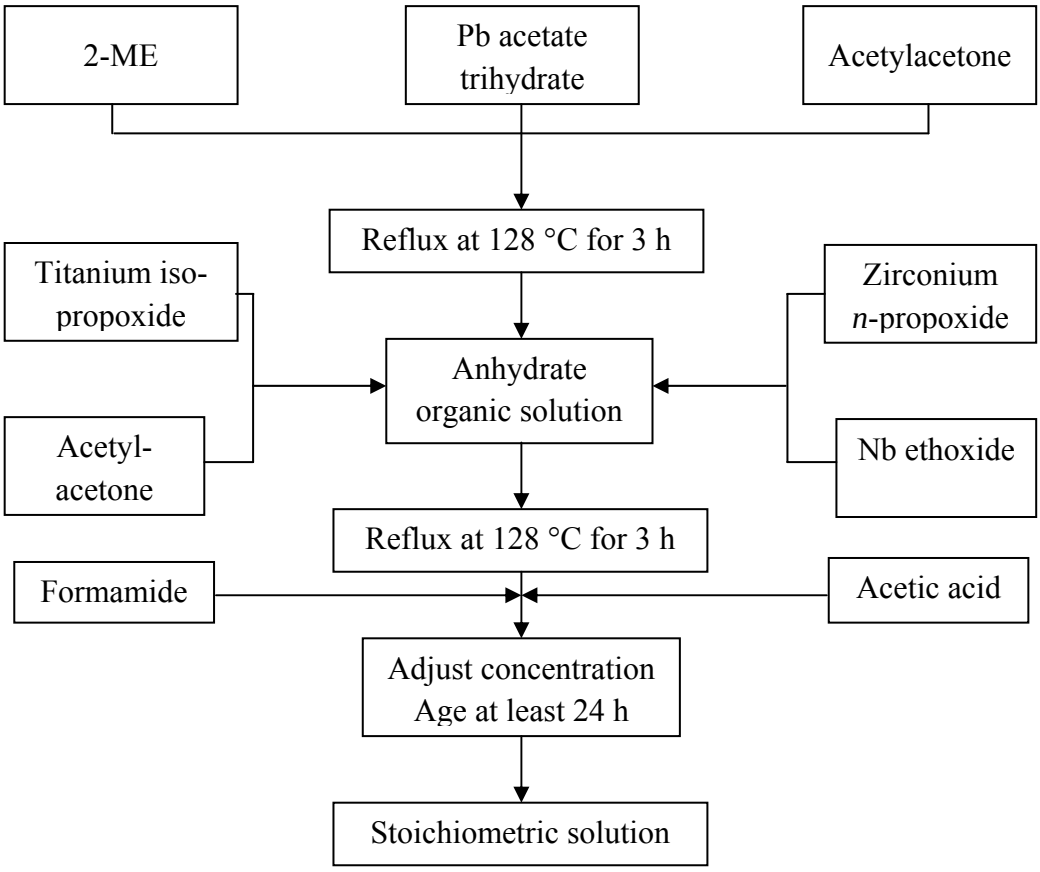

Figure 3.1 Flow chart of the preparation of PNZT solution.

3.3.2 Preparation of metal containing organic solution

In order to control the phase evolution of the top PNZT film, lead and titanium containing organic solutions were the source of metal elements which were oxidized to deposit as the seeding layers. Similar to the PNZT precursor preparation, the seeding solutions were prepared by dissolving lead acetate or titanium iso-propoxide into the mixing solvent of 2-ME, 1 mL acetylacetone and 1 mL acetic acid. The solution was refluxed at 128 °C for 2 hours to stabilize and to avoid a precipitation. The final solution was diluted to a concentration of 0.05 M and aged at least 24 hours.

3.3.3. PNZT thin film deposition

Commercial Pt(111)/TiO_2/SiO_2/Si(100) substrate was composed of different thickness of the pre-deposited films such as Pt layer of 1500 Å, TiO_2

adhesive layer of 200 Å and SiO_2 layer of 3000 Å. The substrate, which was used to deposit PNZT films was about the size of 0.6x0.6 cm^2. Before PNZT film deposition, each substrate was cleaned with absolute ethanol and then dried on hotplate at 200 °C. Heat treatment for the substrate before coating was necessarily done to prevent surface void and to obtain the best PNZT film surface.

As given in Fig. 3.2, the lead containing solution was first deposited onto the platinized silicon substrate as the lead oxide layer which was employed to control the [100]-orientation of PNZT thin films (Gong *et.al.*, 2004) using a common spin coater at spinning rate 4000 rpm for 30 seconds and then annealed for crystallization at 500 °C for 2 minutes. Two layers of lead oxide were also prepared because it was found that the layer thickness was sufficient for the formation of well [100]-textured PNZT thin films.

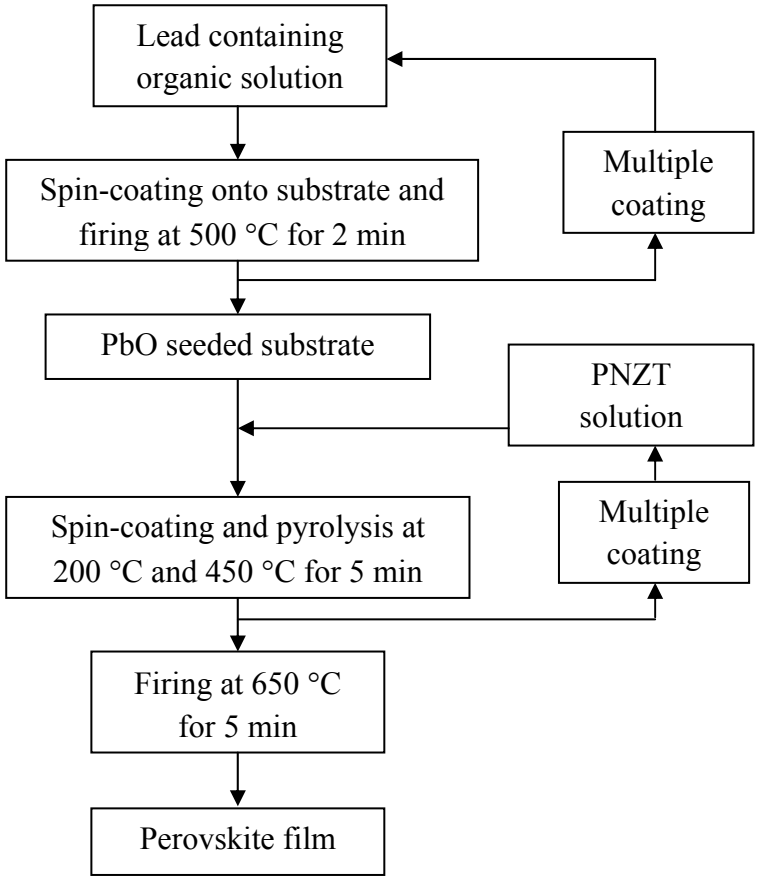

Figure 3.2 Flow chart for the PNZT(100) deposition by sol-gel method.

Subsequently, the PNZT films were deposited onto the lead oxide coated substrate by spin-coating at 4000 rpm for 30 seconds, followed by pyrolysis at 450 °C for 5 minutes for each deposition. The deposition was repeated several times to obtain a desired film thickness. The PNZT films were finally annealed at 650 °C for 5 minutes by rapid thermal processor (RTP) in air. For each PNZT film, the fresh solution of PNZT was employed to control and avoid aging effect.

Similarly, one deposition of TiO_2 served as the seeding layer for the control of [111]-textured PNZT thin films. The seeding precursor solution was derived from the titanium containing organic solution which was then annealed at 600 °C for 2 minutes. One deposition of the TiO_2 thickness was sufficiently employed for the seeding layer in order to avoid the non-ferroelectric TiO_2 layer which would be harmful the electrical properties of the overlaid PNZT films. The PNZT precursor solutions were spin-coated on the TiO_2 seeded substrate under the same heat treatment as the preparation of the PNZT(100) thin films but pyrolysis temperature was set as low as 350 °C.

3.3.4 Thin film characterization

The crystal structure and the texture of the PNZT thin films were analyzed using the high-resolution X-ray diffraction (XRD, Rigaku D/max-RB) with Cu-Kα radiation. Because of the XRD machine set up without Ni filter, each sample was scanned twice: first 2θ ranging from 20° to 39.6° and second from 40.2° to 60° in order to avoid the interference sharp peak of single crystal Pt(111). The XRD patterns were also recorded at a step scanning rate of 2°/min for the crystal structure and texture analysis. The chemical composition of the film was examined using an Auger Electron Spectroscope (AES, ULVAC-PHI, PHI 700 SAN). The Auger spectra were obtained in the derivative mode for the specific energy ranging from 0 to 2400 eV. Argon gas was introduced into the analyzer chamber until the argon and residual gas pressure reached 4×10^{-8} Pa. Sputtering was carried out with a 1.0 kV Ar^+ beam for the spot area of 2×2 mm^2. The surface and cross-sectional fracture morphology of the PZT films were observed using a field-emission scanning electron microscope (FE-SEM, Hitachi S-4800). Furthermore, to investigate the electrical properties, top platinum electrodes, approximately 0.1 μm in thickness and 0.35 mm in diameter,

were sputtered onto the surface of the PNZT films through a shadow mask. A ferroelectric test module (aixACT TF Analyzer 1000, Germany) was employed to evaluate the dielectric and ferroelectric properties. The effective piezoelectric coefficient d_{33} was measured by a scanning probe microscopy system (SPM, Seiko SPI4000 and SPA300HV, Japan).

3.4 Results and discussions

3.4.1 Crystallographic and structural analysis of PbO seeding and PNZT(100) thin films

To confirm the role of the seeding layer, the surface morphology and crystallographic orientation of seeding crystals deposited on the Pt substrate were examined as shown in Figs. 3.3 and 3.4, respectively. The PbO seeding dispersed well uniformly on the surface of the platinized silicon substrate, with the discontinuous crystals and fine crystal size ranging from 50 nm to 130 nm. The XRD result of the seeding layer composed mainly of PbO(001) and PbO(002) compared with PDF card No. 65-2809.

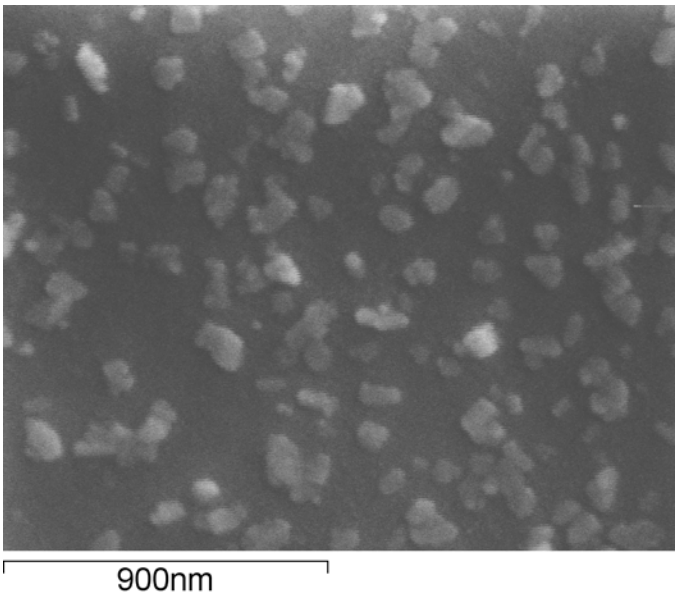

Figure 3.3 SEM surface morphology of the PbO seeding layer.

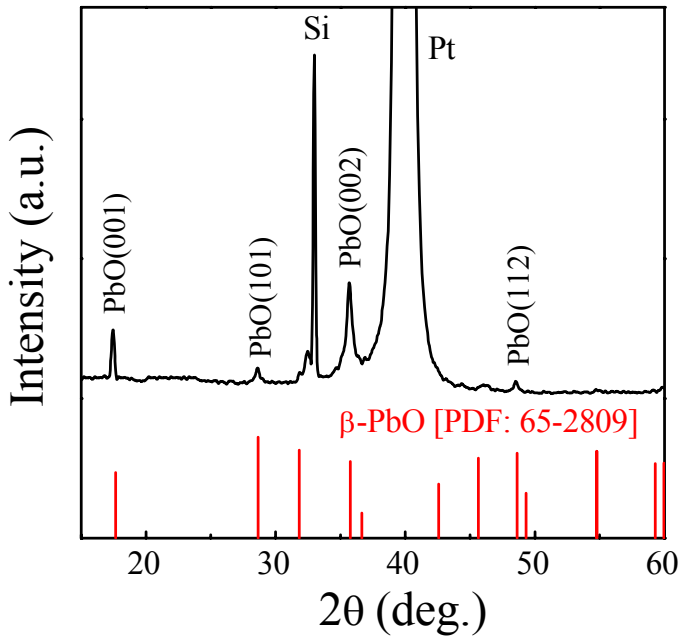

Figure 3.4 XRD pattern of the PbO seeding layer compared with standard PDF card No. 65-2809.

Due to annealing temperature of 500 °C and light yellowish film surface, the PbO(001) seeding layer should be in a form of β-PbO, an orthorhombic phase stable at high temperature (>490 °C) (Veluchamy and Minoura, 1998). As suggested by Gong *et al.* (2004), the formation of [001]-oriented β-PbO crystals provided the nucleation sites and pose good lattice matching to promote [*h*00]-oriented perovskite structure of the overlaid PZT film. The β-PbO(001) crystallizes at annealing temperature of 500 °C but a large number of different polymorphous lead oxide would form with increasing the annealing temperature (Venkataraj *et al.*, 2001). However, the problem of evaporation will be always taken into account for lead-based materials when the lead oxide is heated at crystallization temperature for long time, leading to failure in controlling the overlaid PNZT orientation. Furthermore, the lower annealing temperature contributes to the as-deposited PbO which then interact with the underlying platinum electrode to form a Pb-Pt intermetallic phase, resulting to partly grow the [111]-oriented films, so that the PbO seeding preparation was restricted under the above preparation condition. Therefore, to avoid a surface

degradation and an effect of non-ferroelectric phase, the PbO seeding layers with two layer depositions resulted in a proper thickness in our study.

Figures 3.5 and 3.6 showed the XRD patterns of the PNZT thin films with different Zr/Ti ratios. All the PNZT thin films exhibited the typical XRD patterns of single-perovskite structure without metastable pyrochlore phase. In the entire range of Zr/Ti ratios, all the PNZT films exhibited mainly strong (*h*00) diffraction peaks, which indicated that the crystallites would be textured with *a*-axis out-of-plane orientation.

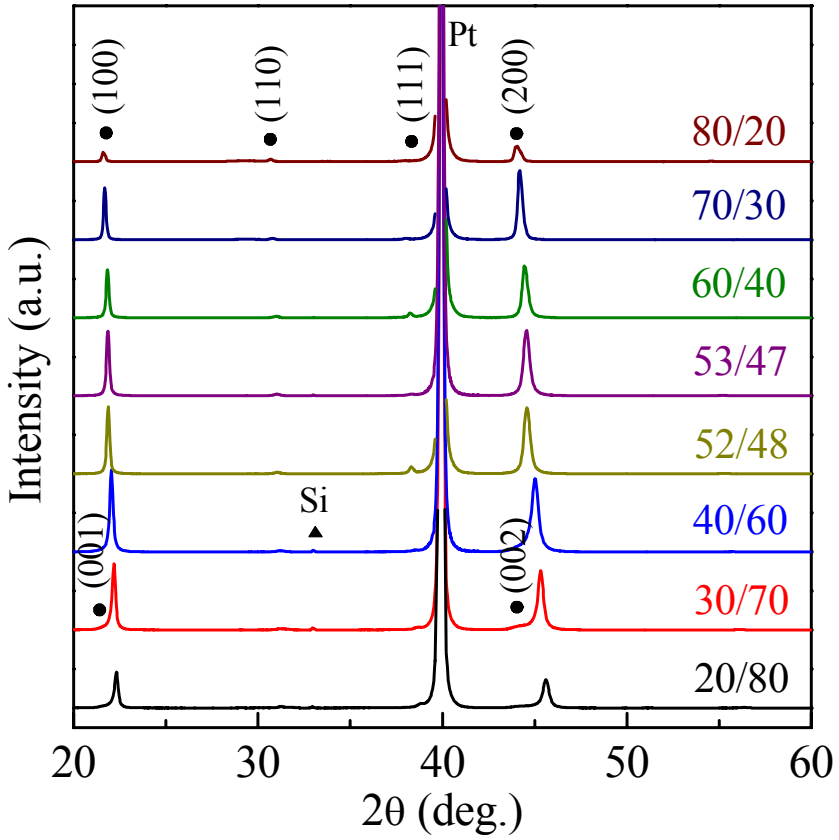

Figure 3.5 XRD patterns of PNZT(100) thin films with different Zr/Ti ratios on PbO seeding layers.

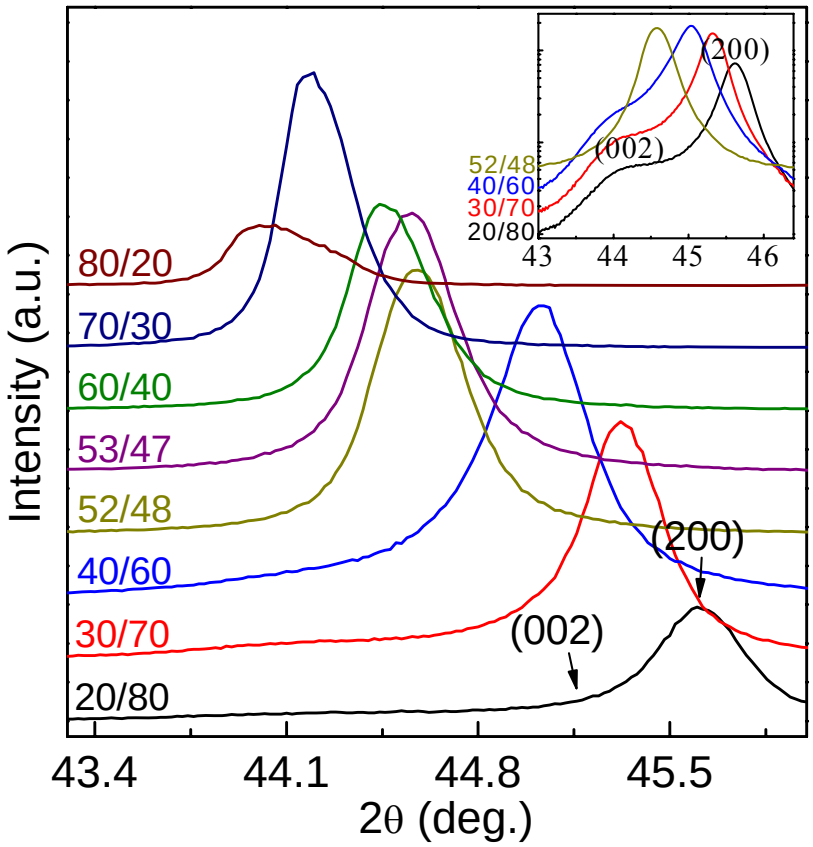

Figure 3.6 XRD patterns of PNZT(100) thin films with different Zr/Ti ratios for step scanning of (002)/(200) peaks. The inset shows the magnification by log scale of (002)/(200) peaks for Ti-rich composition.

Typically, strong (110) peaks with minor (100) and (111) peaks (or random orientation) could be observed in the PZT films on unseeded substrates (Khaenamkaew *et al.*, 2007), but they disappeared in the studied films on the same substrates with the PbO seeding layer. Another experiment showed that the formation of the [100]-oriented PZT films could be obtained from the silicon substrate with the PbO seeding (Gong *et al.*, 2004) and PbO_x (Wu *et al.*, 2007), However, epitaxially grown PZT films would be derived from a single crystal $SrTiO_3$(100) substrate for the selective textures, i.e. [*h*00]-oriented rhombohedral and [00*l*]-oriented tetragonal PZT films (Nagashima, Aratani and Funakubo, 2001).

The preferential orientations were analyzed and quantified through the orientation degree as follows:

$$\alpha_{(hkl)} = \frac{I_{(hkl)}}{\{I_{(100)} + I_{(110)} + I_{(111)}\}} \times 100\%, \tag{3.1}$$

where $I_{(hkl)}$ is the XRD intensity of the corresponding diffraction peaks. In this study, the XRD results of the $\alpha_{(100)}$ values for all the compositions were given in Fig. 3.7 and revealed that all the PNZT thin films behave highly preferred [100]-orientation, whose orientation degree exceeded 88% at most Zr/Ti ratios. For Zr/Ti=80/20, the PNZT film showed a sudden decrease of (100) peak as compared to the others. The reason for this difference is not clear. If *a*-axis oriented PNZT films were closely scrutinized, Zr-rich rhombohedral phase became more stable and probably caused larger lattice-mismatch orientation between [100]-oriented PNZT film and [001]-oriented PbO seeding layer in order to increase a stress. Therefore, when the PbO seeding effect is weakened, the reduction of the $\alpha_{(100)}$ was obtained.

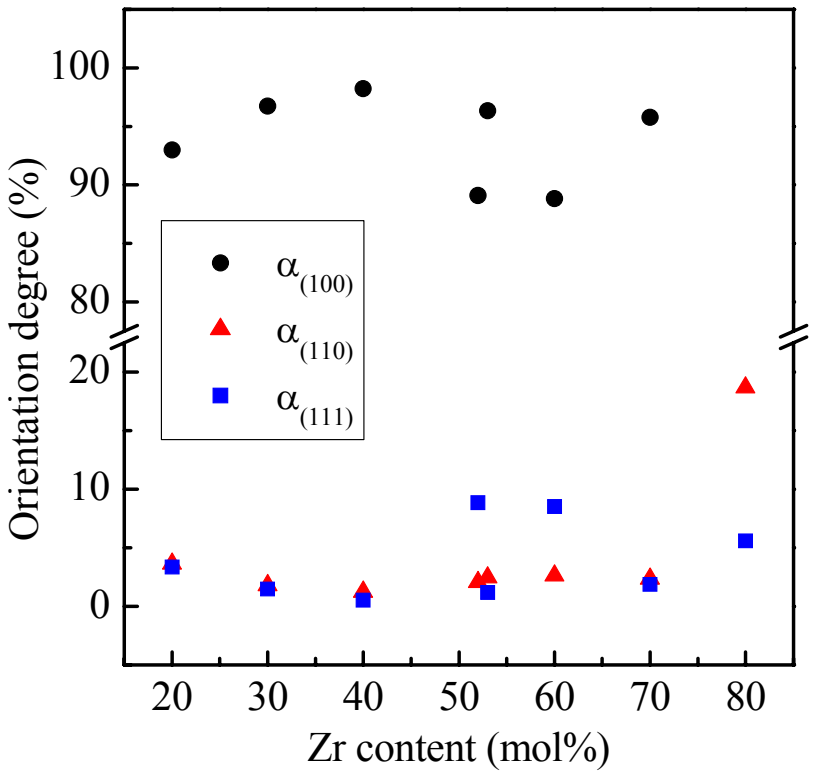

Figure 3.7 Orientation degree summarized for the PbO seeded PNZT thin films.

Using the XRD results from (200) peaks, the *a*-axis lattice parameters as a function of Zr/Ti ratios were calculated and showed in Fig. 3.8. The out-of-plane lattice parameters increased monotonously with increasing Zr content and the (200) peaks shifted to lower 2θ as shown in Fig. 3.6. It is attributed to larger unit cell. Interestingly, the slopes changing at 52-53 mol% Zr of the [100]-oriented PNZT films should be defined as the MPB, suggesting that a phase transition occurred in the present [100]-textured films at the same composition in agreement with that of a bulk PZT materials. The lattice parameters for compositions < 52 mol% Zr were smaller than those extrapolated from compositions > 53 mol% Zr. This indicated that the films with compositions < 52 mol% Zr were of tetragonal phase, which agreed well with the above discussion. The splitting of (002) and (200) in tetragonal composition were scarcely observed in the prepared films owing to their highly [100]-textured structure. The *c*-axis lattice parameters of the films with compositions < 52 mol% Zr corresponding to the in-plane lattice constants were not measured because of the limitation of our XRD equipment. However, in Ti-rich region, small (002) eventually meet (200) at Zr/Ti=52/48 as shown in the inset of Fig. 3.6. It revealed that the in-plane and out-of-plane lattice parameters would meet each other when the phase structure was at the tetragonal-rhombohedral coexisting phase. In PNZT films studied, due to Nb doping and [100]-orientation control, the obtained out-of-plane lattice parameters were in the range of 3.999-4.096 Å. This range was less different from those of random polycrystalline PZT films (3.991-4.115 Å) at the same composition (Khaenamkaew *et al.*, 2007). The stress relaxation would be a possible reason in reducing 2-D tensile thermal stress because of the mismatch of thermal expansion coefficient between the film and the substrate (Zhu *et al.*, 2008).

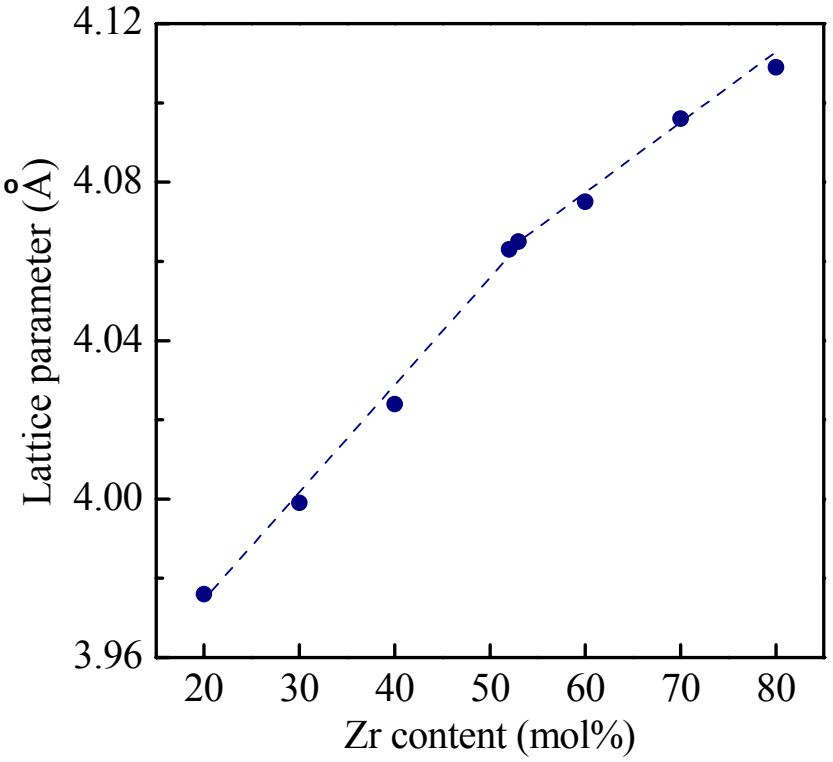

Figure 3.8 Calculated *a*-axis lattice parameters as a function of Zr content for PNZT(100) films.

The typical surface morphology and cross-sectional microstructure of the lead oxide seeded PNZT film (Zr/Ti=52/48) were shown as the FE-SEM images in Figs. 3.9 and 3.10, respectively. The PNZT film was crack-free with a film thickness of 0.4 μm and the well developed columnar grains were observed in Fig. 3.9. The PZT film was doped with Nb exhibited the surface morphology in Fig 3.10. When the lead oxide was introduced as the seeding layer, all the as-deposited PNZT films with varied compositions exhibited the same dense, fine grain and uniform microstructure (not shown). The grain size of PNZT films was in the range of 50-200 nm without observable variation as a function of Zr/Ti ratios. In addition, although the PbO seeding layer was firstly deposited prior to the deposition of the PNZT layer, it was difficult to distinguish interfacial PbO layer between the PNZT film and the substrate by the cross-sectional FE-SEM image. It was evident that the XRD results showed the absence of the PbO seeding layer with no (001)/(002) diffraction peaks due to thin thickness of the films and/or the PbO seeding layer which might dissolve

into the overlaid layer to form the additional PNZT film.

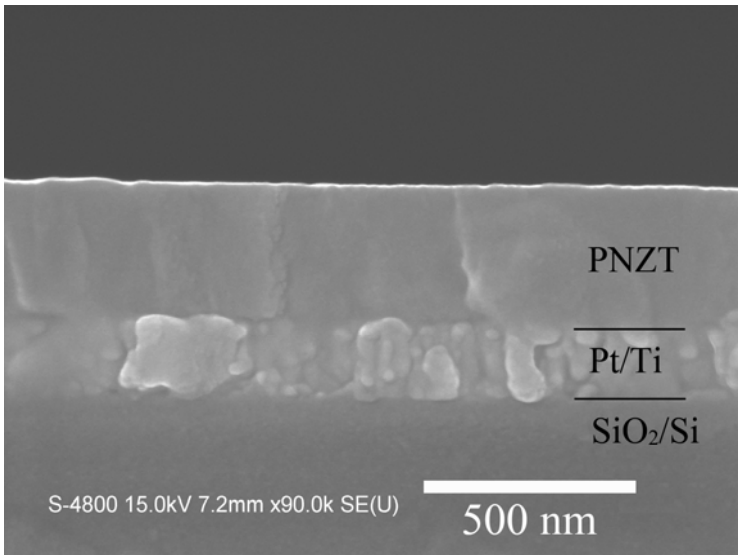

Figure 3.9 FE-SEM cross-sectional image of the PNZT thin film with PbO seeding. The sample contained a Zr/Ti ratio of 52/48.

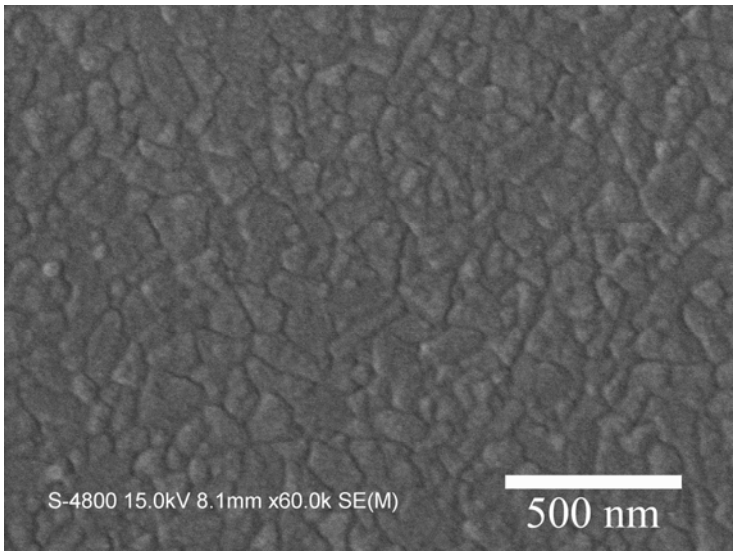

Figure 3.10 FE-SEM planar image of the PNZT thin film with PbO seeding. The sample contained a Zr/Ti ratio of 52/48.

The PNZT films were deposited by the sol-gel method and the Auger Emission Spectroscopy (AES) was used to confirm the stoichiometry of the PNZT films deposited. The compositional depth profiles of the PNZT thin films with two compositions were shown in Figs. 3.11 and 3.12 for Zr/Ti = 52/48 and 70/30, respectively. The compositional distributions exhibited almost constant in the thickness direction, except for the outmost surface layer and the transient layer close to the surface of Pt electrodes. On the surface (indicated as region I), the existing oxygen and lead elements were slightly higher due to a little evaporation of the PbO during the annealing process. In the film interior (region II), no compositional fluctuation was observed even though the film was deposited layer by layer. The elemental contents were almost uniform across the film thickness. The homogeneity of the PNZT films was obtained throughout the film thickness. The calculated values of the Zr content were approximately 0.524 and 0.715 for the nominated Zr/Ti= 52/48 and 70/30, respectively. The desired stoichiometry was under the acceptable control. The signal of the Nb-doping was not clearly shown in the figure because of its small amount which was out of the detectable range. The seeding of PbO crystal was not found evidently at the interface region. The lead element in the seeding layers would diffuse to the bulk region in order to compensate for the lead loss during the annealing process.

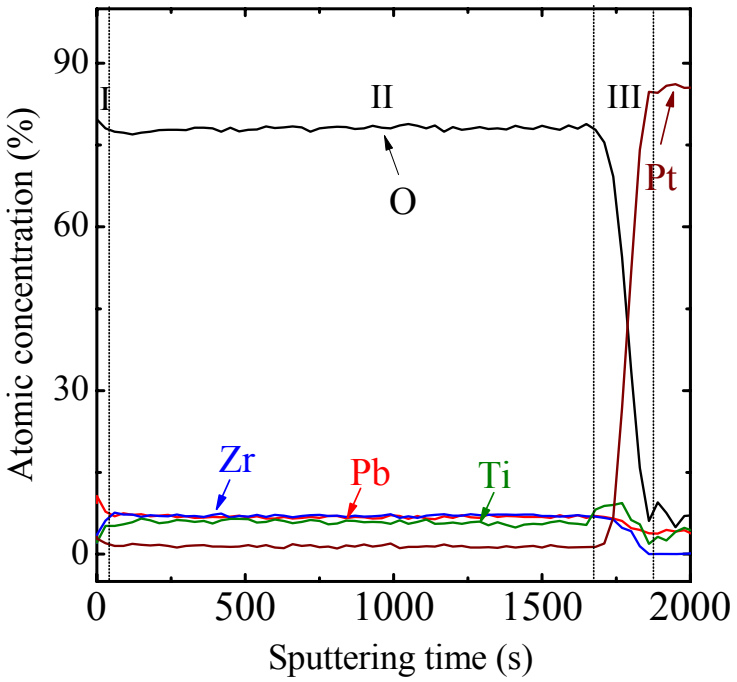

Figure 3.11 Compositional depth profile of PNZT thin films with Zr/Ti= 52/48 on PbO seeding layers; regions I: the surface and II: the interior of the PNZT film, and III: the film-Pt interface.

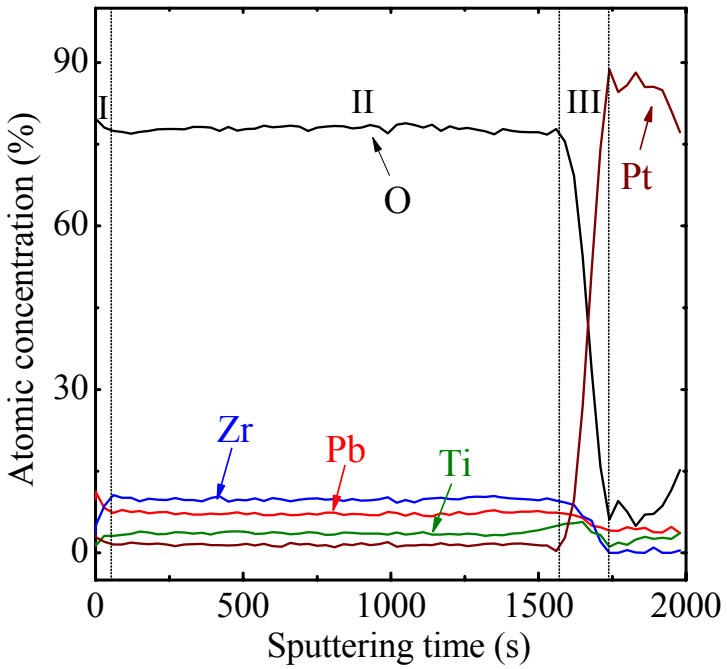

Figure 3.12 Compositional depth profile of PNZT thin films with Zr/Ti= 70/30 on PbO seeding layers; regions I: the surface and II: the interior of the PNZT film, and III: the film-Pt interface.

3.4.2 Crystallographic and structural analysis of TiO_2 seeding and PNZT(111) thin films

Discontinuous and fine grains of the TiO_2 seeding layer exhibited irregular polyhedral morphology in Fig. 3.13. The crystalline texture showed in Fig. 3.14, indicating the seeding layer only composes of [101]-oriented rutile phase as compared with PDF card No. 73-1232.

The TiO_2 diffraction peak in our study did not accord to the (110) peak of the other report (Gong *et al.*, 2004). The TiO_2 was necessarily controlled to give the phase evolution of the overlaid PNZT thin film for desired [111] orientation. The thickness of the seeding layer could be obtained by controlling the concentrate of the seeding solution. The complete of orientation would concern with the seeding-layer thickness. In this study, the titanium solution of 0.05 M was higher concentration than that used by Gong *et al.* (2004) (0.02 M). However, the concentration of 0.02 M was used to produce the PNZT(111) films and the resultant XRD patterns of the PNZT(111) gave the undesired diffraction peak, e.g. (110) and (100) peaks. Therefore, the 0.05 M titanium solution was introduced to all PNZT(111) production.

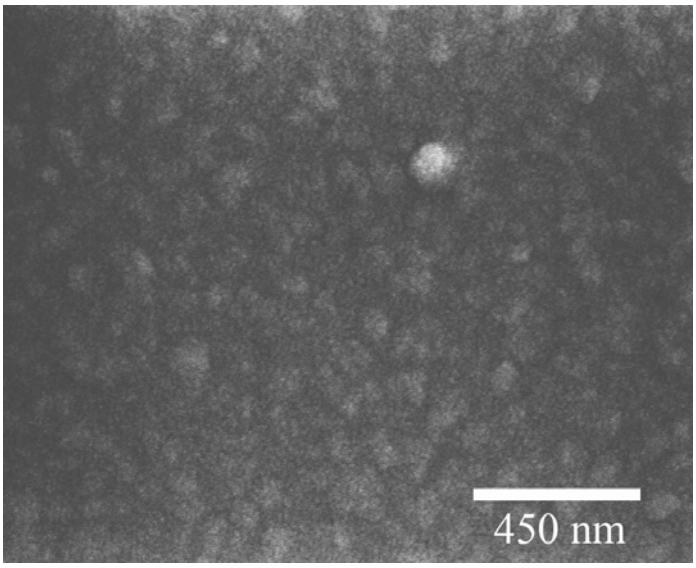

Figure 3.13 SEM surface morphology of the TiO_2 seeding layer.

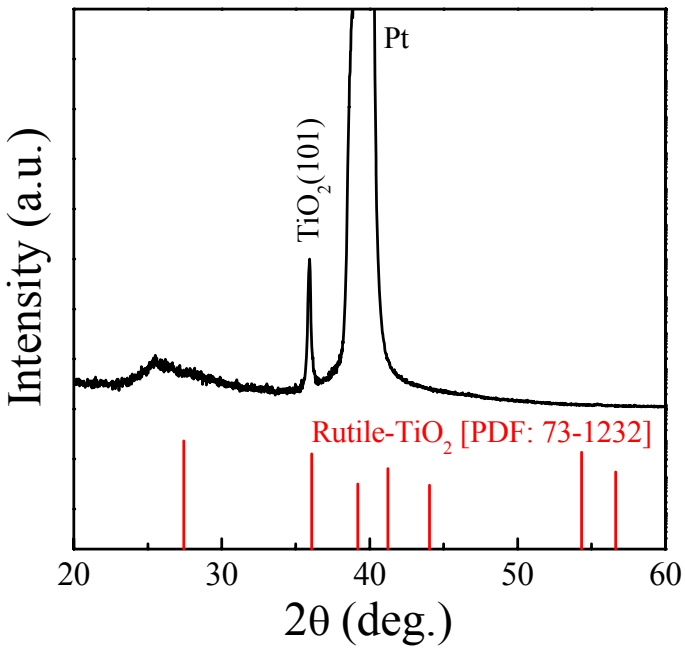

Figure 3.14 XRD pattern of the TiO_2 seeding layer compared with standard PDF card No. 73-1232.

The XRD patterns shown in Fig. 3.15(a) revealed that strong (111) peaks were obtained for the films within the investigated compositional range. All of the films showed a single perovskite phase without the undesired pyrochlore phase. Figure 3.15(b) showed the step scanning of XRD patterns and the (111) peak shifted toward the lower 2θ angel in accordance with the composition which indicated that the unit cell became larger. The peak shifts changed rapidly for Zr/Ti ratio lower than 52/48 but slowly when the Zr/Ti ratio exceeded 52/48. The trace of decreased lattice parameter *c* could not be observed while Zr/Ti ratios were in the range of the tetragonal compositions. It seemed to derive the MPB around 52/48 for the PNZT films. However, it still need to be confirmed by the following results of property characterization.

In several reports (Kim, Kim and Kim, 2006; Gong *et al.*, 2004), the TiO_2 layer coated on the Pt(111)/Ti/SiO_2/Si substrates was employed to conduct the [111]-textured growth of PZT films. The seeding layer of titanium dioxide would play an important role on the phase evolution. Muralt *et al.* (1998) suggested that TiO_2-seeded thin layer with 1-5 nm in thickness was the most effective and posed pure

rutile phase with preferred [110] orientation at a crystallized temperature of 600 °C. This seed layer could induce the growth of PNZT(111) due to a reduction of the activation energy. Owing to a low concentration of 2 at% of Nb, the pure perovskite phase was mainly influenced by the aid of the inserting seed layer even in the case of the PbO seeding. Minor peaks of (100) and (110) were detected, particularly in the films with Zr-rich compositions, but their strengths were quite low.

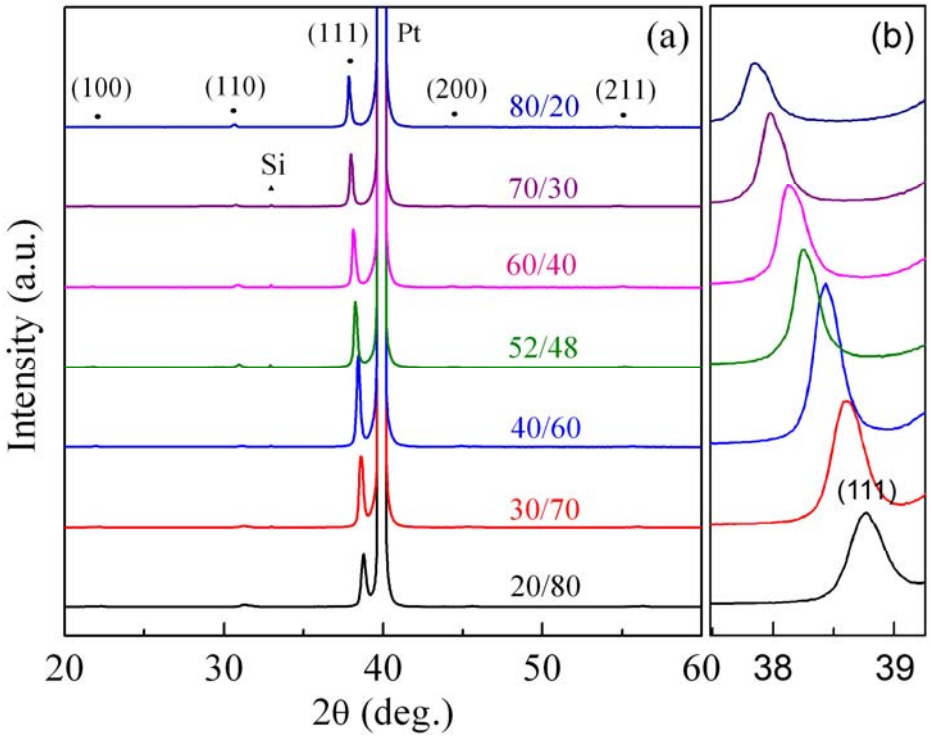

Figure 3.15 XRD patterns of PNZT(111) thin films with different Zr/Ti ratios on TiO_2 seeding layers; (a) overall patterns and (b) step scanning.

As shown in Fig. 3.16, the [111] orientation degree extracted by Eq. 3.1 revealed the remarkable information of the phase evolution. Almost all of the PNZT thin films posed the orientation degree more than 90%, indicating that the PNZT thin films deposited were highly [111] oriented. However, for the Zr/Ti ratio at 80/20 and 20/80, the orientation degrees were slightly low as compared with those of other compositions. No precise elucidation explains this evidence but it is reasonable to consider that the role of TiO_2 seeding layer was probably weak due to the increase of stress, resulting from lattice mismatch between PNZT thin film and the TiO_2

seeding layer. As stated in the experimental procedure, other appropriate fabrication parameters, including the pyrolysis temperature at 350 °C and much lead excess at 20 mol% would be very crucial to support the nucleation control of the [111]-oriented films.

Generally, competition among parameters of the PNZT film fabrication determined the texture of the PNZT films. High pyrolysis temperature was not suitable to control the [111]-oriented PNZT films due to the existing PbO which prefered PNZT(100) growth (Gong *et al.*, 2004). Much lead excess easily contributed to the Pb-Pt intermetallic phase in order to partly enhance [111]-oriented film.

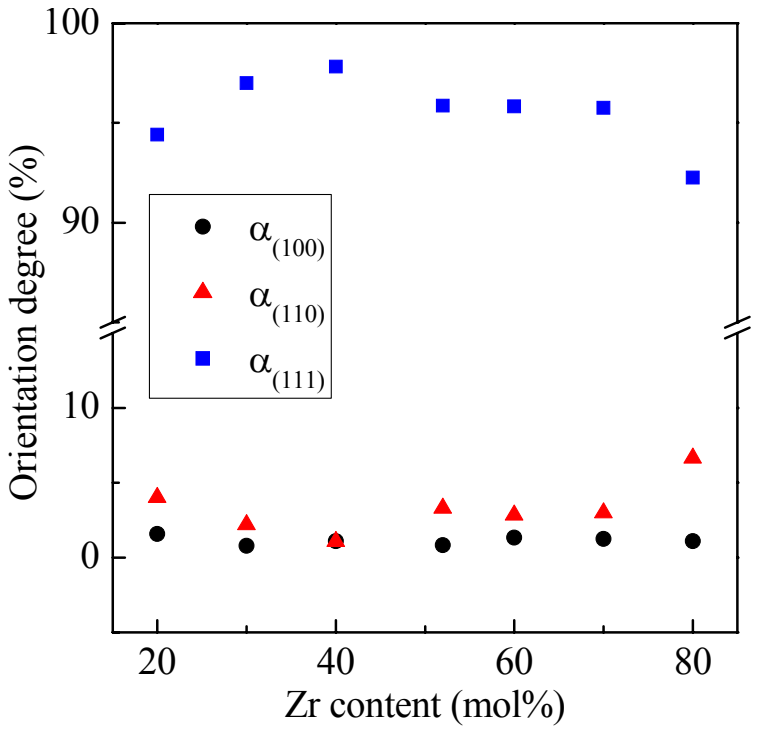

Figure 3.16 Orientation degree summarized for the TiO_2 seeded PNZT thin films.

Representative FE-SEM images of the [111]-oriented PNZT thin film at Zr/Ti = 52/48 were shown in Figs. 3.17 and 3.18. These images showed the PNZT thin film with dense, crack free and a uniform structure. The overall thickness of the film was 450 nm, suggesting that each deposited layer was approximately 90 nm thick.

It was reported that the niobium doping influenced the size of grains in the PZT materials. Nb dopants could suppress grain growth because of an

accumulation of doping ions near grain boundaries, reducing the lattice diffusion of vacancies from pores to grain boundaries (Pereira, Peixoto and Gomes, 2001) and the average grain size was obtained as small as 50 nm. In the other work, Nb doping could result in the grain growth but still in argument (Haccart, Rémiens and Cattan, 2003; Souza *et al.*, 2004). Under the same doping of Nb, the grain size of PNZT(111) was much smaller than that of PNZT(100). The other results have been reported in such comparison for PZT film but were highly similar in all cases (Kim *et al.*, 2002). Although the platinum electrode was seeded by the TiO_2 seeding layer, no segregated or interfacial layer was observed between the substrate and the PNZT film in the cross-sectional Fe-SEM image. TiO_2 seeding crystals might not remain as an individual phase because it was dissolved into the overlaid PNZT films during the annealing process. Thus, the XRD patterns of the PNZT films showed no TiO_2 reflective peaks.

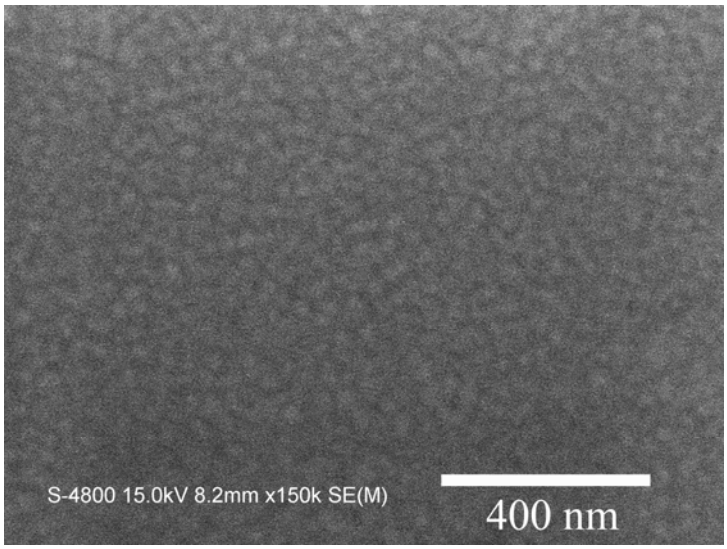

Figure 3.17 FE-SEM planar image of the PNZT thin film with TiO_2 seeding. The sample contained a Zr/Ti ratio of 52/48.

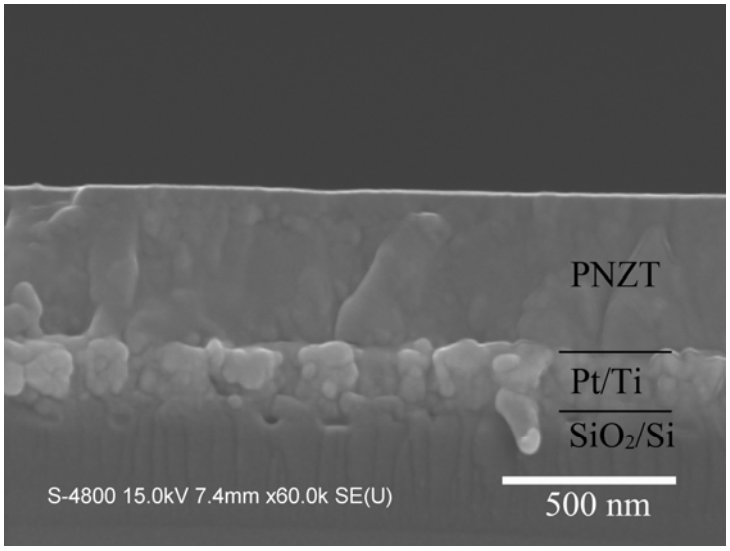

Figure 3.18 FE-SEM cross-sectional image of the PNZT thin film with TiO_2 seeding. The sample contained a Zr/Ti ratio of 52/48.

3.4.3 Electrical properties of PNZT(100) thin films

P-E hysteresis loops were measured using a triangular signal at a frequency of 100 Hz to determine the compositional dependence of the ferroelectric properties for the [100]-oriented PNZT thin films. As shown in Figs. 3.19 and 3.20, all of the films exhibit the typical *P-E* hysteresis loops. There *P-E* hysteresis loop was slightly asymmetries on both polarization and electric field axes.

The asymmetry along the polarization axis would attribute to the presence of trapped space charge at an electrode-ferroelectric interface. The electric field asymmetry was the contribution of an internal electric field, which was mainly related to work function difference of top and bottom platinum electrodes under different heat treatments (Stancu *et al.*, 2007).

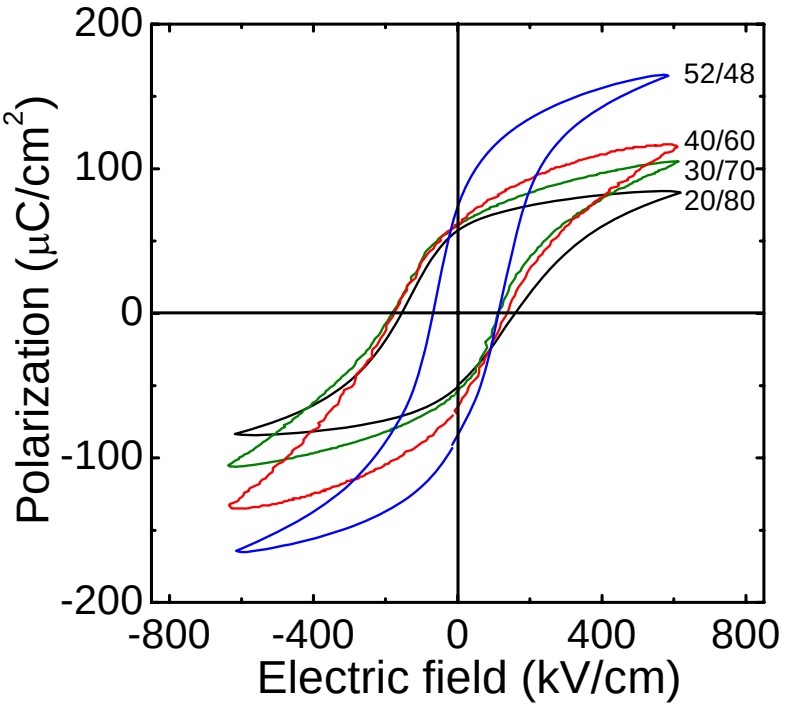

Figure 3.19 *P–E* hysteresis loops of PNZT thin films with different Zr/Ti ratios on PbO seeding layers for Zr/Ti= 20/80, 30/70, 40/60 and 52/48.

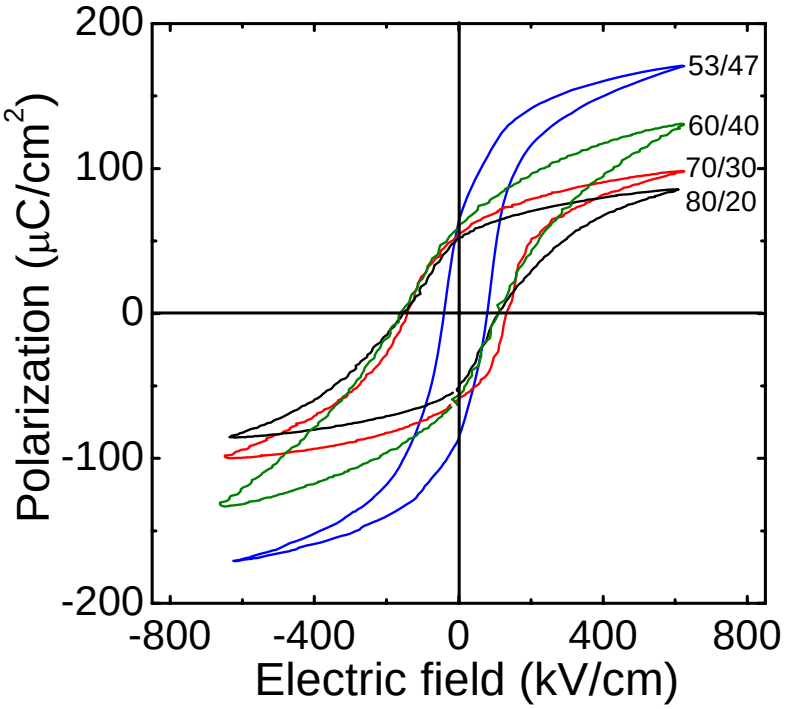

Figure 3.20 *P–E* hysteresis loops of PNZT thin films with different Zr/Ti ratios on PbO seeding layers for Zr/Ti = 53/47, 60/40, 70/30 and 80/20.

As shown in Fig. 3.21, the Zr- or Ti-rich compositions showed lower remanent polarization (P_r) and higher coercive field (E_c). The trend was consistent with randomly oriented PZT films with various Zr/Ti ratios (Khaenamkaew *et al.*, 2007). These values both in Ti- and Zr-rich composition were not significantly different in magnitude. If compared with the same [100]-textured PZT films without Nb-doping, all PNZT films posed higher P_r values ranging from 50 to 75 μC/cm^2. In other work (Zhu *et al.*, 2008), the same [100]-textured PZT films $Pb(Zr_{0.3}Ti_{0.7})O_3$ with and without 2 at% Nb doping were prepared by the same process used in this study, and it was found that the P_r value increased from 44 to 62 μC/cm^2 for the films with the same thickness (0.4 μm) to the PNZT films. Therefore, it was thought that the Nb doping contributed to the enhanced polarization values were in the PNZT films. The maximal P_r value of 75 μC/cm^2 with the minimal E_c value of 82 kV/cm was obtained at the Zr/Ti ratio of 52/48, corresponding to the MPB composition in the bulk PZT system. Usually, dielectric permittivity showed a peak around the MPB composition, but it was difficult to understand why the present PNZT films with a MPB composition showed a peak P_r, which was significantly higher than those for other compositions. This was due to that the PNZT films were *a*-axis-textured, but not 100% *a*-axis-oriented, as shown by the XRD patterns in Fig. 3.6, which showed a broad shoulder of (200) peak in each tetragonal film. For the Ti-rich compositions with tetragonal structure, it was reasonable to presume that the films contain more *a*-domains, whose polar axis was parallel to the film plane. Because the spontaneous polarization direction of the tetragonal PZT was the *c*-axis, the *P*-*E* hysteresis loops should contain predominant extrinsic contribution from non-180° domain switching. For the Zr-rich compositions with rhombohedral structure, whose spontaneous direction is <111>. It was more difficult to analyze the intrinsic and extrinsic contributions to the *P*-*E* hysteresis loops. Nevertheless, it was reasonable to consider that extrinsic contributions from domain rotation were dominant for the *P*-*E* hysteresis behavior of the present [100]-textured polycrystalline PZT films. Due to the reduced coercive field benefiting from the coexistence of two phases, a peak P_r value was obtained at the MPB composition.

Many studies have been conducted to investigate the ferroelectric properties of PZT epitaxial films. For example, Morioka *et al.* (2004) obtained a

larger P_r value of 97 μC/cm^2 in the 100% *c*-axis-oriented epitaxial tetragonal $Pb(Zr_{0.35}Ti_{0.65})O_3$ thin films (about 50 nm thick) on the (100)$SrRuO_3$/(100)$SrTiO_3$ substrates, which is due to the intrinsic contributions of the *c*-axis-oriented domains to the polarization. Vrejoiu *et al.* (2006) reported a perfect square-shaped *P*-*E* hysteresis curve with a further large P_r value of 105 μC/cm^2 for the defect-free epitaxial tetragonal $Pb(Zr_{0.2}Ti_{0.8})O_3$ thin films (90 nm thick). Even compared with these data reported for *c*-axis-oriented epitaxial PZT films, the ferroelectric properties of the present Nb-doped textured polycrystalline PZT films were fairly good. It was expected that further larger polarization could be obtained in Nb-doped PZT films with *c*-axis-orientation. However, as discussed later, the [100]-textured Nb-doped PZT films would show good piezoelectric response due to the domain switching effects.

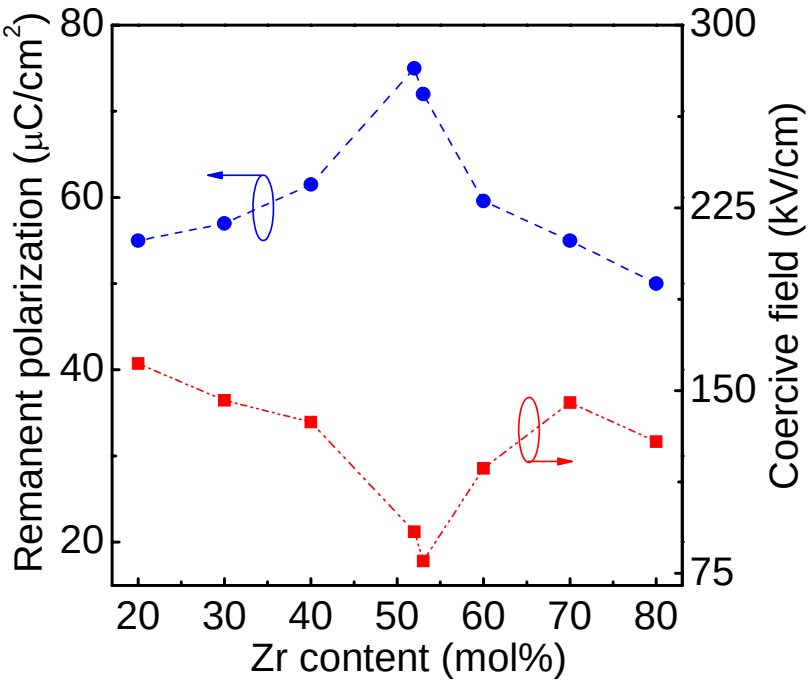

Figure 3.21 Remanent polarization and coercive field of PNZT(100) thin films as a function of Zr content.

Figure 3.22 showed the longitudinal piezoelectric coefficients (d_{33}) of the [100]-oriented PNZT thin films as a function of Zr/Ti ratios. The inset was the typical *Z*-*V* curve of the PNZT film at Zr/Ti=52/48. A strong compositional

dependence of the piezoresponse was also observed in agreement with *P*–*E* behavior at MPB composition. A resulting d_{33} value of 161 pm/V yielded to a distinct peak fallen at Zr/Ti=52/48, which should be verified the MPB, corresponding to XRD results and P_r values.

The maximum d_{33} value obtained in the present PNZT films was almost double as much as that of the [100]-textured PZT film without Nb doping and slightly lower than that of epitaxial PZT films (170 pm/V) deposited on $SrTiO_3$ substrate (Zhu *et al.*, 2007). Undoubtedly, the maximum d_{33} value of oriented PNZT films was much larger than those of randomly oriented PZT films even measured in polling condition as summarized in Table 3.1. Piezoelectric in ferroelectric materials is affected by displacement of domain walls and can be classified into two classes on the basis of their origin: one is intrinsic contributions originated from the piezoelectric and dielectric response of single domains; another is extrinsic contributions arisen from domain wall motion (Kim *et al.*, 2003). In addition, it is well known that the longitudinal d_{33} in thin films is affected by clamping of the film by the substrate. Note that the d_{33} values obtained in our present rhombohedral PNZT films with compositions close to the MPB were higher than those in tetragonal films. It is more difficult to analyze the present films which were *a*-axis-textured, but not 100% *a*-axis oriented. Indeed, previous theoretical analysis suggests that, for epitaxial tetragonal PZT, d_{33} has the maximum value in the spontaneous polarization direction [001] (Du *et al.*, 1998); however, for epitaxial rhombohedral PZT, the smaller d_{33} has its maximum value in a direction of 59.4° away from the polarization direction [111]. Due to excellent d_{33} values measured, the present Nb-doped and [*h*00]-oriented PZT films on silicon substrates would be suitable for applications in many miniaturized components and devices produced by the current microfabrication technology.

Table 3.1 The piezoelectric coefficient of oriented PNZT(100) films compared with randomly oriented PZT films without Nb doping.

Zr/Ti ratios	d_{33} (pm.V^{-1})						
	20/80	30/70	40/60	52/48	60/40	70/30	80/20
PNZT(100) films	42	70	80	161	90	52	60
Randomly oriented PZT films (Khaenamkaew *et al.*, 2007)	-	-	44.3	117.5	41	-	-

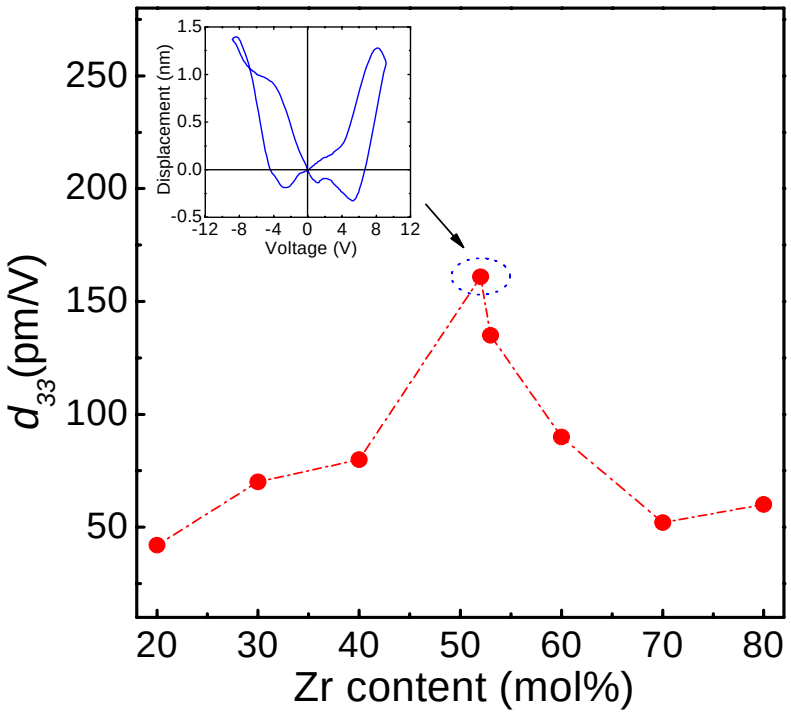

Figure 3.22 Piezoelectric coefficient of PNZT(100) thin films as a function of Zr content. The inset is a typical *Z-V* curve of PNZT film with Zr/Ti = 52/48.

3.4.4 Electrical properties of PNZT(111) thin films

The typical capacitance-voltage (*CV*) property and loss factor were characterized under 10 V signal amplitude at 100 Hz. Figure 3.23 exhibited the typical butterfly shape of *CV* and loss factor curves for the PNZT films with different Zr/Ti ratios. The calculated relative dielectric constants (ε_r) and loss factors ($tan\ \delta$) of

the prepared [111]-textured PNZT thin films were varied as a function of Zr content as shown in Fig. 3.24. The results showed a compositional dependence both for ε_r and *tan* δ.

The non-linear phenomenon of *CV* curves in Fig. 3.23 derived from the result of reversal polarization or switching behavior when the ferroelectric film was in polar state. The maximum near the coercive field attributed to the large number of coexisting domain wall. There was slight asymmetry on voltage axis that was the contribution from an internal electric field due to the difference of work function of the top and bottom platinum electrodes caused by different heat treatments (Stancu *et al.*, 2007).

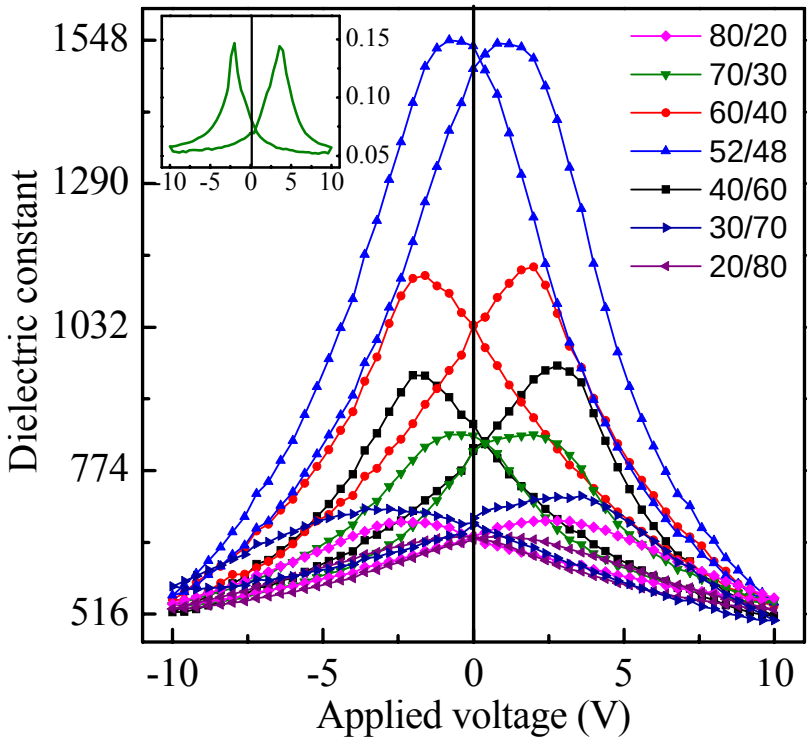

Figure 3.23 Dielectric constant-voltage curve of PNZT(111) thin films with different Zr/Ti ratios. The inset shows loss factor at Zr/Ti = 52/48.

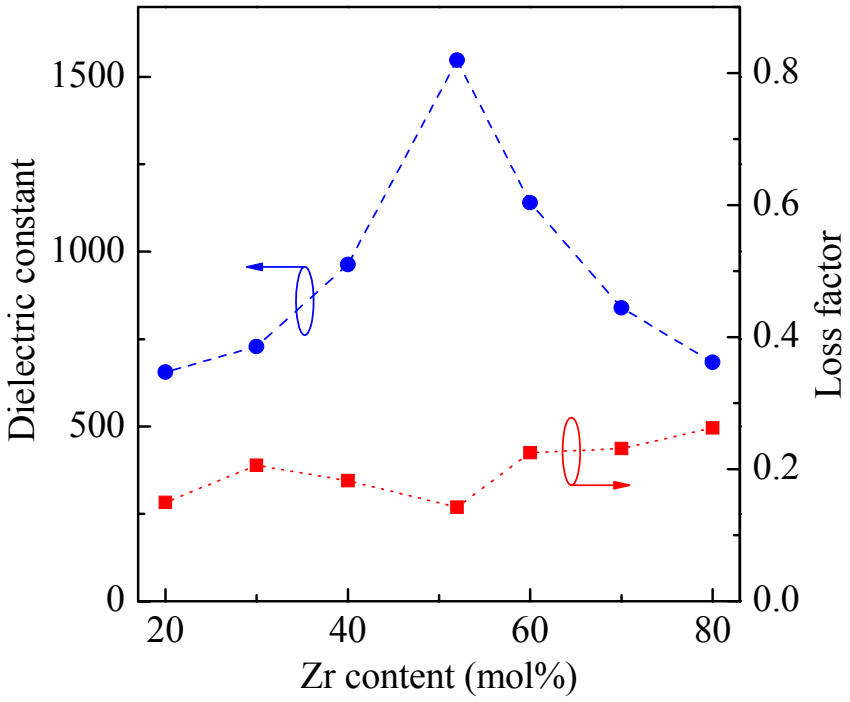

Figure 3.24 Dielectric constant of PNZT(111) films as a function of Zr content.

For the result in 3.24, the maximum relative dielectric constant (ε_r=1550) and loss factor ($tan\ \delta$ = 0.14) at the Zr/Ti ratio of 52/48 was obtained for PNZT(111) films. These values were consistent with the MPB in bulk materials (Yamamoto, 1996) and [100] oriented PNZT films. For PZT ferroelectric films, the contribution of the permittivity could be divided into two categories: intrinsic component and extrinsic component (Xu *et al.*, 2001). Particularly, the intrinsic permittivity exhibited a weak relationship with the Zr/Ti ratio (Kim *et al.*, 2003). With respect to the extrinsic contribution, the enhanced dielectric properties in the MPB region may be attributed to the reversible domain wall motion, which also enhances the loss factor in ferroelectric films (Xu *et al.*, 2001). Furthermore, large lattice distortion of the perovskite structure at the MPB region and the domain wall density would result in increase for relaxing the stress and decreasing the strain energy. The maximum value for the PNZT film was observed near the MPB composition. The maximum ε_r obtained in the present [111]-textured films was much larger as compared to the [111]-textured PZT film without Nb doping (Gong *et al.*, 2004) and non-doped randomly oriented films (Khaenamkaew *et al.*, 2007). It is due to that the

soft donor B-site Nb^{5+} substituting Ti^{4+} and Zr^{4+} would enhance the electrical properties in PZT films including ferroelectric, dielectric and piezoelectric properties. In general, oxygen vacancies from oxygen losses as a result of PbO evaporation during the final annealing are majority defects reducing the domain wall motion. The addition of Nb-dopant was required to lower the concentration of oxygen vacancies (Haccart, Remiens and Cattan, 2003). The values of dielectric constant of our PNZT film compared with the other conditions are summarized in Table 3.2.

Table 3.2 The dielectric constant of oriented PNZT(111) films compared with highly and randomly oriented PZT films without Nb doping.

	ε_r						
Zr/Ti ratios	20/80	30/70	40/60	52/48	60/40	70/30	80/20
PNZT(111) films	656	728	963	1548	1140	840	684
PZT(111) films (Gong *et al.*, 2004)	-	-	900	1130	1040	-	-
PZT(100) films (Gong *et al.*, 2004)	-	-	790	1030	970	-	-
Randomly oriented PZT films (Khaenamkaew *et al.*, 2007)	-	458	929	1194	1119	384	-

Well saturated *P-E* hysteresis loops for the PNZT thin films were presented in Figs. 3.25 and 3.26. For the Zr/Ti ratio of 52/48, the highest remanent (P_r) was obtained at 80 $\mu C/cm^2$ and the corresponding coercive field (E_c) was 70 kV/cm.

The P_r values measured in this study, was much larger than those reported in our previous work for the highly [111]-oriented PZT films and the same compositions. But the lower value was obtained as compared to that of in epitaxial PZT films on single crystal substrates (Zhu *et al.*, 2007). Such high P_r might be concerned with a preparation technique for the precursor solution. In some chemical routes, pyrochlore phase can be reduced or waived out through an addition of stabilizer, e.g. acetic acid and acetyl acetone (Weng, Bao and Sagoe-Crentsil, 2002;

Fe *et al.*, 2001), The present results revealed that the Nb-modified and [111]-oriented PZT films on the platinized substrates would be suitable for ferroelectric device fabrication.

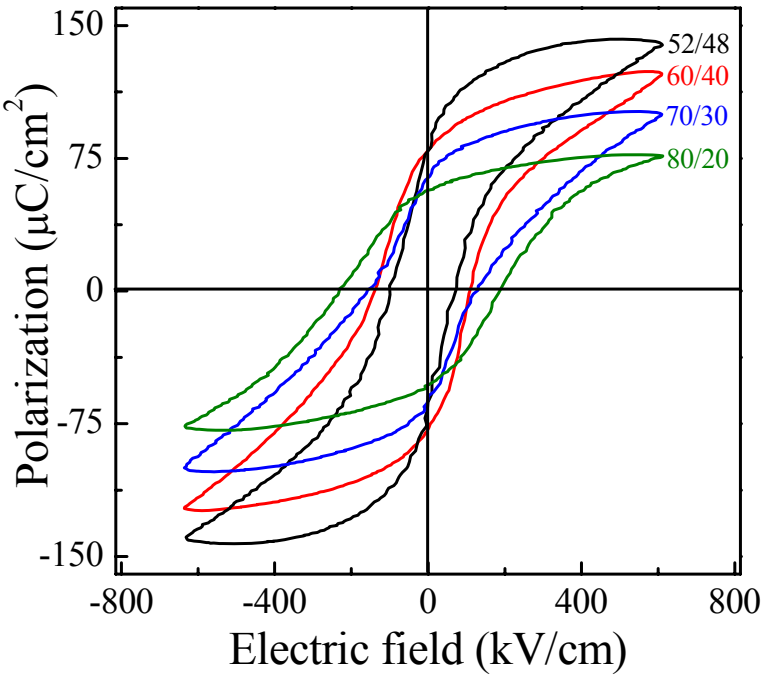

Figure 3.25 *P-E* hysteresis loops for PNZT(111) thin films with Zr-rich composition.

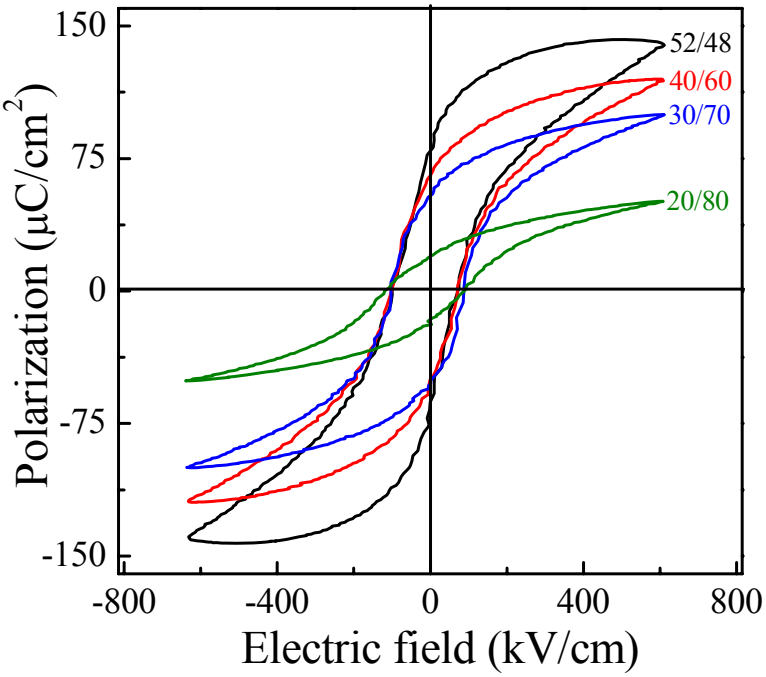

Figure 3.26 *P-E* hysteresis loops for PNZT(111) thin films with Ti-rich composition.

Figure 3.27 showed the compositional dependence of polarization and coercive field. Both values of remanent and saturation polarization were consistent with their compositions. When the Zr/Ti ratios were far from the MPB region, the film properties showed the increasing P_r values and the decreasing E_c values.

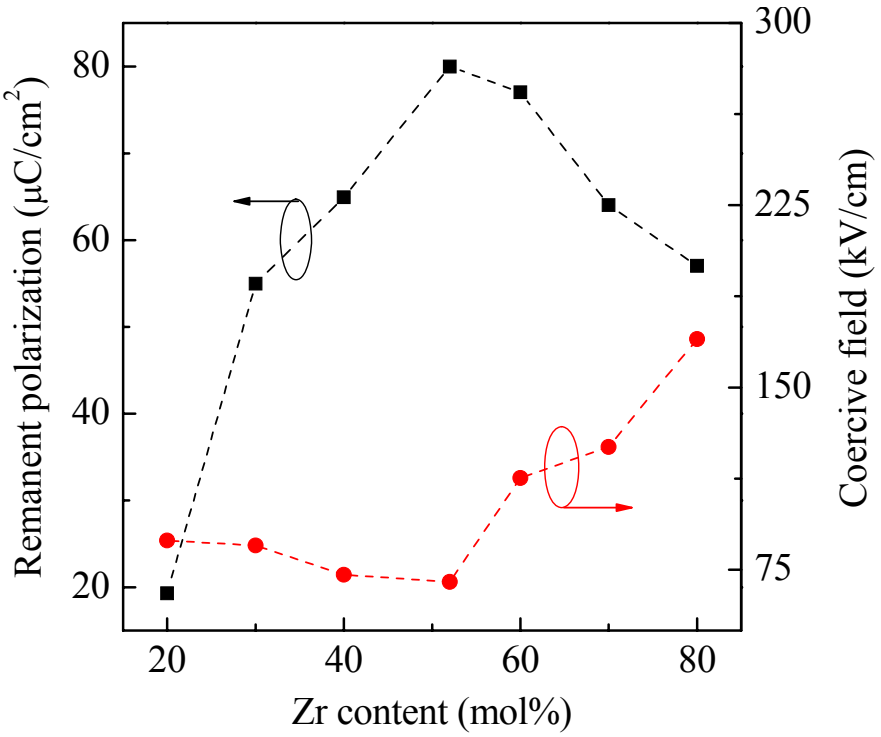

Figure 3.27 Remanent polarization and coercive field as a function of Zr content for PNZT(111) thin films.

This similar trend was obtained from electrical properties of the randomly oriented PZT films with various Zr/Ti ratios (Khaenamkaew *et al.*, 2007) and the PNZT(100) films. The polarization in Zr-rich region composition was greater than that in Ti-rich region. This could be explained that the domain structure of [111]-oriented films resulted in different mobility of the domain walls. Some of polar axis in rhombohedral structure would lie normal to the film surface. For the tetragonal structure, all the polar axis would tilt away with an applied electric field. Consequently, the domain alignment under the applied field would effort to reorient polarization in case of rhombohedral phase. The P_r value of [111]-oriented films was larger than that of [100]-oriented ones for rhombohedral composition. This is due to

that the rhombohedral structure would lie polarization directions along [111] direction in [111]-oriented unit cell as reviewed previously in chapter 2. However, the lower P_r value would result in the composition of the Ti-rich region. This behavior could be attributed to the coexisting of minority (001)- together with majority (100)-peak in tetragonal PNZT(100) films and the polarization vector in the [100]-oriented tetragonal unit cell reorients along [001] direction (in-plane direction). Values of remanent polarization of highly oriented PNZT films and randomly oriented PZT films are summarized in Table 3.3.

Table 3.3 The remanent polarization of oriented PNZT films compared with randomly oriented PZT films without Nb doping.

	P_r ($\mu C.cm^{-2}$)						
Zr/Ti ratios	20/80	30/70	40/60	52/48	60/40	70/30	80/20
PNZT(100) films	55	57	61	75	59	55	50
PNZT(111) films	19	55	65	80	77	64	57
Randomly oriented PZT films (Khaenamkaew *et al.*, 2007)	-	14.7	19.2	23.7	20.1	7.6	-

3.4.5 Role of niobium modification on electrical properties

One experimental work showed that, when PZT solid solution was annealed at crystallized temperature, lead oxide evaporation seems to occur with lead and oxygen vacancies according to the following formula (Zhang *et al.*, 2006):

$$\text{null} \rightarrow V_{Pb}^{''} + V_{O}^{oo}, \tag{3.2}$$

where null: a position Pb-O bonding in porovskite structure, $V_{Pb}^{''}$: lead-atom vacancy and V_{O}^{oo}: oxygen-atom vacancy. Consequently, the pinning effects on domain wall by planes of the oxygen vacancies which can form complex dipolar defects (Haccart, Remiens and Cattan, 2003; Zhang *et al.*, 2008) leads to reduction in the domain wall mobility. Generally, Nb^{5+} ion is considered as donor doping to replace B-site atoms.

The introduction of Nb^{5+} is also compatible with the ionic radii of B-sites for perovskite phase formation (Pereira, Peixoto and Gomes, 2001). The introduction of the niobium doping with excessive oxygen atoms has a strong effect to increase domain reorientation by reducing the oxygen vacancies density through (Zhang *et al.*, 2006):

$$Nb_2O_5 \xrightarrow{2TiO_2} 2Nb_{Ti}^{o} + 5O_o, \tag{3.3}$$

where Nb_{Ti}^{o}: the substitution of niobium to titanium atom and O_o: the substitution of oxygen atom from niobium oxide to oxygen atom vacancy in the perovskite structure. Because of such doping effect, remanent polarization, dielectric constant and piezoelectric coefficient were found to enhance in agreement with our measured results. By the same composition, we obtained much larger P_r and ε_r compared to those reported in literature of highly [111]-oriented PZT thin films (Gong *et al.*, 2004) and polycrystalline PZT thin films (Khaenamkaew *et al.*, 2007) but much lower than the reported values of epitaxial PNZT films deposited on single crystal substrates (Zhu *et al.*, 2007). Such the enhancement was also confirmed by results of the present piezoelectric measurement (Kwok *et al.*, 2004). The improvement of electrical properties by various dopings has been discussed (Zhang *et al.*, 2008; Kuscer *et al.*, 2007; Yu *et al.*, 2003). The donor doping, in turn, introduces immobile defect dipoles, resulting to net mobile defect density and leading to a reduction of imprint and fatigue (Zhang and Whatmore, 2004). Some authors have studied the variation of the electrical properties with niobium doping level (Haccart, Remiens and Cattan, 2003; Kwok *et al.*, 2004), 2 at% niobium is reported not only for enhanced dielectric and ferroelectric properties but also for pyroelectric and piezoelectric properties. For more doping, higher crystallization temperature is needed in which it may lead to the degradation of electrical properties and the coexisting non-ferroelectric pyrochlore phase (Kurchania and Milne, 2003) due to the unfavorable increase of crystallized temperature for perovskite phase formation. To avoid harmful pyrochlore phase, the appropriate temperature used must be concerned. However, there are arguments of such optimal level reported by other authors (Souza *et al.*, 2004; Chu *et al.*, 2004).

3.5 Conclusions

Preferentially oriented and Nb-modified PZT (PNZT) films with different compositions were deposited on Pt(111)/TiO_2/SiO_2/Si(100) substrates by sol-gel method. With the insertion of the seeding layers, the prepared PNZT films showed single perovskite phase and exhibited highly [100]- and [111]-preferred orientation for each type of seeding layer. The measured out-of-plane lattice parameters indicated that the existence of MPB in PNZT(100) films was consistent with that of PZT bulk materials. Although lattice parameter could not be extracted for PNZT(111), the change in XRD result seemed to point out that the MPB for such films agreed with the PNZT(100) films. The polycrystalline PNZT films with varied composition displayed dense, fine-grained and uniform microstructures.

The measurements of electrical properties indicated that the electrical properties had a strong dependence of Zr/Ti ratio. Typical *P-E* hysteresis loops were obtained for all the PNZT films. The Zr/Ti ratio at 52/48 possessed the maximum P_r of 75 μC/cm^2 and low E_c of 82 kV/cm for PNZT(100). In addition, the d_{33} values varying with the composition showed the similar trend to that for P_r and reached its maximum of 161 pm/V at the Zr/Ti ratio of 52/48.

For PNZT(111) thin films, the composition dependent P_r reached the best value of 80 μC/cm^2 at MPB (Zr/Ti=52/48) which was also consistent with that in PNZT(100) thin films. The film with MPB composition possessed low E_c of 70 kV/cm and high dielectric constant of 1550. Furthermore, by comparing with the pure PZT films, the 2 mol% Nb-doping showed a significant contribution for improvement of the electrical properties of PZT films.

CHAPTER 4

TEXTURE AND THICKNESS DEPENDENT NIOBIUM MODIFIED PNZT THIN FILMS

4.1 Introduction

Lead zirconate titanate (PZT) has been growing interest in ferroelectric materials for applications in devices, especially in ferroelectric memories due to their two stable and large polarized stages (Lee, Ahn and Yoon, 2005). One considerable issue is to develop high quality PZT thin film integrated in silicon-based technology whose operation requires the reduced coercive voltage of the films. Scaling down thickness is one of major concerns necessary which, in turn, lead to deterioration of retaining high remanent polarization and dielectric constant, and lowering coercive field (Lin *et al.*, 2001; Ellerkmann *et al.*, 2008). This is because the adverse ferroelectric properties come at thinner film due to the effect of an interfacial layer of low dielectric permittivity and small grain size (Kundu and Lee, 2000). However, although most research has concentrated on epitaxial films grown on single crystal substrates (Contreras *et al.*, 2003; Nonomura *et al.*, 2002), scaling down the thickness of polycrystalline PZT films is more important from the practical point of view, especially in decreasing the operating voltage of FeRAMs (Summerfelt *et al.*, 2001).

The problems also arise with the loss of preferred orientation (Ellerkmann *et al.*, 2008). It is reported that niobium modified PZT with optimal 2 at% Nb was verified to behave good ferroelectric material (Haccart, Remiens and Cattan, 2003). In addition, $Pb(Zr_{0.3}Ti_{0.7})O_3$ thin films have been reported their high remanent polarization (Yan *et al.*, 2002). This chapter thus aims to prepare Nb-modified PZT 30/70 using the sol-gel process. The control of film texture is achieved under an inserting buffer layer between the substrate and the PNZT film. During the deposition cycles, the thickness of the film is controlled by the spinning rate and varied from 80 to 400 nm. Thin films (0.3-3 μm) are generally required for incorporations in microelectronics and microsystems. Therefore, the understanding

and tailoring of the PNZT thin films with different thicknesses are of interest from both an engineering and a basic science viewpoint.

4.2 Review of previous works

Ferroelectric in thin film form have several key advantages over bulk materials as active elements in electromechanical devices. Ferroelectric thin films pose significantly higher dielectric strengths so that higher energy densities can be achieved and require a relatively low driving voltage, thus leading to small inertia, which allows for higher frequency applications (Lian and Sottos, 2000)

Authors have reported the dielectric and ferroelectric properties that showed strong thickness dependence in all of the following measurements: polarization-electric field, current-voltage, and capacitance-voltage (Lin *et al.*, 2001; Bouregba *et al.*, 2006; Etin *et al.*, 2007; Lin *et al.*, 2008). Because of the formation of Schottky barriers at ferroelectric/electrode interfaces, built-in electric fields are present (Lin *et al.*, 2001). An increment in carrier concentration and interfacial built-in electric field versus reducing PZT film thickness was observed, which is believed to be a dominant factor controlling the measured dielectric/ferroelectric properties. Similarly, nonferroelectric space-charge layers at both ferroelectric-electrode interfaces were proposed to the degradation of the switching properties in order to explain the electrical properties dependent to film thickness (Bouregba *et al.*, 2006). The reduction of the ferroelectric properties of PZT thin film capacitors encountered when their thickness is reduced. It probably arises from a mechanism of modulation of density and sign of the space charge at both interfaces. In addition, simulation of hysteresis loops including nonswitching dielectric layer reproduced quite well and the increased tilt often observed when the thickness of the ferroelectric film is reduced (Miller *et al.*, 1990). This is consistent with the serial model since the voltage drop across the interface capacitance is expected to yield a reduction of the field applied to the bulk ferroelectric layer, hence a decrease of the polarization. However, the observed thickness dependence of true coercive field cannot be recovered if the interface dielectric layers are considered as insulating or passive layers (Cillessen, Prins and Wolf, 1997).

Scott *et al.* (1988) reported a $d^{-1/3}$ thickness dependence of the coercive field in a thick film regime (0.2-0.5 μm), and a $d^{-4/3}$ behavior for the intermediate film thickness d regime ($0.15<d<0.35$ μm). Tagantsev *et al.* (1994) interpret the thickness dependence in thin films as a result of the differences in the threshold fields required for domain wall motion and reversed domain nucleation at the electrode-film interfaces that could arise from the semiconducting properties of the metal-ferroelectric interface. Therefore, the key to obtaining good ferroelectricity in thinner films is a clean interface between the PZT and bottom electrode because the decrease in ferroelectric properties with decreasing film thickness has been related to this interface, the so-called dead layer (Kijima and Ishiwara, 2002; Larsen *et al.*, 1994). Another important factor is the diminishing leakage current density when film thickness decreases (Aratani, Nagashima and Funakubo, 2001).

4.3 Materials and methods

Lead acetate trihydrate, zirconium *n*-propoxide, titanium iso-propoxide and niobium ethoxide were used as raw materials. The precursor solution was prepared in 2-methoxyethanol and diluted to 0.5 M. The mole ratio between zirconium and titanium was 30:70 and 2 at% Nb was added to replace B-site atom. 20 and 8 mol% lead excesses were used to compensate for lead losses in PNZT(111) and PNZT(100), respectively, and to prevent pyrochlore formation. By similar method, 0.05 M lead- and titanium-containing organic solutions were prepared for seeding solutions.

The lead containing organic solution was first deposited on $Pt(111)/TiO_2/SiO_2/Si(100)$ substrate by the spin coater and then annealed at 500 °C for 2 min for PbO seeding layer to control for PNZT(100). Similarly, titanium containing solution was deposited and annealed at 600 °C to control for PNZT(111). Details of the fabrication of thin films with highly orientation were described in chapter 3. The PNZT with seeded substrate and different thicknesses: 80, 160, 240 and 400 nm were fired at 650 °C for 5 min by rapid thermal processing in air while the film thickness was controlled through deposition cycles in which each deposited cycle gave 80 nm in film thickness. For random orientation, the PNZT films were

directly deposited on the non-seeded substrate. The prepared films were examined the crystallization and orientation using an X-ray diffractometer (XRD, Rigaku D/max-RB, Cu-K_α).

For the electrical measurements, ~0.1 μm-thick of gold metal was sputtered through a shadow mask to form an electrode of an area of ~0.3 mm^2 on the surface of the film. The electrical properties including dielectric constant and *P-E* hysteresis loops were carried out using a standard ferroelectric test module (aixACT TF Analyzer 1000, Germany).

4.4 Results and discussions

4.4.1 X-ray characterization for different thicknesses and orientations

All XRD patterns of PNZT films, which were annealed at 650 °C for 5 min, showed typical single-phase perovskite structure without detectable pyrochlore phase as shown in Figs. 4.1-4.3. The PNZT films with the inserting PbO seeding layer favorable stronger (*h*00) peaks over (00*l*) peaks for the films at bigger thickness in Fig. 4.1, indicating that strong [100]/[001] orientations were ascertained for influence of the seeding layer. Thus, the thin films would have mainly the tetragonal single phase. The (100) peaks shifted slightly to lower 2θ as thickness of films were increased. This could be attributed that the out-of-plane lattice constant became smaller. Figure 4.2 represented the XRD patterns of the PNZT films with the inserting TiO_2 buffer layer. The crystallized thin films showed mainly preferred [111] orientation. Although the seeding layer was applied prior to the deposition of the PNZT film, Figs. 4.1 and 4.2 did not show seeding diffraction peaks of either PbO(001) or TiO_2(101) even in 80 nm thick PNZT films. As discussed early in chapter 3, Pb and Ti were the main elements for PNZT solid solution and PbO and TiO_2 may diffuse to the overlaid the PNZT layer during annealing procedure and formation of the thinner PNZT layer. Figure 4.3 showed the XRD patterns of the PNZT thin films without any buffer layer. The XRD results also showed that all the textures transformed into either [110]- or random orientation.

As similar film behavior obtained from experiment in chapter 3, the seeding buffer layer would play the important role in reducing the nucleation energy

during the heat treatment process. However, as compared to the films with the PbO buffer layer, no splitting peak occurred when the thin films were crystallized into preferred [111]- and random orientation irrespective to the precursor solutions of PNZT 30/70. Experimental results on the thickness dependence of the XRD patterns suggested that, with increasing film thickness, the diffraction intensity increased obviously. The corresponding results showed the slightly increased grain size in thicker films (Li *et al.*, 2002; Etin *et al.*, 2007).

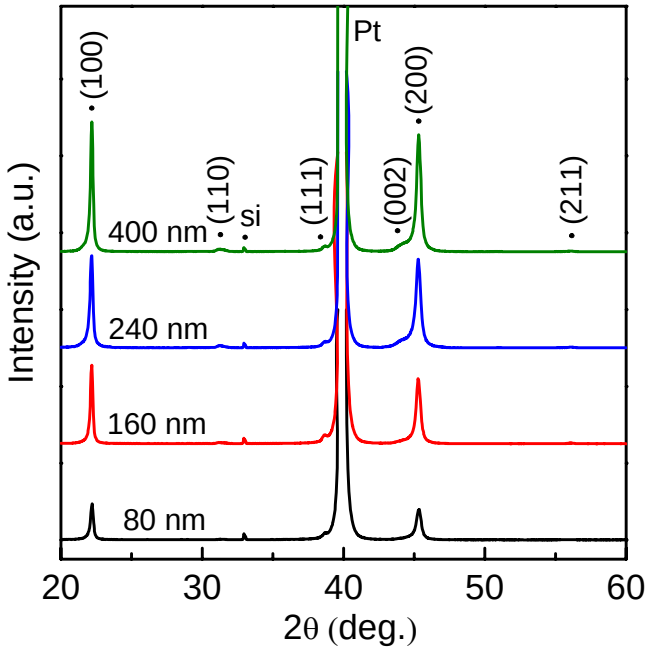

Figure 4.1 XRD patterns of different thicknesses in PNZT films with [100]-preferred orientation.

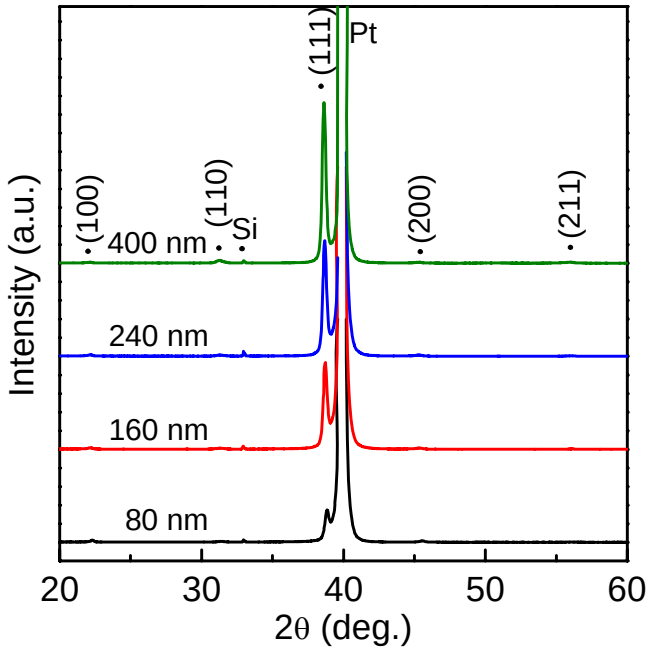

Figure 4.2 XRD patterns of different thicknesses in PNZT films with [111]-preferred orientation.

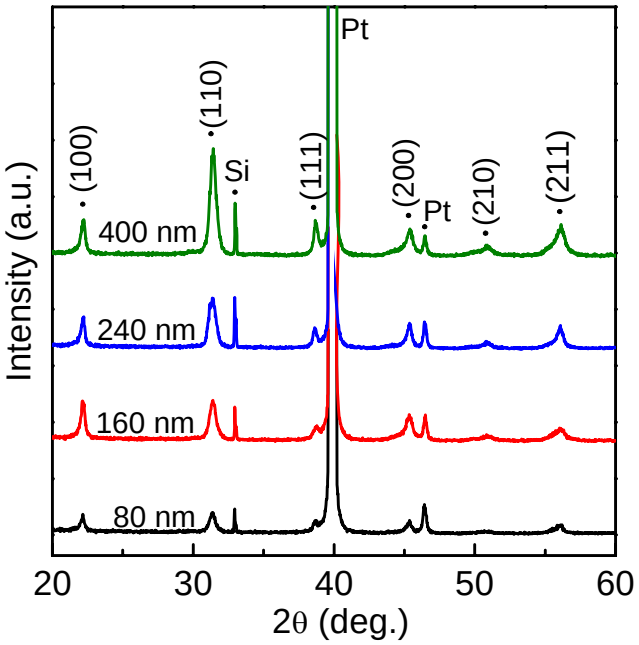

Figure 4.3 XRD patterns of different thicknesses in PNZT films with random orientation.

Analysis of such preferential orientation was performed by calculating orientation ratio of the desired (*hkl*) according to Eq. 3.1. As shown in Fig. 4.4, the orientation ratios of (100), (111) and (110) peaks in PbO-buffered, TiO_2-buffered and non-buffered PNZT thin films, respectively, increased with increasing film thickness. This was probably attributed to that the underlying PNZT layers would promote the nucleation and crystallization for overlaid PNZT layers (Lin *et al.*, 2008). The similar mechanism was employed for the growth of PZT thick film by the hybrid process which consists of the sol-gel method and other technique with a high continuous deposition rate, e.g. PLD (Wang, Kokawa and Maeda, 2005). The PZT deposited by sol-gel method required a lower crystallized temperature, leading to reduce the overall temperature used whereas the PLD method used later required a higher temperature due to the exist of nucleation site by PZT.

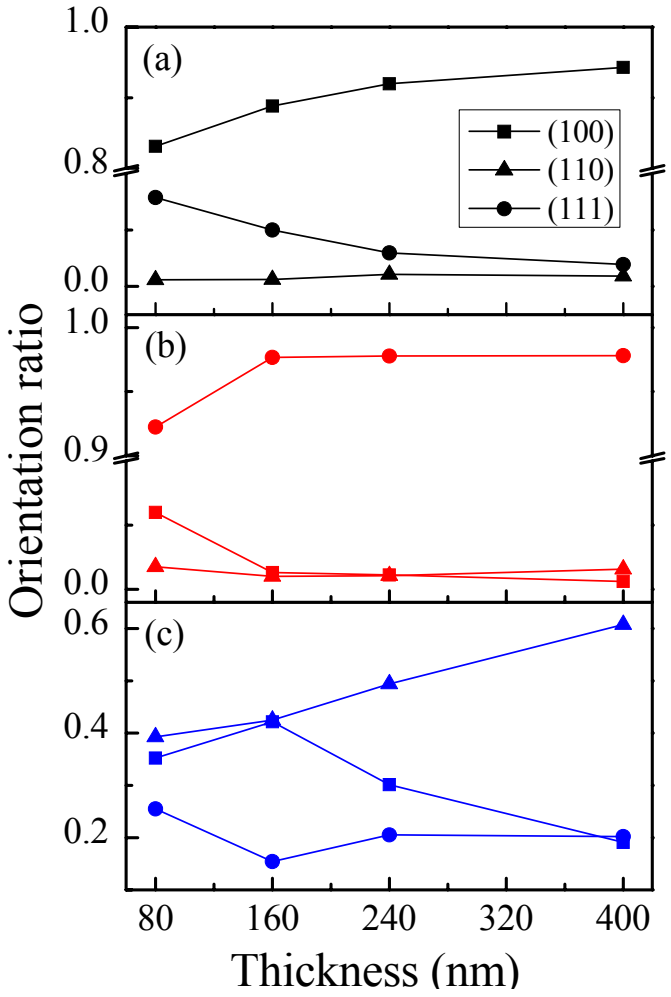

Figure 4.4 Orientation ratio as a function of film thickness. Films posses (a) [100]-preferred, (b) [111]-preferred and (c) random orientation.

4.4.2 Electrical characterization for different thicknesses and orientations

Figure 4.5 showed the leakage current characteristics recorded at room temperature of the PNZT(100) thin films. The leakage current density increased with decreasing film thickness. There was a slightly asymmetric behavior for negative and positive voltage.

The asymmetric characteristic should be resulted from the different work function of electrodes (Lee, Ahn and Yoon, 2005); even top and bottom electrodes were the same platinum metal but different heat treatments were used after the final annealing. As discussed in previous work (Cheng and Meng, 2001), the leakage current density at low applied voltage increased linearly, indicating that

ohmic conduction results from contact barrier at the film-electrode interface in reducing the injection current and thermally excited electrons. In comparison, the leakage current density of 80 nm film was approximately 1 A/cm^2, larger than that reported in film prepared in vacuum system (Lisca *et al.*, 2006). The inferior leakage current density would be attributed to poor microstructure of ceramic film which involved in preparation with the different processing conditions and/or other contributions such as lead vacancies, residual organics and micro cracks (Gong *et al.*, 2004). In recent articles (Kim and Lee, 2005; Oikawa *et al.*, 2004), the reduction of the leakage current could obtained by improving the film surface roughness during in situ or post annealing process.

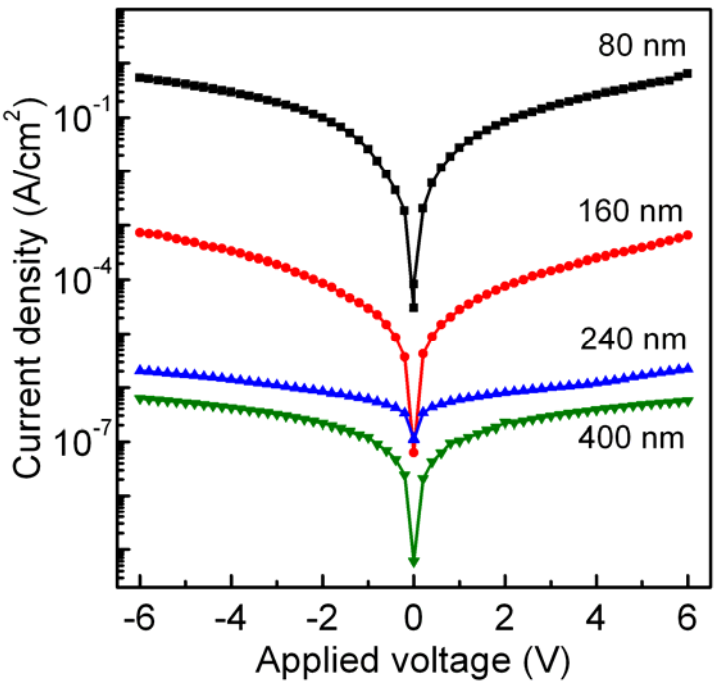

Figure 4.5 Leakage current density of [100]-preferentially oriented PNZT films with different thicknesses.

Figures 4.6 and 4.7 revealed the dielectric nonlinearity and hysteresis in ferroelectric PNZT thin films. The butterfly-type shapes were the natural result of switching behavior where the maximum occured near the coercive voltage. This is due to the large number of coexisting domain walls at these voltages.

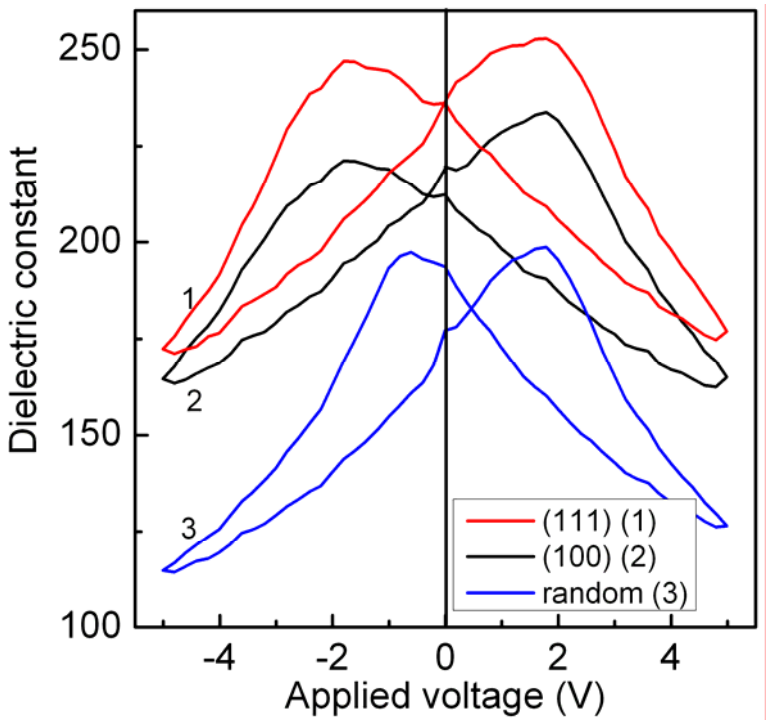

Figure 4.6 Dielectric constant–voltage curves for [100]-, [111]- and randomly oriented PNZT films with film thickness of 160 nm.

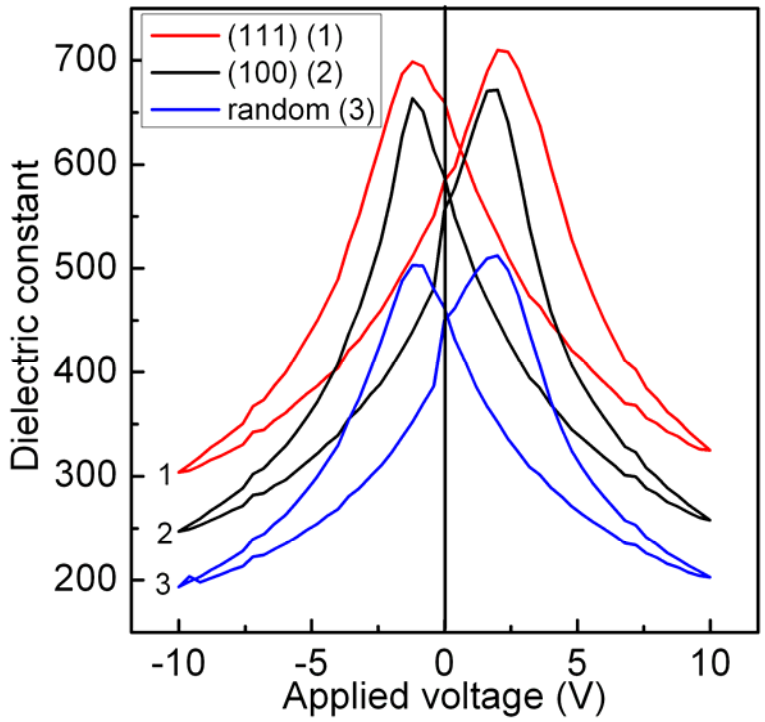

Figure 4.7 Dielectric constant–voltage curves for [100]-, [111]- and randomly oriented PNZT films with film thickness of 400 nm.

Ferroelectric properties were carried out from *P-E* hysteresis loops measured at 100 Hz for each sample with different thicknesses. The measurements were performed to keep films under the similar magnitude of the applied electric field. The results were shown in Fig. 4.8 for the [100]-oriented films, Fig. 4.9 for the [111]-oriented films and Fig. 4.10 for the randomly oriented ones. The PNZT films exhibited a relatively well-saturated hysteresis loop.

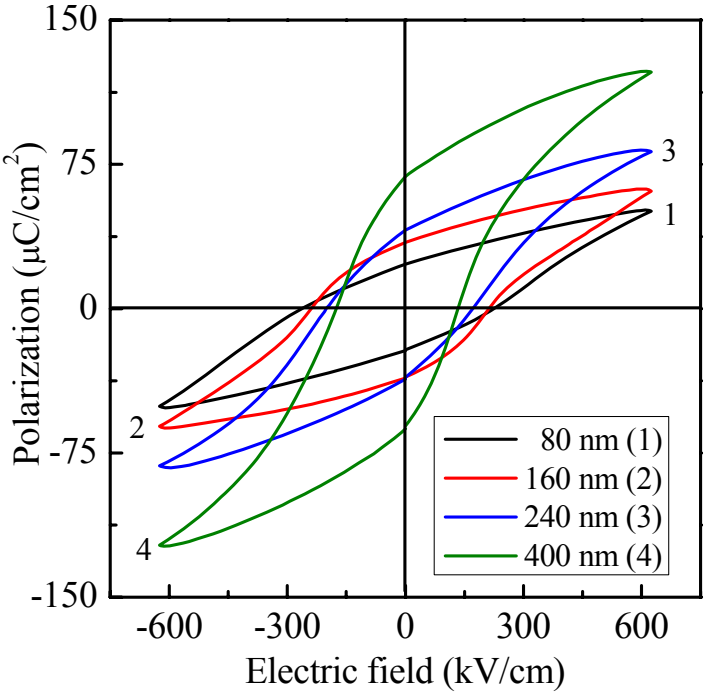

Figure 4.8 *P-E* hysteresis loops of different thicknesses in PNZT films with [100]-preferred orientation.

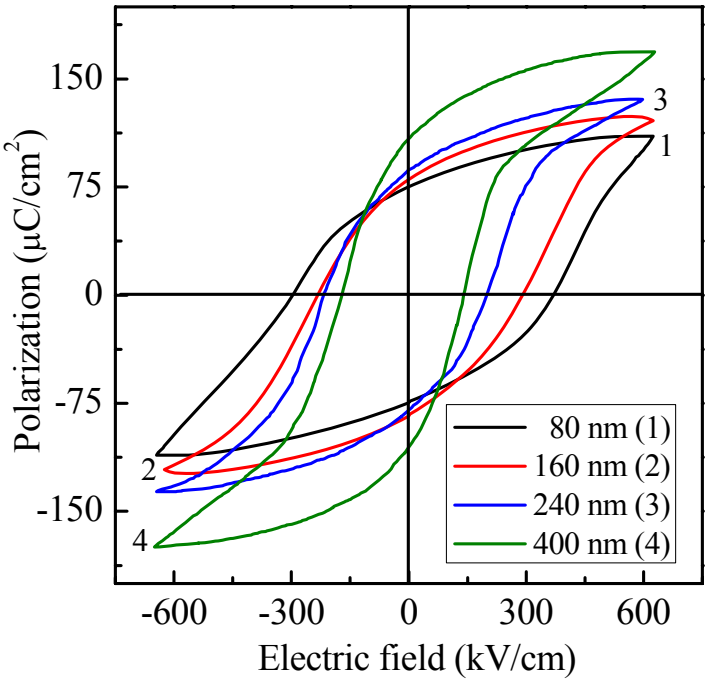

Figure 4.9 *P-E* hysteresis loops of different thicknesses in PNZT films with [111]-preferred orientation.

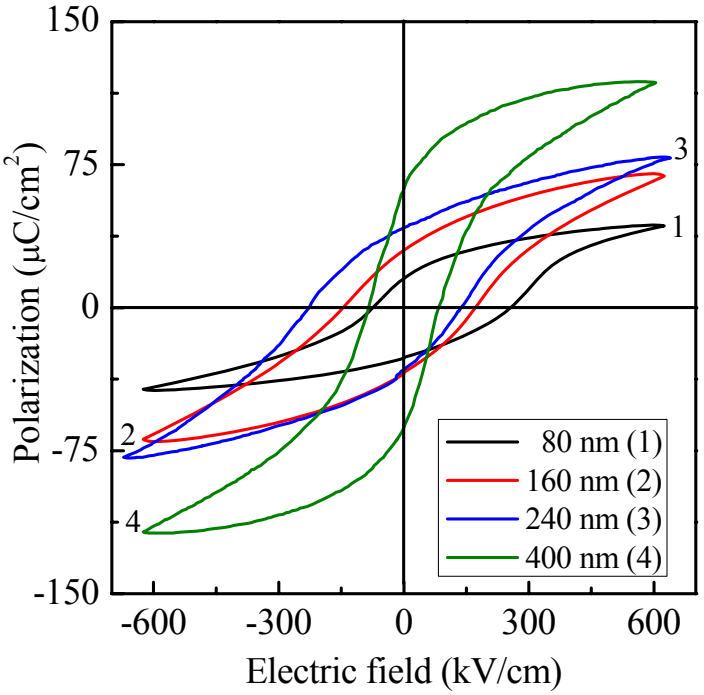

Figure 4.10 *P-E* hysteresis loops of different thicknesses in PNZT films with random orientation.

In Fig. 4.11, the coercive field (E_c) and remanent polarization (P_r) as a function of film thickness with different orientations were shown. Each oriented film posed the same trend of the increased E_c with reduced thickness.

The origin of this would be described thought the formation of a predominant interfacial layer with low dielectric permittivity between the film and the substrate. This occurrence would be influenced by a nonstoichiometric phase, a chemical reaction with platinum electrode, a space-charge layer, stress and the size effect (Sakashita *et al.*, 1993). An imprint behavior in which the hysteresis loop shifts along electric field axis was significantly exhibited in thinner films. The formation of model explaining the imprint effect based on interface space-charge layer was detailed elsewhere (Rhun, Bouregba and Poullain; 2004). The increase of the film thickness also led to increase the P_r value ranging from 78 to 108 μC/cm^2 in [111]-oriented films. The increasing film thickness might result in the domain wall density becoming larger with less domain wall pinning.

Considering the possible orientations of domain for crystallographic orientations, for tetragonal structure, the polarization axis aligned along [001] direction. The reoriented 90° domain from [001] to [100] would not be favored by applied electric field normal to the film surface but there were small (00*l*) peaks or *c*-domains. Thus the resulting P_r values in [100]-oriented films were smaller than those in [111]-oriented films (Chen and Sun, 2001). In randomly oriented films, all possible orientations in perovskite crystal occured but mostly in [110] orientation which were clearly observed in thicker films. The coexisting (100)-, (110)- and (111)-unit cells would lead to the measured P_r value lower in randomly oriented than those of preferred oriented films due to different polarization directions, resulting to energy loss and poor electrical properties. As the polarization was switching one poling stage to the other, the larger E_c in [111]-oriented film was due to non-90° domain reorientation from the first stage to the later one when the domains fall in opposite electric field. This would induce more strain. In turn, the E_c was obtained the smallest in randomly oriented films.

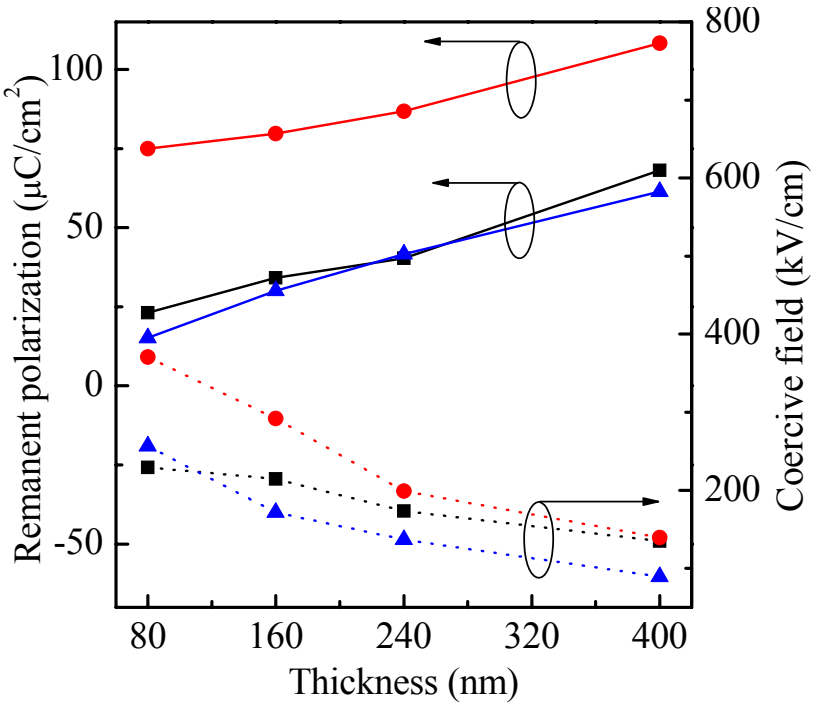

Figure 4.11 Dependence of remanent polarization (solid line) and coercive field (dotted line) on film thickness with (■) [100]-preferred, (●) [111]-preferred and (▲) random orientation.

4.5 Conclusions

Highly [100]-, [111]- and randomly oriented PNZT thin films with thickness ranging from 80 to 400 nm were fabricated onto platinized silicon substrates by the sol-gel process and spin coating method. The crystalline structure and preferred orientation of the PNZT films were examined by XRD analysis and showed that all the thin films with thickness dependence were crystallized into single perovskite structure. XRD analysis indicated that the preferred orientation of PNZT films could be controlled using the seeding layer.

The tetragonal perovskite structure of Nb-modified $Pb(Zr_{0.3}Ti_{0.7})O_3$ is of interest in this work due to that polarizable directions were close to the polar axes. The electrical properties were a function of thickness in which the largest dielectric constant and remanent polarization were obtained in [111]-oriented PNZT thin films at film thickness of 400 nm. However, the smallest dielectric constant and coercive field were obtained in randomly oriented films.

CHAPTER 5

THIN POROUS PZT FILMS

This chapter presents the PZT thin film prepared by using the conventional 2-methoxyethanol-sol-gel process discussed earlier. The modification made is adding the CNTs during the preparation of the PZT precursor. The material properties of the obtained PZT thin films have been tailored and possible for pyroelectric detector applications as described below.

5.1 Introduction

In recent years, there is a continuous growth of interest in pyroelectric materials for radiation energy detection, radiation power detection, and radiation configuration imaging for continuous wave signal, pulse signal, and modulated signal (Lines and Glass, 2001; Kruse, 2001). Unlike semiconductor or photon detectors, pyroelectric IR detectors could be operated well at room temperature which makes them very applicable for uncooled IR detection and imaging applications, thereby eliminating the need for expensive multistage thermal regulation systems (Kruse, 2001). They also have broader and more uniform spectral responsively as well. The task of designing more economical IR detection devices with a better performance has led to the use of ferroelectric thin films as potential candidates as the operational component of such devices (Shi *et al.*, 2000; Björmander *et al.*, 1995). In particular, the integration of hybrid arrays of ferroelectric thin films detectors with silicon readout integrated circuits can offer a high performance for infrared imaging (Mantese *et al.*, 1993).

PZTs are considered leading candidates as the active materials for pyroelectric sensors because these compounds provide a relatively large response at room temperature (Whatmore, Osbond and Shorrocks, 1987). Owing to the superior dielectric and piezoelectric properties, the PZT film with x = 0.52, i.e. a well-known

MPB is of our interest. The pure PZT (52/48) thin film is demonstrated to be a good pyroelectric material (Akai, 2005).

One way to improve the pyroelectric device performances is the artificial reduction of physical properties through chemical or physical modification. If its dielectric constant can be reduced without sacrificing the pyroelectric property, a higher figure of merit can be obtained. A method to decrease ε_r is to prepare porous films. The porous ferroelectric studies showed that the porosity is influenced by the annealing rate (Muralt, 2001), the method based on burning out carbon-based fillers (Stancu *et al.*, 2007) or the doping as PZT/low dielectric material composite solid solution (Sakamoto, Marin-Franch and Das-Gupta, 2002).

There are methods of adding the CNTs into a host material. In this work, CNTs were directly mixing into the precursor solution. However, reports of the fabrications and measurements of the sol-gel derived PZT film with CNT fillers are scarce. It is possible that the difficulties encountered in obtaining uniform dispersion of the CNTs in the precursor solution are a part of the reason for this. Our purpose is to investigate the role of the multiwalled CNTs (MWNTs) as fillers on the electrical properties in which high ferroelectric property is sustained with reduced dielectric property.

5.2 Review of previous works

In the present study, the aim was to produce PZT films with low dielectric constant and low dielectric loss (or loss factor). Consequently, high figure of merits yield for such PZT films. As reviewed in the introduction, porous PZT films are to obtain for low dielectric constant in different ways. Generally, porous PZT with different pore size and porosities can be made by burning pore formers with different sizes and contents such as starch (Lyckfeldt and Ferreira, 1998), PVA (Chao and Chou, 1996), PVB (Liu, 1996), yeast (Chi *et al.*, 2004), during heat treatment process.

Stancu *et al.* (2007) have reported the effect of an addition of organic macromelecular polyvinylpyrrolidone (PVP) at different amounts (7-15 wt%) in the PZT precursor solution prior to spin coating which proves to be an excellent method for obtaining porous films. The dielectric constant decreases from 246.32 for dense

films to the minimum value of 42.37 for 40% porous films at PVP doping of 7 wt%. The addition of polymer phase also affects the crystallographic growth of the ceramics matrix. The substantial presence of [110] orientation for porous films occurs in comparison with more epitaxial dense films.

In addition, 5-45% porous lead zirconate titanate (PZT) ceramics were fabricated by adding pore formers such as polymethyl methacrylate (PMMA) and dextrin (Zeng *et al.*, 2007). With an increase in the content of pore formers, the porosity of sintered ceramics increased, leading to reduction of dielectric constant and longitudinal piezoelectric coefficient as well as increase of hydrostatic piezoelectric voltage coefficient (g_h) and hydrostatic figures of merit ($d_h g_h$). The hydrostatic figures of merit of 41% porous PZT were 10 times more than that of 95% dense PZT.

Suyal and Setter (2004) studied different molecular weight of the filler and found that the pore volume can be easily controlled by changing the molecular weight and the concentration of the polymer used. Introduction of pores creates a matrix void composite, resulting in high figures of merit for pyroelectric applications. For PZT (Zr/Ti=45/55), the F_v and F_d values were increased from 0.28 to 1.0 $\mu C/m^2K$ and 38 to 80 $\mu C/m^2K$, respectively, due to incorporating a nanoporous structure into films.

Addition to porous films, reducing electric constant of the ferroelectric materials will meet to improve pyroelectric operation through other possible ways. Zhang *et al.* (2005) proposed increasing the thickness of a single layer introduced pores into PZT films. Seifert *et al.* (1999) have synthesized porous thin films of $Pb_xCa_{1-x}TiO_3$ by controlling the nucleation and growth during RTP of the material. In stacking structure (Sun, Tan and Zhu, 2006), PZT and $PbTiO_3$ layers deposited alternately in multilayer PZT/$PbTiO_3$ thin films characterized that the 5PZT/4PT multilayer thin film has reduced dielectric constant, comparable pyroelectric coefficient and dielectric loss when compared with the pure PZT thin film. Consequently, the detectivity figure of merit of 2.1×10^{-5} $Pa^{-1/2}$ for multilayer film is found to be better than that of pure PZT thin film.

5.3 Materials and methods

The $Pb_{1.2}(Zr_{0.52},Ti_{0.48})O_3$ thin films were prepared by a sol-gel process and a spin-on method. The solution components were lead acetate trihydrate, zirconium *n*-propoxide and titanium iso-propoxide in 2-methoxyethanol as a solvent. The procedure of the preparation of precursor solution was based on that described in chapter 3. The precursor solution was diluted to 0.6 M.

Purified MWNTs (Shenzhen Nanotech) at concentrations of 0.4 and 0.6 wt% were mixed into the solution and dispersed using a sonic tip (Ultrasonic Homogenizer 150VT) for 30 min to form a uniform suspension. 2 mL of the solution was partially dried at 80 °C for 24 h. The obtaining dry gel was then performed the thermo-gravimetric analysis (TGA) at a rate of 10 °C/min. The thin films were obtained by spin-coating at the spinning rate of 3000 rpm for 30 s on a commercial $Pt(111)/Ti/TiO_2/SiO_2/Si(100)$ substrate, followed by pyrolysis at 400 °C for 2 min. The coating-drying-pyrolysis procedure was repeated 4 times for the desired film thickness before final annealing at 650 °C for 30 min. Figure 5.1 summarized steps of the preparation of thin films.

Phase and microstructure were characterized by X-ray diffractometer (XRD), Philips X-Pert, Cu-Kα and scanning electron microscope (SEM), JEOL2000. For electrical measurements, a gold electrode with an area of ~0.3 mm^2 was sputtered on the surface of the films. Frequency-dependent dielectric constants were measured using an HP 4192A LF Impedance Analyzer and polarization hysteresis loops were determined with a Radiant Technologies RT66A at a frequency of 1 kHz.

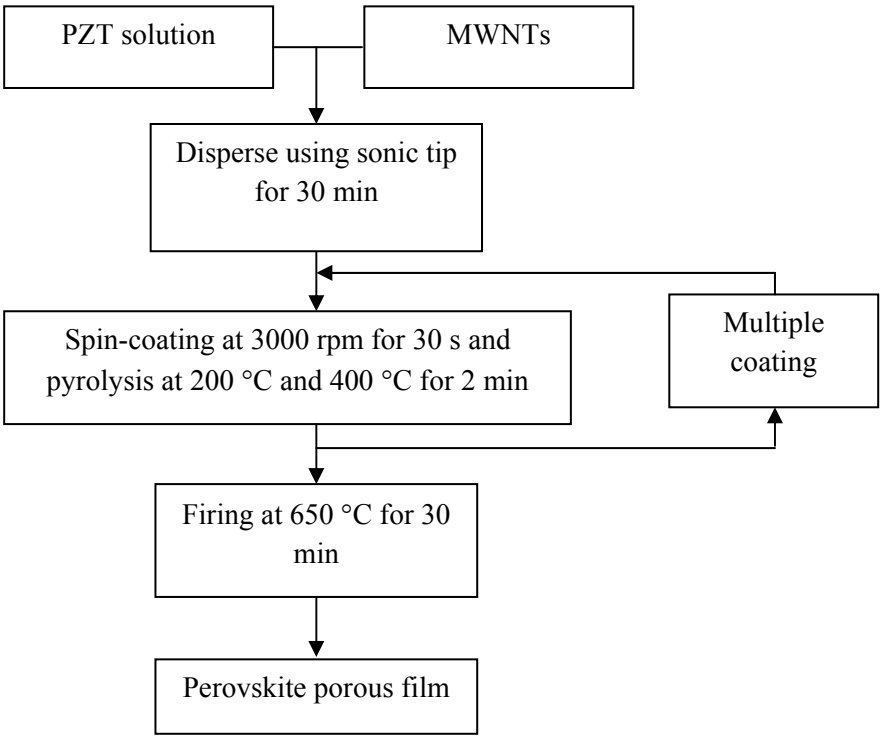

Figure 5.1 Flow chart of the MWNT mixed PZT film deposition.

5.4 Results and discussions

5.4.1 Thermo gravimetric analysis of PZT dried gels

TGA data of the MWNT, PZT and PZT-MWNT dried gels were shown in Fig. 5.2. MWNTs were burnt out rapidly in nitrogen atmosphere when the temperature increased above 600 °C. For PZT films, three weight losses were observed up to 550 °C, due to the decomposition of the organic products. No weigh loss was observed above 550 °C because the PZT film was completely transferred into perovskite structure. The weight loss at the temperature around 1000-1200 °C was probably associated with the burnt out some amount of the PZT itself. The insertion of MWNT at level of 2 wt% would not significantly affect the thermal decomposition behavior of the PZT-MWNT films. At 650 °C, the incorporation of MWNT into PZT films was expected to induce porosity due to the presence of the MWNT's dimensional material.

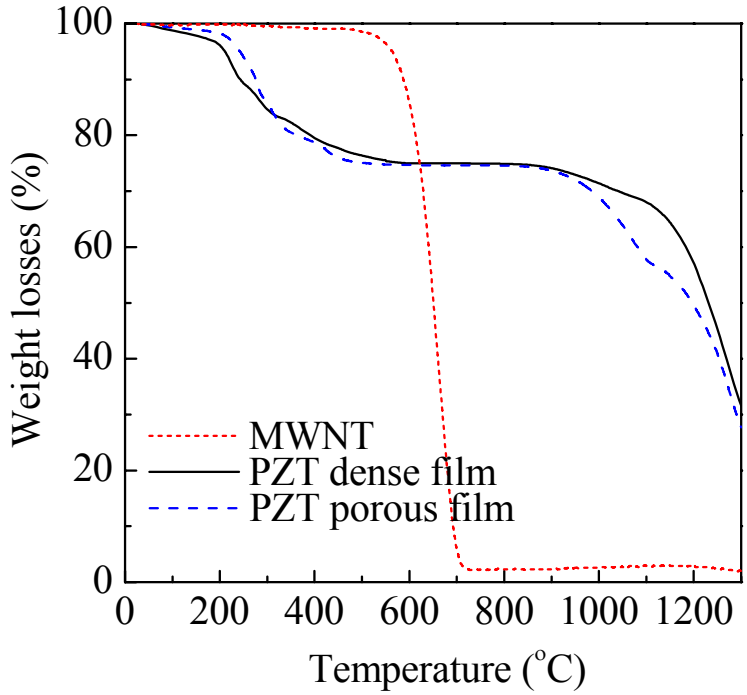

Figure 5.2 TGA curves of MWNTs and PZT dried gels with and without additional MWNTs.

5.4.2 X-ray characterization of the dense and porous PZT films

Typical XRD results for the dense and porous PZT films were shown in Fig. 5.3. The PZT dense film showed predominant perovskite phase with random orientation posing a strong (110) peak. The X-ray patterns of the porous films, after heat-treatment at 650 °C, showed the absence of MWNT, indicating that MWNT was well decomposed. The peaks at 40° and 46.5° were the Pt(111) and Pt(200) reflections, respectively, and the peak at 33° was the Si(200) reflection. The broadening of the peak around 29° identified as microcrystalline detectable pyrochlore phase because of lead loss during the annealing process at 650 °C for long time in the conventional tube furnace.

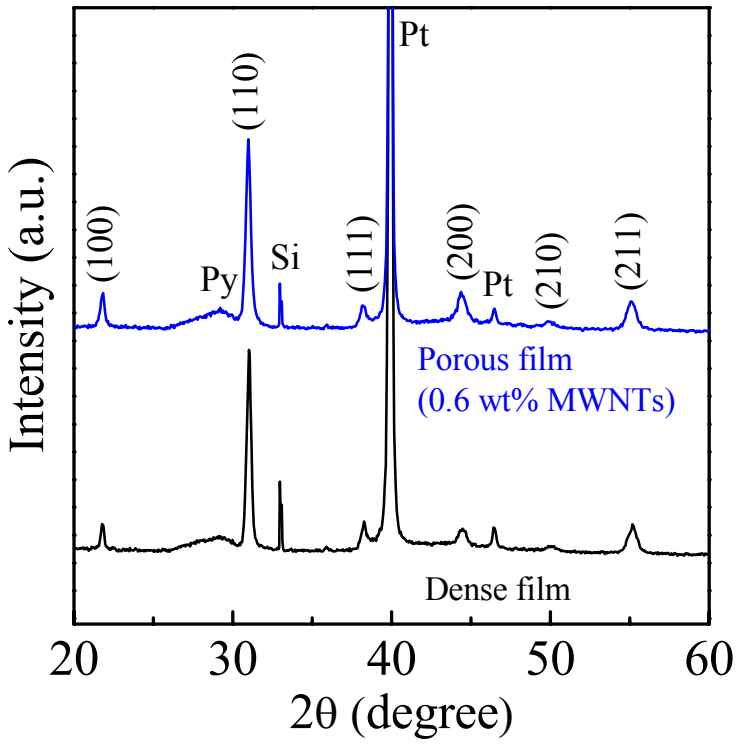

Figure 5.3 XRD patterns of PZT films with and without additional MWNTs.

The SEM micrographs of the PZT thin films with dense (0 wt% MWNT) and porous (0.4 and 0.6 wt% MWNT) structures were shown in Figs. 5.4-5.6. The burnt out some amounts of MWNT and the PZT film would left behind voids and microcracks. Figures 5.7-5.9 showed the cross-sectional images of the samples. The voids and pores in the film were not clearly observed from the top to the bottom of the film. It is possible due to nanoscale dimensions of MWNT.

Kozuka and Kajimura (2000), and Stancu *et al.* (2007) reported the effect of PVP on the thickness of the sol-gel deposited films. The PVP demonstrated to suppress the condensation reaction during the heat treatment and subsequently increase the thickness of the films. The PZT porous films in this study resulted the same film thickness whereas an amount of MWNT was increased from 0.4 to 0.6 wt%. The MWNT doping level was much lower than the amount of PVP which was used at the starting level of 7 wt%. Although there was no evidence to prove the existence of the porosity induced by MWNT in porous films by the SEM micrographs, the porosity would affect the electrical properties as discussed later. The globular structure of grain growth occurred in agreement with the previous films without the

additional MWNT produced by Seifert *et al.* (1999). Without presence of the MWNT, typical columnar structure of the PZT thin film was clearly observed. All the thin films had a thickness of approximately 600 nm.

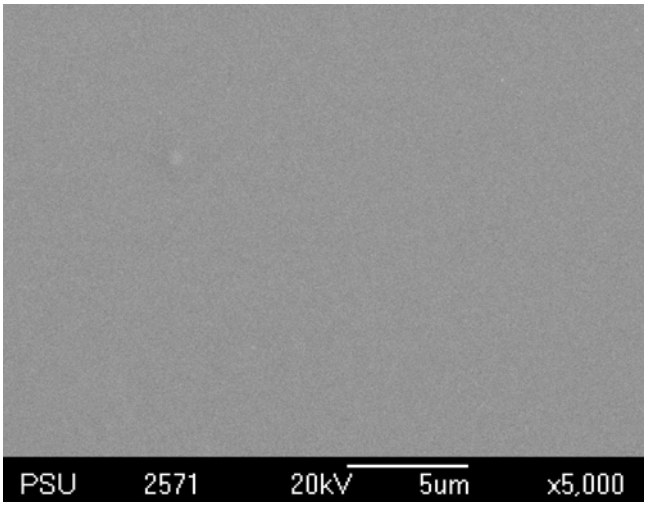

Figure 5.4 SEM planar image of PZT dense film.

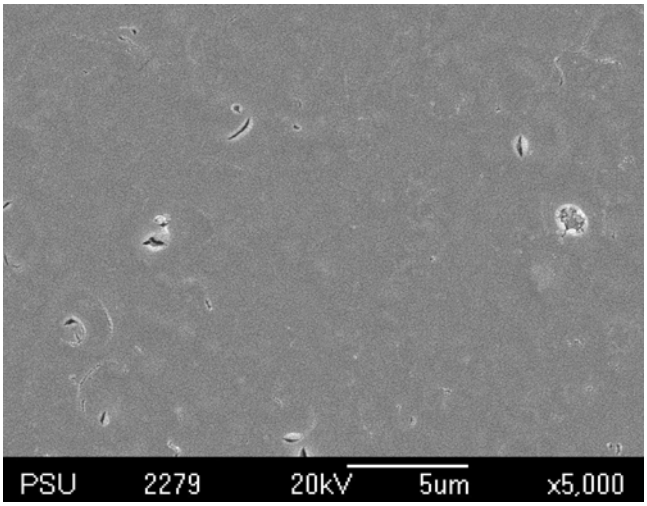

Figure 5.5 SEM planar image of the PZT porous film with 0.4 wt% MWNTs.

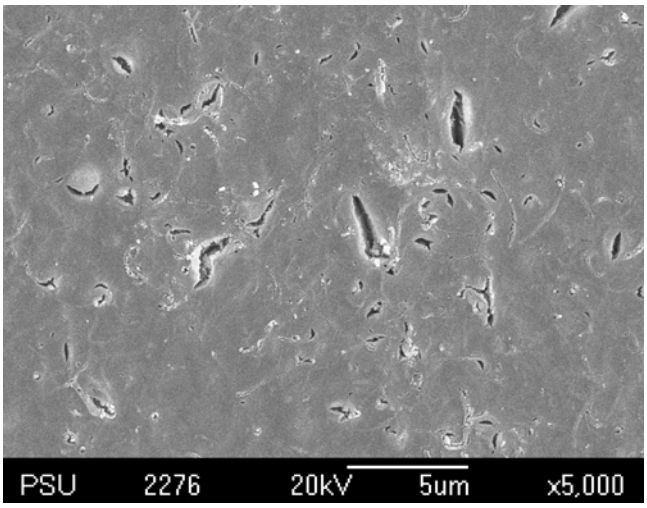

Figure 5.6 SEM planar image of the PZT porous film with 0.6 wt% MWNTs.

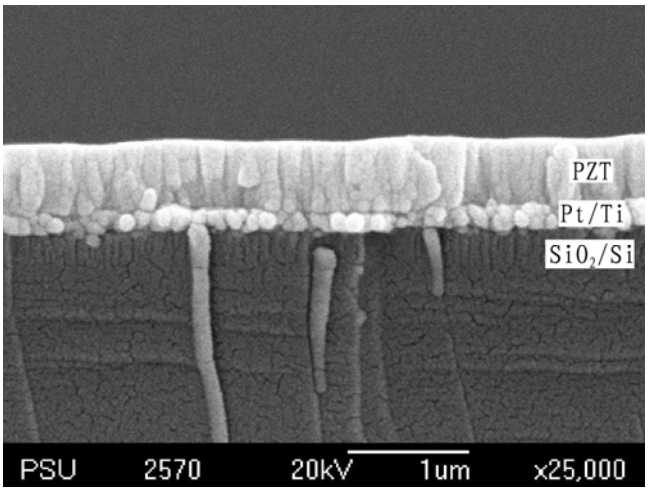

Figure 5.7 SEM cross sectional image of PZT dense film.

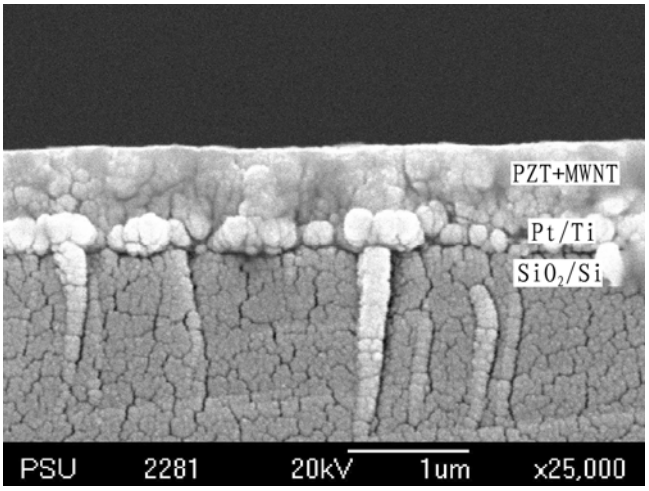

Figure 5.8 SEM cross sectional image of PZT porous film with 0.4 wt% MWNTs.

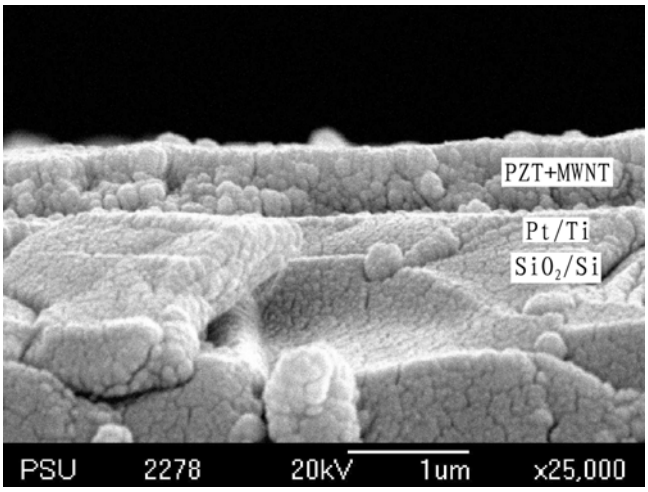

Figure 5.9 SEM cross sectional image of PZT porous film with 0.6 wt% MWNTs.

5.4.3 Electrical characterization of dense and porous PZT films

Ferroelectric hysteresis loops were obtained from the thin films with dense and porous structures as shown in Figs. 5.10-5.12. The polarization curves changed as a function of the applied electric field intensity. It is found that when the applied voltage was 10 V, the hysteresis loops showed typical ferroelectric characteristics, except for the PZT/MWNT films which exhibited irregular hysteresis loop. Asymmetry and slightly changes in the spontaneous polarization were observed while there were no changes in the remanent polarization. It seemed that the

ferroelectricity was accompanied by other special properties although the small amount of MWNTs was used. This is possibly related to the large shape anisotropy and high elastic modulus of CNTs, resulting in a decrease in the polarizibility in the crystalline ferroelectric film (Bell and Moulson, 1985). Indeed, the main purpose of this chapter is to carry out the influence of the carbon based filler on the pyroelectric operation of the material but there was no pyroelectric coefficient measured out. Thus the pyroelectric coefficient would be determined through the ferroelectric properties of the as-deposited samples. Because it would be implied that the increase in net polarization would directly affect to improve the pyroelectric coefficient. Pyroelectric properties of the films as a function between the net polarization and temperature were not mainly emphasized since the process fabrication of the quality films was the main aim in this study.

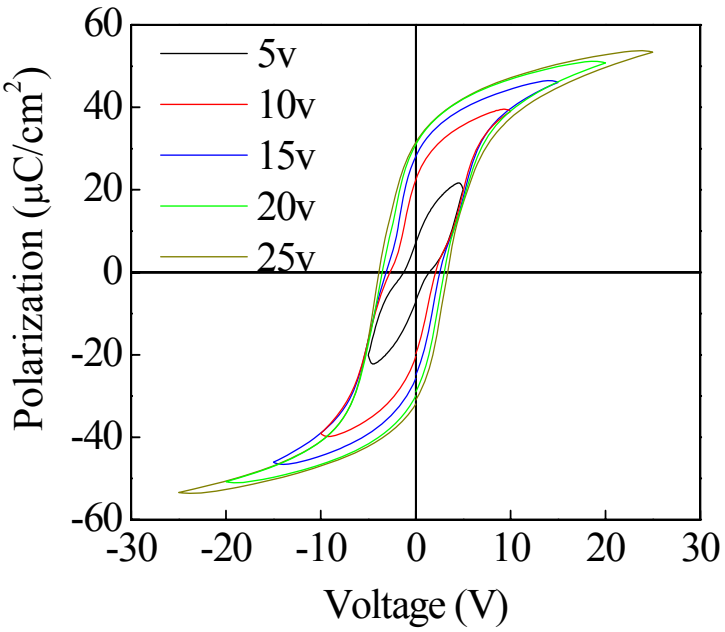

Figure 5.10 Ferroelectric hysteresis loops of PZT dense film.

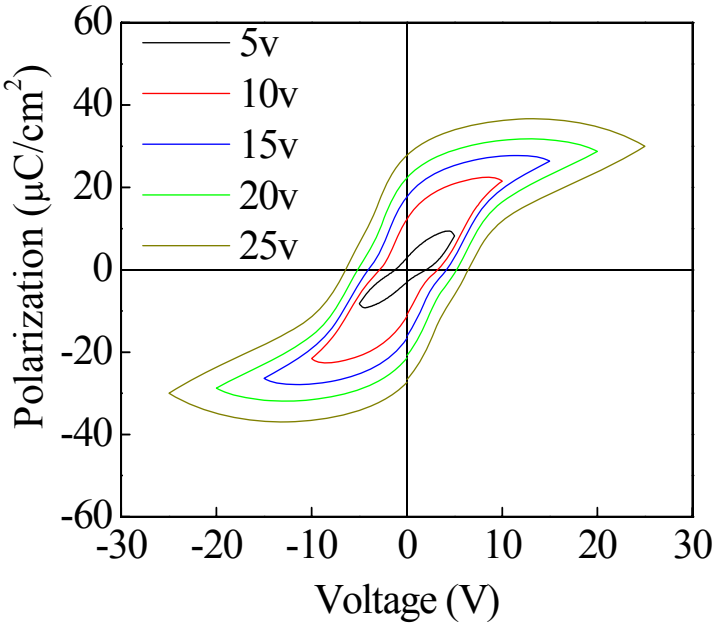

Figure 5.11 Ferroelectric hysteresis loops of PZT porous film with 0.4 wt% MWNTs.

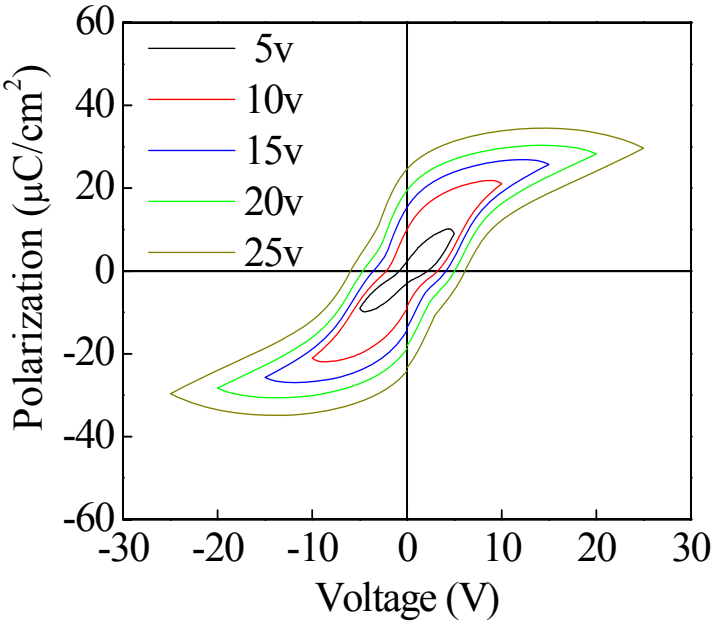

Figure 5.12 Ferroelectric hysteresis loops of PZT porous film with 0.6 wt% MWNTs.

Frequency-dependent dielectric constant and loss tangent (or loss factor) data were shown in Figs. 5.13-5.15. The cause of relatively high loss tangent within the 0.4 wt%-MWNT thin film was possibly the presence of microcracks. In comparison to the PZT dense film, the dielectric constant of the PZT porous films was

decreased by approximately 50%. This significant change would be induced by the addition of MWNTs. Despite of introducing the porosity into the PZT films to reduce the dielectric constant and to enhance the pyroelectric property of the materials as reported by publications (Stancu *et al.*, 2007; Suyal and Setter, 2004; Shaw, Whatmore and Alcock, 2007), the addition of CNTs surprisingly led to the low-dielectric constant composite PZT film. The decrease of the dielectric constant in PZT/CNT porous films would have the potential pyroelectric applications. Assuming that the pyroelectric coefficient was about the same in porous and dense films, a larger figure of merit in the case of the porous films could be expected because of the advantage of the lower dielectric constant.

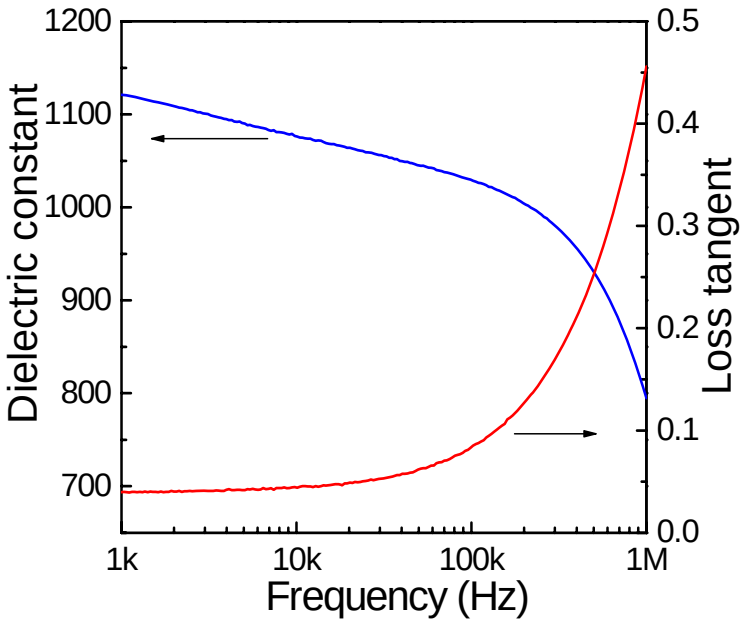

Figure 5.13 Frequency-dependent dielectric constant of PZT dense film.

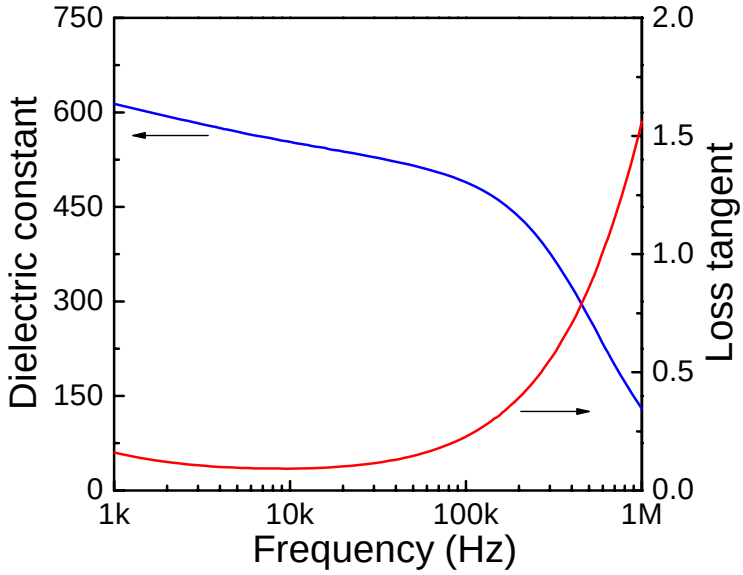

Figure 5.14 Frequency-dependent dielectric constant of PZT porous film with 0.4 wt% MWNTs.

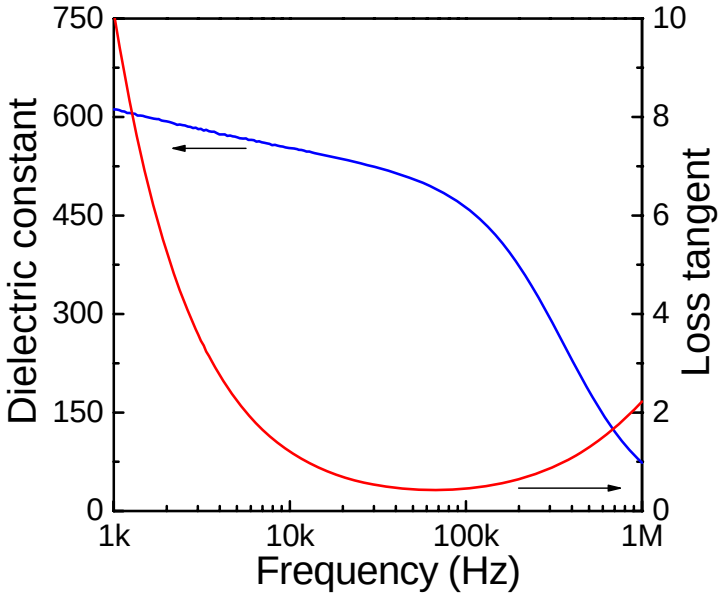

Figure 5.15 Frequency-dependent dielectric constant of PZT porous film with 0.6 wt% MWNTs.

5.5 Conclusions

The sol-gel precursor solution of the $Pb(Zr_{0.52},Ti_{0.48})O_3$ thin films were used as a matrix and MWNT as a filler in this work. The difficulties in obtaining uniform dispersion of the CNTs were encountered. The PZT/MWNT porous film deposited on platinized silicon substrates showed some microcracks caused by either inappropriate annealing temperature or prolonged heating time. A small amount of MWNTs introduced the porosity which resulted to the reduction of the dielectric constant and slight decrease of the spontaneous polarization when compared to the dense film without MWNT addition. However, further investigations are needed to overcome the difficulties in obtaining uniform dispersion of the CNTs in the precursor solution which was the main problem of reproducing these films in this work.

CHAPTER 6

CONCLUSIONS AND FUTURE WORKS

6.1 Main conclusions

(1) Highly oriented and niobium modified $Pb(Zr_xTi_{1-x})O_3$ (PNZT) films (x=0.2, 0.3, 0.4, 0.52, 0.53, 0.6, 0.7 and 0.8) of 400 nm in thickness were prepared on $Pt(111)/TiO_2/SiO_2/Si(100)$ substrates by sol-gel method. [100] and [111] orientations were controlled under the influence of PbO and TiO_2 seeding layer, respectively. The XRD results and measured out-of-plane lattice parameters evidenced that the PNZT films were crystallized into tetragonal perovskite phase with x<0.52 while the perovskite phase evolution yielded rhombohedral structure with x>0.52. The electrical properties were a strong dependence of composition for both orientations. For PNZT(100) films, Zr/Ti ratio of 52/48 posed the maximum remanent polarization P_r of 75 μC/cm^2 with the corresponding low coercive field E_c of 82 kV/cm. The piezoelectric coefficients were carried out to reach the maximum value of 161 pm/V at the same composition. For PNZT(111) films, the composition dependent P_r reached the best value of 80 μC/cm^2 and low E_c of 70 kV/cm at Zr/Ti ratio=52/48. The film with a Zr/Ti ratio of 52/48 had a maximum dielectric constant of 1550. This confirmed that the existence of MPB was located near Zr/Ti ratio=52/48 irrespective to oriented crystallographic films which was consistent with bulk PZT materials. The electrical properties of all films were higher due to the effect of niobium doping which lowered oxygen vacancies, resulting to increase domain wall mobility. The enhancement of ferroelectric, dielectric and piezoelectric properties could bring the PNZT films to use in memory, capacitor and MEMs applications.

(2) Highly [100]-, [111]- and randomly oriented PNZT thin films with thickness ranging from 80 to 400 nm were deposited on $Pt(111)/TiO_2/SiO_2/Si(100)$ substrates by the sol-gel method. XRD analysis indicated that the PNZT films presented highly oriented perovskite structure under the influence of the seeding layer and random orientation while the films were directly deposited on the platinized

silicon substrate. The perovskite phase evolution took place without pyrochlore phase even film thickness increasing up to 80 nm. The tetragonal perovskite structure of Nb-modified $Pb(Zr_{0.3}Ti_{0.7})O_3$ would be of interest in this work due to polarizable directions which were close to the polar axes. The dielectric and ferroelectric properties showed thickness dependence in which the largest dielectric constant and remanent polarization was found for [111]-oriented PNZT thin films with 400 nm in thickness. However, the smallest dielectric constant and coercive field were obtained for randomly oriented films. Larger remanent polarization and smaller coercive field indicated that the thickness dependent PNZT films would be possible for non-volatile memory device applications to operate with less consumed energy. As a result of scaling down the film thickness with relatively acceptable ferroelectric and dielectric properties, thinner PNZT films would be attractive to beyond capacitive limitation in solid state data storage and memory technology.

(3) The use of MWNT as a volatile phase to introduce porosity in $Pb(Zr_{0.52},Ti_{0.48})O_3$ thin films was carried out by sol-gel method. The difficulties in obtaining uniform dispersion of the CNTs were encountered. The porous thin film deposited on platinized silicon substrates would present some microcracks caused by either high annealing temperature or prolong heating time. A small amount of MWNTs induced significant reduction of the dielectric constant and slightly decrease of the spontaneous polarization when compared to the film without MWNT.

6.2 Future works

Some difficulties arisen during the courses of this work are:

(1) relatively high dielectric loss for PNZT(111) films and very high dielectric loss with asymmetry on voltage axis in dielectric-voltage curves for PNZT(100) films,

(2) high leakage current during ferroelectric and dielectric measurements and short contact between top and bottom electrode,

(3) problem occurred from some platinized silicon substrate that the desired orientation cannot be completely control,

(4) lack of profound understanding the behavior and the influence of seeding mechanism on the perovskite growth of highly oriented PZT films,

(5) shortage of high technology equipment for thin film measurement, e.g. AFM/PFM, high resolution XRD with φ mode, HRTEM,

(6) produce a uniform CNT incorporated ferroelectric film and investigate the possibility of using this material in the pyroelectric applications.

The following topics are of considerable interest to study:

(1) nanoscale-structure images of the PNZT films by AFM/PFM to indicate the grain growth behavior under textured control and to map the ferroelectric or piezoelectric domain for such materials,

(2) comparison of piezoelectric and pyroelectric coefficients of PNZT(100) to PNZT(111) films,

(3) XPS, TEM and Raman characterizations,

(4) epitaxial growth of PNZT film on single crystalline substrate to study the orientation dependent on the electrical properties,

(5) fabrication of highly oriented thick film (>> 1 μm),

(6) the effect of other chemical dopings on the electrical properties and perovskite phase evolution,

(7) the integration of ferroelectric films in nowadays electrical device for realistic application.

REFERENCES

Adachi H. and Wasa K., (1991). Sputtering preparation of ferroelectric PLZT films and their optical applications, IEEE trans. Ultra. Ferro. Freq. Control, Vol. 38, p. 645.

Akai D., (2005). Ferroelectric properties of sol-gel delivered epitaxial $Pb(Zr_x,Ti_{1-x})O_3$ thin films on Si using epitaxial γ-Al_2O_3 Layers, Appl. Phys. Lett., Vol. 86, p. 202906.

Aoki K., Fukuda Y., Numata K. and Nishimura A., (1995). Effects of Titanium Buffer Layer on Lead-Zirconate-Titanate Crystallization Processes in Sol-Gel Deposition Technique, Japan. J. Appl. Phys. Part 1, Vol. 34, p. 192.

Aratani M., Nagashima K. and Funakubo H., (2001). Preparation of $Pb(Zr_x, Ti_{1-x})O_3$ Thin Films by Source Gas Pulse-Introduced Metalorganic Chemical Vapor Deposition, Japan. J. Appl. Phys. Part 1, Vol. 40, p. 4126.

Araujo P. de C., Scott J.F. and Taylor G.W., (1996). Ferroelectric thin films: synthesis and basic properties, Gordon and Breach, Amsterdam.

Arlt G., (1990). Review: Twinning in ferroelectric and ferroelectric ceramics; stress relief, J. Mater. Sci., Vol. 25, p. 2655.

Auciello O., Scott J.F. and Ramesh R., (1998). The physics of ferroelectric memories, Physics Today, July, p. 22.

Auciello O. and Foster C., (1998). Processing technologies for Ferroelectric thin films and heterostructures, Annu. Rev. Mater. Sci., Vol. 28, p. 501.

Aurivillius B., (1949). Mixed bismuth oxides with layer lattices: I. structure type of $CaBi_2B_2O_9$, Ark. Kemi, Vol. 1, p. 463.

Banno H., (1995). Piezoelectric transducer and piezoelectric ceramics, encyclopedia of advanced materials, Pergamon Press, Oxford, U.K., p. 2017.

Bauer S., (1996). Poled polymers for sensors and photonic applications, J. Appl. Phys., Vol. 80, p. 5531.

Bell A.J. and Moulson A.J., (1985). The Effect of Grain Size on the Dielectric Properties of Barium Titanate Ceramics, Br. Ceram. Proc., Vol. 36, p. 57.

Björmander C., Sceenivas K., Grishin A.M. and Rao K.V., (1995). Pyroelectric $PbSc_{0.5}Ta_{0.5}O_3/Y_1Ba_2Cu_3O_{7-x}$ thin-film heterostructures, Appl. Phys. Lett., Vol. 67, p. 58.

Boikov Y.A., Esayan S.K., Ivanov Z.G., Brorsson G., Cleason T., Lee J. and Safari A., (1992). Epitaxial growth and properties of $YBa_2Cu_3O_x$-$Pb(Zr_{0.6}Ti_{0.4})O_3$-$YBa_2Cu_3O_x$ trilayer structure by laser ablation, Appl. Phys. Lett., Vol. 61, p. 528.

Bouregba R., Rhun G.L., Poullain G. and Leclerc G., (2006). Investigation of thickness dependence of the ferroelectric properties of $Pb(Zr_{0.6}Ti_{0.4})O_3$ thin-film capacitors, J. Appl. Phys., Vol. 99, p. 34102.

Brooks K.G., Reaney I.M., Klissurska R., Huang Y., Bursill L. and Setter N., (1994). Orientation of rapid thermally annealed lead zirconate titanate thin films on (111) Pt substrates, J. Mater. Res., Vol. 9, p. 2540.

Bruncková H., Medvecký L'., Briančin J. and Saksl K., (2004). Influence of hydrolysis conditions of the acetate sol-gel process on the stoichiometry of PZT powders, Ceram. Int., Vol. 30, p. 453.

Buchal C. and Siegert M., (1999). The Physics of Modulators", Proceedings of the International School of Physics "Enrico Fermi", IOS Press, Amterdam.

Budd K.D., Dey S.K., Payne D.A., (1985). Sol-gel processing of $PbTiO_3$, $PbZrO_3$, PZT and PLZT thin films, Br. Ceram. Soc. Proc., Vol. 36, p. 107.

Calzada M.L., Sirera R., Carmona F. and Jimenez B., (1995). Investigations of a Diol-based Sol-Gel Process for the Preparation of Lead Titanate Materials, J. Am. Ceram. Soc., Vol. 78, p. 1802.

Chao W.J. and Chou K.S., (1996). Studies on the control of porous properties in the fabrication of porous supports, Key Eng. Mater., Vol. 113, p. 93.

Chen S.-Y. and Chen I.-W., (1998). Texture development, microstructure evolution, and crystallization of chemically derived PZT thin films, J. Am. Ceram. Soc., Vol. 81, p. 97.

Chen C., Ryder D.F. and Spurgeon W.A., (1989). Synthesis and microstructure of highly oriented lead titanate thin films prepared by a Sol-Gel method, J. Am. Ceram. Soc., Vol. 72, p. 1495.

Chen S.Y. and Sun C.L., (2001). Ferroelectric characteristics of oriented $Pb(Zr_{1-x}Ti_x)O_3$ films, J. Appl. Phys., Vol. 90, p. 2970.

Cheng J. and Meng Z., (2001). Thickness-dependent microstructures and electrical properties of PZT films derived from sol–gel process, Thin Solid Films, Vol. 385, p. 5.

Chi W.G., Jiang D.L., Huang Z.G. and Tan S.H., (2004). Sintering behavior of porous SiC ceramics, Ceram. Int., Vol. 30, p. 869.

Chiang Y.-M., Farrey G.W., Soukhojak A.N., (1998). Lead-free high-strain single-crystal piezoelectrics in the alkaline-bismuth-titanate perovskite family, Appl. Phys. Lett., Vol. 73, p. 3683.

Chow A.F., Lichtenwalner D.J., Woolcott Jr. R.R., Graettinger T.M., Auciello O., Kingon A.I., Boatner L.A. and Parikh N.R., (1994). Epitaxial $KNbO_3$ thin films on $KTaO_3$, $MgAl_2O_4$, and MgO substrates, Appl. Phys. Lett., Vol. 65, p. 1073.

Chu S.-Y., Chen T.-Y., Tsai I.-T. and Water W., (2004). Doping effects of Nb additives on the piezoelectric and dielectric properties of PZT ceramics and its application on SAW device, Sensors and Actuators A, Vol. 113, p. 198.

Cillessen J.F.M., Prins M.W.J. and Wolf R.M., (1997). Thickness dependence of the switching voltage in all-oxide ferroelectric thin-film capacitors prepared by pulsed laser deposition, J. Appl. Phys., Vol. 81, p. 2777.

Coffman P.R., Barlingay C.K., Gupta A. and Dey S.K., (1996). Structure evolution in the PbO-ZrO_2-TiO_2 sol-gel systems: Part II-Pyrolysis of acid and base-catalyzed bulk and thin film gels, J. Sol-Gel Sci. Technol, Vol. 6, p. 83.

Contreras J., Kohlstedt H., Poppe U., Waser R. and Buchal C., (2003). Surface treatment effects on the thickness dependence of the remanent polarization of $PbZr_{0.52}Ti_{0.48}O_3$ capacitors, Appl. Phys. Lett., Vol. 83, p. 126.

Cross L.E., (1995). Boundary conditions for shape memory in ceramic material system, J. Intell. Mater. System Struct., Vol. 6, p. 55.

Cross L.E., (1995). Ferroelectric materials for electromechanical transducer applications, Japan. J. Appl. Phys., Vol. 34, p. 2525.

Cross L.E. and Newham R.E., (1987). Ceramics and civilization, Volume III, High Technology Ceramics – Past, Present, and Future, chapter History of Ferroelectrics, The American Ceramic Society, Inc., p 289.

Damjanovic D., Muralt P. and Setter N., (2001). Ferroelectric sensors, IEEE Sens. J., Vol. 1, p. 191.

Darlington C.N.W., (1988). Transitions in the glassy ferroelectric PLZT (8.7/65/35), J. Phys. C.: Solid State Phys., Vol. 21, p. 3851.

Dey S.K., Budd K.D. and Payne D.A., (1987). Structure of polymeric $PbTiO_3$ gels, J. Am. Ceram. Soc., Vol. 70, p. 296.

Dogheche E., Jaber B., Remiens D., and Thierry B., (1995). Determination of optical properties of lead based ferroelectrics thin films for integrated optics applications, Microelect. Eng., Vol. 29, p. 315.

Du X.-H., Zheng J., Belegundu U. and Uchino K., (1998). Crystal orientation dependence of piezoelectric properties of lead ziroconate titanate near the morphotropic phase boundary, Appl. Phys. Lett., Vol. 72, p. 2421.

Durruthy M.D., Fuentes L., Hernandez M. and Camacho H., (1999). Influence of the niobium dopant concentration on the $Pb(Zr_{0.54}Ti_{0.46})O_3$ ceramics sintering and final properties, J. Mater. Sci., Vol. 34, p. 2311.

Eng L.M., Guntherodt H.-J., Rosenman G., Skliar A., Oron M., Katz M. and Eger D., (1998). Nondestructive imaging and characterization of ferroelectric domains in periodically poled crystals, J. Appl. Phys., Vol. 83, p. 5973.

Ellerkmann U., Schneller T., Nauenheim C., Bottger U. and Waser R., (2008). Reduction of film thickness for chemical solution deposited $PbZr_{0.3}Ti_{0.7}O_3$ thin films revealing no size effects and maintaining high remanent polarization and low coercive field, Thin Solid Films, Vol. 516, p. 4713.

Es-Souni M., Kuhnke M., Piorra A. and Solterbeck C.-H., (2005). Pyroelectric and piezoelectric properties of thick PZT films produced by a new sol-gel route, J. Eur. Ceram. Soc., Vol. 25, p. 2499.

Es-Souni M., Piorra A., Solterbeck C.-H. and Abed M., (2001). Processing, crystallization behavior and dielectric properties of metallorganic deposited Nb doped PZT thin films on highly textured 111-Pt, Mater. Sci. Eng. B, Vol. 86, p. 237.

Etin A., Shter G.E., Grader G.S. and G.M. Reisner, (2007). Interrelation of Ferroelectricity, Morphology, and Thickness in Sol-Gel-Derived $PbZr_xTi_{1-x}O_3$ Films, J. Am Ceram. Soc., Vol. 90, p. 77.

Fe L., Norga G.J., Wouters D.J., Maes H.E. and Maes G., (2001). Chemical structure evolution and orientation selection in sol-gel-prepared ferroelectric $Pb(Zr,Ti)O_3$ thin films, J. Mater. Res., Vol. 16, p. 2499.

Fork D.K., Armani-Leplingard F. and Kingston J.J., (1996). Application of electroceramic thin films to optical waveguide devices, MRS Bulletin, p. 53.

Fu D.S., Suzuki H., Ogawa T. and Ishikawa K., (2002). High-piezoelectric behavior of c-axis-oriented lead zirconate titanate thin films with composition near the morphotropic phase boundary, Appl. Phys. Lett., Vol. 80, p. 3572.

Fujitsuka N., Miyachi Y., Mizuno K., Ohtsuka K., Taga Y. and Tabata O., (1988). Mnolithic pyroelectric infrared image sensor using PVDF thin film, Sensor and Actuators A, Vol. 66, p. 237.

Fukushima J., Kodaira K. and Matsushita T., (1984). Preparation of ferroelectric PZT films by thermal decomposition of organometallic compounds, J. Mater. Sci., Vol. 19, p. 595.

Gerson R., (1960). Variation in ferroelectric characteristics of lead zirconate titanate ceramics due to minor chemical modifications, J. Appl. Phys., Vol. 31, p. 188.

Glazer A.M., Mabud S.A. and Clarke R.R., (1978). Powder profile refinement of lead zirconae titanate at several temperatures. I. $PbZr_{0.9}Ti_{0.1}O_3$, Acta Crystal, Vol. B34, p. 1060.

Glazer A.M., Thomas P.A., Baba-Kishi K.Z., Pang G.K.H. and Tai C.W., (2004). Influence of short-range and long-range order on the evolution of the morphotropic phase boundary in $Pb(Zr_{1-x}Ti_x)O_3$, Phys. Rev. B, Vol. 70, p. 184123.

Gong W., Li J.-F., Chu X.-C., Gui Z.-L. and Li L.-T., (2004). Combined effect of preferential orientation and Zr/Ti atomic ratio on electrical properties of $Pb(Zr_xTi_{1-x})O_3$ thin films, J. Appl. Phys., Vol. 96, p. 590.

Gong W., Li J.-F., Chu X.-C., Gui Z.-L. and Li L.-T., (2004). Preparation and characterization of sol–gel derived (1 0 0)-textured Pb(Zr,Ti)O_3 thin films: PbO seeding role in the formation of preferential orientation, Acta Mater., Vol. 52, p. 2787.

Gong W., Li J.-F., Chu X.-C., Gui Z.-L. and Li L.-T., (2004). Effect of pyrolysis temperature on preferential orientation and electrical properties of sol-gel derived lead zirconate titanate films, J. Eur. Ceram. Soc., Vol. 24, p. 2977.

Grossmann M., Lohse O., Bolten D., Boettger U., Schneller T. and Waser R., (2002). The interface screening model as origin of imprint in $PbZr_xTi_{1-x}O_3$ thin films. I. Dopant, illumination, and bias dependence, J. Appl. Phys., Vol. 92, p. 2680.

Gruverman A. and Kalinin S.V., (2006). Piezoresponse force microscopy and recent advances in nanoscale studies of ferroelectrics, J. Mater. Sci., Vol. 41, p. 107.

Gruverman A., Tokumoto H., Prakash A., Aggarwal S., Yang B., Wuttig M., Ramesh R., Auciello O. and Venkatesan V., (1997). Nanoscale imaging of domain dynamics and retention in ferroelectric thin films, Appl. Phys. Lett., Vol. 71, p. 3492.

Guo Y.P., Akai D., Swada K. and Ishida M., (2007). Ferroelectric and pyroelectric properties of highly (110)-oriented $Pb(Zr_{0.40}Ti_{0.60})O_3$ thin films grown on $Pt/LaNiO_3/SiO_2/Si$ substrates, Appl. Phys. Lett., Vol. 90, p. 232908.

Guthner P. and Dransfeld K., (1992). Local poling of ferroelectric polymers by scanning force microscopy. Appl. Phys. Lett., Vol. 61, p. 1137.

Haertling G.H., (1986). “Piezoelectric and Electrooptic ceramics” in Ceramic materials for electronics: processing, properties, and applications. Ed. By Buchanan, R.C., NewYork, Basel: Dekker, p. 135.

Haertling G.H., (1999). Ferroelectric Ceramics: History and Technology, J. Am. Ceram. Soc., Vol. 82, p. 797.

Haccart T., Remiens D. and Cattan E., (2003). Substitution of Nb doping on the structural, microstructural and electrical properties in PZT films, Thin Solid Films, Vol. 423, p. 235.

Han H., Kotru S., Zhong J. and Pandey R.K., (2008). Effect of Nb doping on pyroelectric property of lead zirconate titanate films prepared by chemical solution deposition, Infrared Phys. Technol., Vol. 51, p. 216.

Hiboux S. and Muralt P., (2004). Mixed titania-lead oxide seed layers for PZT growth on Pt(111): a study on nucleation, texture and properties, J. Eur. Ceram. Soc., Vol. 24, p. 1593.

Iijima K., Tomita Y., Takayama R. and Ueda I., (1986). Preparation of c-axis oriented $PbTiO_3$ thin films and their crystallographic, dielectric, and pyroelectric properties, J. Appl. Phys., Vol. 60, p. 361.

Ikeda T., (1959). A few quaternary systems of perovskite type $A^{2+}B^{4+}O_3$ solid solutions., J. Phys. Soc. Japan, Vol. 14, p. 1286.

Irie H., Miyayama M. and Kudo T., (2001). Structure dependence of ferroelectric properties of bismuth layer-structured ferroelectric single crystals, J. Appl. Phys., Vol. 90, p. 4089.

Jacobs R.N. and Salamanca-Riba L., (2003). Role of Pb excess in the crystallization of lead zirconate titanate films derived via sol-gel processing, J. Mater. Res., Vol. 18, p. 1405.

Jaffe H. and Berlincourt D.A., (1965). Piezoelectric transducer materials, Proc. IEEE., Vol. 53, p. 1372.

Jaffe B., Cook W.R. and Jaffe H., (1971). Piezoelectric Ceramics, NewYork: Academic, p.1

Jaffe B. and Roth R.S., (1954). Piezoelectric properties of lead zirconate-lead titanate solid solution ceramics, J. Appl. Phys., Vol. 25, p. 809.

Jiang S.W., Zhang Q.Y., Huang W., Jiang B., Zhang Y. and Li Y.R., (2006). Texture control of $Pb(Zr,Ti)O_3$ thin films with different post-annealing processes, Appl. Surf. Sci., Vol. 252, p. 8756.

Jona F., Ferroelectric crystals, 1st edition, NewYork, Dover, 1993.

Kalinin S.V., Karapetian E. and Kachanov M., (2004). Nanoelectromechanics of piezoresponse force microscopy, Phys. Rev. B, Vol. 70, p.184101.

Kalpat S. and Uchino K., (2001). Highly oriented lead zirconium titanate thin films: Growth, control of texture, and its effect on dielectric properties, J. Appl. Phys., Vol. 90, p. 2703.

Khaenamkaew P., Muensit S., Bdikin I.K. and Kholkin A.L., (2007). Effect of Zr/Ti ratio on the microstructure and ferroelectric properties of lead zirconate titanate thin films, Mater. Chem. Phys., Vol. 102, p. 159.

Kijima T. and Ishiwara H., (2002). Si-Substituted Ultrathin Ferroelectric Films, Japan. J. Appl. Phys. Part 2, Vol. 41, p. L716.

Kim C.J., Kim B.I. and Kim J., (2006). Effects of $PbTiO_3$ seeding layer on electrical properties of $PbZr_{0.4}Ti_{0.6}O_3$ thin films, Sensors and Actuators A, Vol. 125, p. 353.

Kim C.J. and Lee Y.K., (2005). Characteristics of nano-thickness lead zirconate titanate thin film for high-density storage applications, Mater. Sci. Eng. B, Vol. 122, p. 12.

Kim D.-J., Maria J.-P., Kingon A.I. and Streiffer S.K., (2003). Evaluation of intrinsic and extrinsic contributions to the piezoelectric properties of $Pb(Zr_{1-x}T_x)O_3$ thin films as a function of composition, J. Appl. Phys., Vol. 93, p. 5568.

Kim S.-H., Park D.-Y., Woo H.-J., Lee D.-S., Ha J., Hwang C.-S., Shim I.-B. and Kingon A.I., (2002). Orientation effects in chemical solution derived $Pb(Zr_{0.3},Ti_{0.7})O_3$ thin films on ferroelectric properties, Thin Solid Films, Vol. 416, p. 264.

Kingon A., (1999). Memories are made of …, Nature, Vol. 401, p. 658.

Klissurka R.D., Tagantsev A.K., Brooks K.G. and Setter N., (1997). Use of ferroelectric hysteresis parameters for evaluation of niobium effects in lead zirconate titanate thin films, J. Am. Ceram. Soc., Vol. 80, p. 336.

Kosec M. and Malic B., (1998). Relationship between precursor chemistry and microstructure of CSD derived PZT films, J. Phys. IV France, Vol. 8, p.9.

Kozuka H. and Kajimura M., (2000). Single-Step Dip Coating of Crack-Free $BaTiO_3$ Films >1 μm Thick: Effect of Poly(vinylpyrrolidone) on Critical Thickness, J. Am. Ceram. Soc., Vol. 83, p. 1056.

Kruse P.W., (2001). Uncooled Thermal Imaging, Arrays, Systems, and Applications, SPIE.

Kundu T.K. and Lee J.Y., (2000). Thickness-Dependent Electrical Properties of $Pb(Zr,Ti)O_3$ Thin Film Capacitors for Memory Device Applications, J. Electrochem. Soc., Vol. 147, p. 326.

Kurchania R. and Milne S., (2003). Effect of Niobium Modifications to PZT (53/47) Thin Films Made by a Sol-Gel Route, J. Sol-Gel Sci. Technol., Vol. 28, p. 143.

Kuscer D., Korzekwa J., Kosec M. and Skulski R., (2007). A- and B-compensated PLZT x/90/10: Sintering and microstructural analysis, J. Eur. Ceram. Soc., Vol. 27, p. 4499.

Kwok K.W., Tsang R.C.W., Chan H.L.W. and Choy C.L., (2004). Effects of niobium doping on the piezoelectric properties of sol–gel-derived lead–zirconate–titanate films, J. Appl. Phys., Vol. 95, p. 1372.

Kwon Y.T., Lee I.-M., Lee W.I., Kim C.J. and Yoo I.K., (1999). Effect of Sol-Gel precursors on the grain structure of PZT thin films, Mater. Res. Bull., Vol. 34, p. 749.

Larsen P., Dormans G., Taylor D. and Veldhoven P., (1994). Ferroelectric properties and fatigue of $PbZr_{0.51}Ti_{0.49}O_3$ thin films of varying thickness: Blocking layer model, J. Appl. Phys., Vol. 76, p. 2405.

Lee W.-S., Ahn K.-C. and Yoon S.-G., (2005). Effect of film thickness on the ferroelectric properties of $Pb(Zr_{0.2}Ti_{0.8})O_3$ thin films for nano-data storage applications , J. Vac. Sci. Technol. B, Vol. 23, p. 1901.

Lefki K. and Dormans G.J.M., (1994). Measurement of piezoelectric coefficients of ferroelectric thin films, J. Appl. Phys., Vol. 76, p. 1764.

Li A.D., Mak C.L., Wong K.H., Shao Q.Y., Wang Y.J., Wu D. and Ming N., (2002). Thickness-dependent structural characteristics of sol–gel-derived epitaxial $Pb(ZrTi)O_3$ films using inorganic zirconium salt, J. Crystal Growth, Vol. 235, p. 307.

Li L., Zhang L., Yao X. and Li B., (2004). Computer simulation of temperature field of multilayer pyroelectric thin film IR detector, Ceramics International, Vol. 30, p. 1847.

Lian L. and Sottos N.R., (2000). Effects of thickness on the piezoelectric and dielectric properties of lead zirconate titanate thin films, J. Appl. Phys., Vol. 87, p. 3941.

Lin C.H., Friddle P.A., Ma C.H., Daga A. and Chen H., (2001). Effects of thickness on the electrical properties of metalorganic chemical vapor deposited $Pb(Zr,Ti)O_3$ (25-100 nm) thin films on LaNiO3 buffered Si, J. Appl. Phys., Vol. 90, p. 1509.

Lin P., Ren W., Wu X.Q., Shi P., Chen X.F. and Yao X., (2008). Thickness effects on structures and electrical properties of lead zirconate titanate thick films, Ceram. Int., Vol. 34, p. 991.

Lines M.E. and Glass A.M., (2001). Principles and Applications of Ferroelectrics and Related Materials, Oxford University Press, New York.

Lisca M., Pintilie L., Alexe M. and Teodorescu C.M., (2006). Thickness effect in $Pb(Zr_{0.2}Ti_{0.8})O_3$ ferroelectric thin films grown by pulsed laser deposition, Appl. Surf. Sci., Vol. 252, p. 4549.

Liu D.M., (1996). Control of pore geometry on influencing the mechanical property of porous hydroxyapatite, J. Mater. Sci. Lett., Vol. 15, p. 419.

Liu J.-M., Pan B., Chan H.L.W., Zhu S.N., Zhu Y.Y. and Liu Z.G., (2002). Piezoelectric coefficient measurement of piezoelectric thin films: an overview, Mater. Chem. Phys., Vol. 75, p. 12.

Liu Y. and Phule P.-P., (1996). Nucleation- or growth-controlled orientation development in chemically derived ferroelectric lead zirconate titanate ($Pb(Zr_xTi_{1-x})O_3$, x=0.4), J. Am. Ceram. Soc., Vol. 79, p. 495.

Livage J., Henry M. and Sanchez C., (1988). Sol-Gel chemistry of transition metal oxides, Prog. Solid State Chem., Vol. 18, p. 259.

Lyckfeldt O. and Ferreira J.M.F., (1998). Processing of porous ceramics by ‘starch consolidation’, J. Eur. Ceram. Soc., Vol. 184, p. 134.

Malic B., Kosec M., Arcon I. and Kodre A., (2005). Homogeneity issues in chemical solution of $Pb(Zr,Ti)O_3$ thin films, J. Eur. Ceram. Soc., Vol. 25, p. 2241.

Mantese J.V., Micheli A.L., Schubring N. W., Catalan A. B., Soch K. L., Ng K., Kapper S.H., Lopez R.J., and G. Lung, (1993). Infrared imaging using uncooled focal plane arrays of unreticulated 10-μm potassium tantalum niobate films, IEEE Trans. Electron Devices, Vol. 40, p. 320.

Matsuzaki T. and Funakubo H., (1999). Preparation and characterization of $Pb(Nb,Ti)O_3$ thin films by metalorganic chemical vapor deposition, J. Appl. Phys., Vol. 86, p. 4559.

Miller S.L., Nasby R.D., Schwank J.R. Rodgers M.S. and Dressendorfer P.V., (1990). Device modeling of ferroelectric capacitors, J. Appl. Phys., Vol. 68, p. 6463.

Millon C., Malhaire C. and Barbier D., (2004). Ti and TiO_x seeding influence on the orientation and ferroelectric properties of sputtered PZT thin films, Sens. Act. A, Vol. 113, p. 376.

Morioka H., Yokoyama S., Oikawa T., Funakubo H., and Saito K., (2004). Spontaneous polarization change with Zr/(Zr + Ti) ratios in perfectly polar-axis-orientated epitaxial tetragonal $Pb(Zr,Ti)O_3$ films, Appl. Phys. Lett., Vol. 85, p. 3516.

Moulson A. J., and Herbert J. M., (1990). Electroceramics – Materials, Properties & Applications, Chapman & Hall.

Muralt P., (2001). Micromachined infrared detectors based on pyroelectric thin films, Rep. Prog. Phys., Vol. 64, p. 1339.

Muralt P., (2008). Recent Progress in Materials Issues for Piezoelectric MEMS, J. Am. Ceram. Soc., Vol. 91, p. 1385.

Muralt P., Maeder T., Sagalowicz L., Hiboux S., Scalese S., Naumovic D., Agostino R.G., Xanthopoulos N., Mathieu H.J., Patthey L., and Bullock E.L., (1998). Texture control of $PbTiO_3$ and $Pb(Zr,Ti)O_3$ thin films with TiO_2 seeding, J. Appl. Phys., Vol. 83, p. 3835.

Nagashima K., Aratani M. and Funakubo H., (2001). Orientation dependence of ferroelectricity of epitaxially grown $Pb(Zr_xTi_{1-x})O_3$ thin films prepared by metalorganic chemical vapor deposition, J. Appl. Phys., Vol. 89, p. 4517.

Newham R.E., (1997). Molecular mechanism in smart materials, MRS. Bulletin, p. 20.

Nagel N., Mikolajick T., Kasko I., Hartner W., Moert M., Pinnow C.-U., Dehm C. and Mazure C., (2001). An overview of FeRam technology for high density applications, Mater. Res. Symp. Proc., Vol. 655, p. 1.1.1.

Noheda B., (2002). Structure and high-piezoelectricity in lead oxide solid solutions, Curr. Opin. Solid State Mater. Sci., Vol. 6, p. 27.

Noheda B., Cox D.E., Shirane G., Gonzalo J.A., Cross L.E., Park S.E., (1999). A monoclinic ferroelectric phase in the $Pb(Zr_{1-x}Ti_x)O_3$ solid solution., Appl. Phys. Lett., Vol. 74, p. 2059.

Noheda B., Cox D.E., Shirane G., Guo R., Jones B. and Cross L.E., (2000). Stability of the monoclinic phase in the ferroelectric perovskite PbZr1-xTixO3., Phys. Rev. B, Vol. 63, p. 14103.

Nonomura H., Fujisawa H., Shimizu M. and Niu H., (2002). Epitaxial Growth and Ferroelectric Properties of the 20-nm-Thick $Pb(Zr,Ti)O_3$ Film on $SrTiO_3(100)$ with an Atomically Flat Surface by Metalorganic Chemical Vapor Deposition, Japan. J. Appl. Phys. Part 1., Vol. 41, p. 6682.

Norga G.J., Fe L., Vasiliu F., Fompeyrine J., Locquet J.-P. and Van der Biest O., (2004). Orientation selection in functional oxide thin films, J. Eur. Ceram. Soc., Vol. 24, p. 969.

Nye J. F., (1985). Physics Properties of Crystals, Oxford University Press, New York.

Ogawa T., (2000). Domain structure of ferroelectric ceramics, Ceram. Int., Vol. 26, p. 383.

Oh S.H. and Jang H.M., (2001). Epitaxial $Pb(Zr,Ti)O_3$ thin films with coexisting tetragonal and rhombohedral phases, Phys. Rev. B, Vol. 63, p. 132101.

Oh S.H. and Jang H.M., (2000). Two-dimentional thermodynamic theory of epitaxial Pb(Zr,Ti)O3 thin films, Phys. Rev. B, Vol. 62, p. 14757.

Oikawa T., Morioka H., Nagai A. and Funakubo H., (2004). Thickness scaling of polycrystalline $Pb(Zr,Ti)O_3$ films down to 35 nm prepared by metalorganic chemical vapor deposition having good ferroelectric properties, Appl. Phys. Lett., Vol. 85, p. 1754.

Oikawa T., Aratani M., Funakubo H., Saito K. and Mizuhira M., (2004). Composition and orientation dependence of electrical properties of epitaxial $Pb(Zr_xTi_{1-x})O_3$ thin films grown using metalorganic chemical vapor deposition, J. Appl. Phys., Vol. 95, p. 3111.

Okuyama M., Asano J.-J. and Hamaka Y., (1995). Electron emission from PZT ceramic thin plate by pulsed electric field, Integ. Ferroelectrics, Vol. 9, p. 133.

Padilla J., Zhong W. and Vanderbit D., (1996). First-principles investigation of 180° domain walls in $BaTiO_3$, Phys. Revs. B, Vol. 53, p. 5969.

Park B.H., Kang B.S., Bu S.D., Noh T.W., Lee J. and Jo W., (1999). Lanthanum-substituted bismuth titanate for use in non-volatile memories, Nature, Vol. 401, p.682.

Paz de Araujo C.A., Cuchiaro J.D., McMillan L.D., Scott M.C. and Scott J.F., (1995). Fatigue-free ferroelectric capacitors with platinum electrodes, Nature, Vol. 374, p. 627.

Pereira M., Peixoto A.G. and Gomes M.J.M., (2001). Effect of Nb doping on the microstructural and electrical properties of the PZT ceramics, J. Eur. Ceram. Soc., Vol. 21, p. 1353.

Pérez J., Vyshatko N.P., Vilarinho P.M. and Kholkin A.L., (2007). Electrical properties of lead zirconate titanate thick films prepared by hybrid sol-gel method with multiple infiltration steps, Mater. Chem. Phys., Vol. 101, p. 280.

Pertsev N.A., Kukhar V.G., Kohlstedt H. and Waser R., (2003). Phase diagrams and physical properties of single-domain epitaxial $Pb(Zr_{1-x}Ti_x)O_3$ thin films, Phys. Rev. B, Vol. 67, p. 54107.

Pintilie L., Pereira M., Gomes M.J.M. and Boerasu I., (2004). Pyroelectric current spectroscopy: example of application on Nb doped $Pb(Zr_{0.92}Ti_{0.08})O_3$ ceramics for infrared detection, Sensors and Actuators A, Vol. 115, p. 185.

Ramesh R., (1997). Thin film ferroelectric materials devices, Kluwer Academic Publisher, Boston.

Ramesh R., Gilchrist H., Sands T., Keramidas V.G., Haakenaasen R. and Fork D.K., (1992). Ferroelectric La-Sr-Co-O/Pb-Zr-Ti-O/La-Sr-Co-O heterostructures on silicon via template growth, Appl. Phys. Lett., Vol. 63, p. 3592.

Reaney I.M., Brooks K., Klissurska R., Pawlacyk C. and Setter N., (1994). Use of transmission electron microscopy for the characterization of rapid thermally annealed, solution-gel, lead zirconate titanate films, J. Am. Ceram. Soc., Vol. 77, p. 1209.

Remiens D., Cattan E., Soyer C. and Haccart T., (2003). Piezoelectric properties of sputtered PZT films: influence of structure, micro structure, film thickness (Zr,Ti) ratio and Nb substitution, Mater. Sci. Semi. Proc., Vol. 5, p. 123.

Rossinger S.A. and Misat S.I., (2000). unpublished results.

Ruangchalermwong C., Li J.-F., Zhi Z.-X. and Muensit S., (2008). Phase transition and electrical properties of highly [111]-oriented and niobium modified $Pb(Zr_xTi_{1-x})O_3$ thin films with different Zr/Ti ratios, J. Phys. D: Appl. Phys., Vol. 41, p. 225302.

Runt J. and Galgoci E.C., (1984). Polymer/piezoelectric ceramic composites: polystyrene and poly(methyl methacrylate) with PZT, J. Appl. Polymer Sci., Vol. 29, p. 611.

Saito Y., Takao H., Tani T., Nonoyama T., Takatori K., Homma T., Nagaya T. and Nakamura M., (2004). Lead-free piezoceramics, Nature, Vol. 432, p. 84.

Sakamoto W.K., Marin-Franch P. and Das-Gupta D.K., (2002). Characterization and application of PZT/PU and graphite doped PZT/PU composite, Sens. Act. A., Vol. 100, p. 165.

Sakashita Y. and Segawa H., (1995). Preparation and characterization of $LiNbO_3$ thin films produced by chemical-vapor deposition, J. Appl. Phys., Vol. 77, p. 5995.

Sakashita Y., Segawa H., Tominaga K. and Okada M., (1993). Dependence of electrical properties on film thickness in $Pb(Zr_xTi_{1-x})O_3$ thin films produced by metalorganic chemical vapor deposition, J. Appl. Phys., Vol. 73, p. 7857.

Sayer M., Judd B., El-Assal K. and Parsad E., (1981). Poling of piezoelectric ceramics, J. Canadian Ceram. Soc., Vol. 50.

Setter N., (2001). Electroceramics: looking ahead, J. Eur. Ceram. Soc., Vol. 21, p. 1279.

Schmidt H., Rinn G., Nass R. and Sporn D., (1988). Film preparation by inorganic organic Sol-Gel synthesis, Mater. Res. Soc. Symp. Proc., Vol. 121, p. 743.

Schwartz R.W., (1997). Chemical solution deposition of perovkite thin films, Chem. Mater., Vol. 9, p. 2325.

Schwartz R.W., Assink R.A. and Headley T., (1992). Solution Chemistry Effects in PZT Thin Film Processing: Spectroscopic and Microstructural Characterization, Mater. Res. Soc. Sym. Proc., Vol.243, p. 245.

Schwartz R.W., Boyle T.J., Lockwood S.J., Sinclair M.B., Dimos D. and Buchheit C.D., (1995). Sol-gel processing of PZT thin films: A review of the state-of-the-art and process optimization strategies, Integ. Ferroelectrics, Vol. 7, p. 259.

Schwartz R.W., Schneller T., and Waser R., (2004). Chemical solution deposition of electronic oxide films, Compt. Ren. Chimie, Vol. 7, p. 433.

Schwartz R.W., Voigt J.A., Tuttle B.A., Payne D.A., Reichert T.L. and DaSalla R.S., (1997). Comments on the effects of solution precursor characteristics and thermal processing conditions on the crystallization behavior of sol-gel derived PZT thin films, J. Mater. Res., Vol. 12, p. 444.

Scott J.F., (2000). Ferroelectric memories, Springer, Heidelberg, p. 165.

Seifert A., Sagalowicz L., Muralt P. and Setter N., (1999). Microstructural evolution of dense and porous pyroelectric $Pb_{1-x}Ca_xTiO_3$ thin films, J. Mater. Res., Vol. 14, p. 2012.

Seifert A., Muralt P. and Setter N., (1998). High figure-of-merit porous $Pb_{1-x}Ca_xTiO_3$ thin films for pyroelectric applications, Appl. Phys. Lett., Vol. 72, p. 2409.

Shaw C.P., Whatmore R. and Alcock J.R., (2007). Porous, Functionally Gradient Pyroelectric Materials, J. Am. Ceram. Soc., Vol. 90, p. 137.

Shi C., Meidong L., Churong L., Yike Z. and Costa J.D., (2000). Investigation of crystallographic and pyroelectric properties of lead-based perovskite-type structure ferroelectric thin films, Thin Solid Films, Vol. 375, p. 288.

Shirane G., Hoshino S. and Suzuki K., (1950). X-Ray Study of the Phase Transition in Lead Titanate, J. Phys. Soc. Japan, Vol. 5, p.453; Phys. Rev., Vol. 80, p. 1105.

Souza E.C.F., Simoes A.Z., Cilense M., Longo E. and Varela J.A., (2004). The effect of Nb doping on ferroelectric properties of PZT thin films prepared from polymeric precursors, Mater. Chem. Phys., Vol. 88, p. 155.

Stancu V., Lisca M., Boerasu I., Pintilie L. and Kosec M., (2007). Effects of porosity on ferroelectric properties of $Pb(Zr_{0.2}Ti_{0.8})O_3$ films, Thin Solid Films, Vol. 515, p. 6557.

Steier W.H., Chen A., Lee S.-S., Garner S., Zhang H., Chuyanov V., Dalton L.R., Wang F., Ren A.S., Zhang C. Todorova G., Harper A., Fetterman H.R., Cheng D., Udupa A., Bhattacharpa D. and Tsap B., (1999). Polymer electro-optic devices for integrated optics, Chem. Phys., Vol. 245, p. 487.

Summerfelt S., Moise T., Xing G., Colombo L., Sakoda T., Gilbert S., Loke A., Ma S., Wills L., Kavari R., Shu T., Amano J., Johnson S., Vestoyk D., Russell M., Bilodeau S. and Buskirk P., (2001). Demonstration of scaled ($\geq$0.12 μm^2) $Pb(Zr,Ti)O_3$ capacitors on W plugs with Al interconnect, Appl. Phys. Lett., Vol. 79, p. 4004.

Sun L.L., Tan O.K. and Zhu W.G., (2006). $Pb(Zr_{0.3}Ti_{0.7})O_3/PbTiO_3$ multilayer thin films for pyroelectric infrared sensor application, J. Appl. Phys., Vol. 99, p. 094108.

Sung-Gap L., Young-Jae S., Jin K.C. and Jun-Ki C., (2008). Structural and dielectric properties of $Pb(Zr,Ti)O_3$ heterolayered thick films, J. Alloys Comp., Vol. 449, p. 73.

Suyal G. and Setter N., (2004). Enhanced performance of pyroelectric microsensors through the introduction of nanoporosity, J. Eur. Ceram. Soc., Vol. 24, p. 247.

Tagantsev A.K., Pawlaczyk C.Z., Brooks K. and Setter N., (1994). Built-in electric field assisted nucleation and coercive fields in ferroelectric thin films, Integ. Ferroelectrics, Vol. 4, p. 1.

Takahashi Y., Matsuoka Y., Yamaguchi K., Matsuki M. and Kobayashi K., (1990). Dip coating of PT, PZ and PZT films using an alkoxide-diethanolamine method, J. Mater. Sci., Vol.25, p. 3960.

Tashiro S., Oikawa Y., Igarashi H. and Okazaki K., (1987). Piezoelectric anisotropy in lead titanate system ceramics, Japan. J. Appl. Phys. Suppl., Vol. 26, p. 61.

Taylor D.V. and Damjanovic D., (2000). Piezoelectric properties of rhombohedral $Pb(Zr,Ti)O_3$ thin films with (100), (111), and "random" crystallographic orientation, Appl. Phys. Lett., Vol. 76, p. 1615.

Tu Y.-L., Calzada M.L., Phillips N.J. and Milne S.J., (1996). Synthesis and Electrical Characterization of Thin Films of PT and PZT Made from a Diol-Based Sol-Gel Route, J. Am. Ceram. Soc., Vol. 79, p. 441.

Turik A.V. and Topolove V.Y., (1997). Ferroelectric ceramics with a large piezoelectric anisotropy, J. Phys. D: Appl. Phys., Vol. 30, p. 1541.

Tuttle B.A., Doughty D.H., Schwartz R.W., Garino T.J., Martinez S.L., Goodnow D., Fernandez C.L., Tissot R.G. and Hammeter W.F., (1992). Chemically Prepared PZT Films with Niobium Additions, Ceram. Trans., Vol. 15, p. 179.

Tuttle B.A. and Schwartz R.W., (1996). Solution deposition of ferroelectric thin films, MRS Bull., Vol. 21, p. 49.

Uhlmann D.R., Dawley J.T., Poisl W.H., Zelinski B.J.J. and Teowee G., (2000). Ferroelectric Films, J. Sol-Gel Sci. Technol., Vol. 19, p. 53.

Veluchamy P. and Minoura H., (1998). Surface analysis of anodic lead oxide films prepared in hot alkaline solutions, Appl. Surf. Sci., Vol. 126, p. 241.

Venkataraj S., Geurts J., Weis H., Kappertz O., Njoroge W.K., Jayavel R. and Wuttig M., (2001). Structural and optical properties of thin lead oxide films produced by reactive direct current magnetron sputtering, J. Vac. Sci. Technol. A, Vol. 19, p. 2870.

Verardi P., Cracium F., Dinescu M. and Gerardi C., (1998). Epitaxial piezoelectric PZT thin films obtained by pulsed laser deposition, Thin Solid Films, Vol. 318, p. 265.

Vrejoiu I., Rhun L.G., Pintilie L., Hesse D., Alexe M., and Gosele U., (2006). Intrinsic ferroelectric properties of strained tetragonal $PbZr_{0.2}Ti_{0.8}O_3$ obtained on layer–by–layer grown, defect–free single–crystalline films, Adv. Mater., Vol. 18, p. 1657.

Wadhawan V.K., (2000). Introduction to ferroic materials, Gordon and Breach.

Wang Z.J., Kokawa H. and Maeda R., (2005). In situ growth of lead zirconate titanate thin films by hybrid process: sol–gel method and pulsed-laser deposition, Acta Mater., Vol. 53, p.593.

Wakiya N., Kuroyanagi K., Xuan Y., Shinozaki K. and Mizutani N., (1999). Nucleation and growth behavior of epitaxial $Pb(Zr,Ti)O_3$/MgO(100) observed by atomic force microscopy, Thin Solid Films, Vol. 357, p.166.

Weng L., Bao X. and Sagoe-Crentsil K., (2002). Effect of acetylacetone on the preparation of PZT materials in sol–gel processing, Mater. Sci. Eng. B, Vol. 96, p. 307.

Wessels B.W., (1998). Ferroelectric oxide epitaxial thin films: synthesis and non-linear optical properties, J. Crystal Growth, Vol. 195, p. 706.

Whatmore R.W., Osbond P.C. and Shorrocks N.M., (1987). Ferroelectric materials for thermal IR detectors, Ferroelectrics, Vol. 76, p. 351.

Whatmore R.W., Zhang Q., Huang Z. and Dorey R.A., (2003). Ferroelectric thin and thick films for Microsystems, Mater. Sci. Semicond. Proc., Vol. 5, p. 65.

Wright P.J., Crossbie M.J., Lane P.A., Williams D.J., Jones A.C., Leedham T.J. and Davies H.O., (2002). Metal organic chemical vapor deposition (MOCVD) of oxides and ferroelectric materials, J. Mater. Sci. Mater. Electron., Vol. 13, p. 671.

Xu Y., (1991). Ferroelectric Materials and Their Applications, North-Holland.

Xu F., Trolier-McKinstry S., Ren W., Xu B.M., Xie Z.-L. and Kemker K.J., (2001). Domain wall motion and its contribution to the dielectric and piezoelectric properties of lead zirconate titanate films, J. Appl. Phys., Vol. 89, p. 1336.

Yamaguchi N., Hattori T., Terashima K. and Yoshida T., (1998). High-rate deposition of $LiNbO_3$ films by thermal plasma spray CVD, Thin Solid Films, Vol. 316, p. 185.

Yamamoto T., (1996). Ferroelectric Properties of the $PbZrO_3$–$PbTiO_3$ System, Japan. J. Appl. Phys. Part 1, Vol. 35, p. 5104.

Yan F., Bao P., Chan H.L.W., Choy C.-L. and Wang Y., (2002). The grain size effect of $Pb(Zr_{0.3}Ti_{0.7})O_3$ thin films, Thin Solid Films, Vol. 406, p. 282.

Yi. G. and Sayer M., (1991). Sol-Gel processing of complex oxide films, Ceram. Bull., Vol. 70, p. 1173.

Yokoyama S., Honda Y., Morioka H., Okamoto S., Funakubo H., Iijima T., Matsuda H., Saito K., Yamamoto T., Okino H., Sakata O. and Kimura S., (2005). Dependence of electrical properties of epitaxial Pb(Zr,Ti)O3 thick films on crystal orientation and Zr/(Zr+Ti) ratio, J. Appl. Phys., Vol. 98, p. 94106.

Yu Y. -J., Chan H.-L.-W., Wang F.-P. and Zhao L.-C., (2003). Effects of rare earth Eu doping on ferroelectric properties of $PbZr_{0.52}Ti_{0.48}O_3$ thin films by sol–gel methods, Microelect. Eng., Vol. 66, p. 726.

Zeng T., Dong X., Chen S. and Yang H., (2007). Processing and piezoelectric properties of porous PZT ceramics, Ceram. Int., Vol. 33, p. 395.

Zeng J., Zhang M., Wang L. and Lin C., (1999). Influence of lead titanate seed layer on orientation behavior and ferroelectric characteristics of sol-gel derived PZT thin films, Journal of Physics: Condense Matter, Vol. 11, p. 1139.

Zhang Q., Corkovic S., Shaw C.P., Huang Z. and Whatmore R.W., (2005). Effect of porosity on the ferroelectric properties of sol-gel prepared lead zirconate titanate thin film, Thin Solid Films, Vol. 488, p. 258.

Zhang Q., Huang Z., Vickers M.E. and Whatmore R.W., (1999). Effect of the particle size in PZT precursor sols on the orientation of the thin films, J. Eur. Ceram. Soc., Vol. 19, p. 1417.

Zhang Z., Lu L., Shu C. and Wu P., (2006). Computational investigation of *B*-site donor doping effect on fatigue behavior of lead zirconate titanate, Appl. Phys. Lett., Vol. 89, p. 152909.

Zhang Z., Wang S., Song W., Lu L., Shu C. and Wu P., (2008). Comparative study of effects of Mo and W dopants on the ferroelectric property of $Pb(Zr_{0.3}Ti_{0.7})$ thin films, J. Phys. D: Appl. Phys., Vol. 41, p. 135402.

Zhang Q. and Whatmore R.W., (2004). Low fatigue lead zirconate titanate-based capacitors modified by manganese for nonvolatile memories, Mater. Sci. Eng. B, Vol. 109, p. 136.

Zhang Q., Whatmore R.W. and Vickers M.E., (1999). A comparison of the nanostructure of lead zirconate, lead titanate and lead zirconate titanate sols, J. Sol-Gel Sci. Technol., Vol. 15, p.13.

Zhang S., Xia R and Shrout T.R., (2007). Lead-free piezoelectric ceramics vs. PZT?, J. Electroceram., Vol. 19, p. 251.

Zhu Z.-X., Li J.-F., Lai F.-P., Zhen Y.-H. and Lin Y.-H., (2007). Phase structure of epitaxial $Pb(Zr,Ti)O_3$ thin films on Nb-doped $SrTiO_3$ substrates, Appl. Phys. Lett., Vol. 91, p. 222910.

Zhu Z.-X., Ruangchalermwong C. and Li J.-F., (2008). Thickness and Nb-doping effects on ferro- and piezoelectric properties of highly *a*-axis-oriented Nb-doped $Pb(Zr_{0.3}Ti_{0.7})O_3$ films, J. Appl. Phys., Vol. 104, p. 54107.

Zhu T., and Yang W., (1997). Toughness variation of ferroelectrics by polarization switch under non-uniform electric field, Acta Mater., Vol. 45, p. 4695.

VITAE

Name Mr. Charnwit Ruangchalermwong

Student ID 4823013

Educational Attainment

Degree	Name of Institution	Year of Graduation
B.Sc.(Physics)	Prince of Songkla University	2001
M.Sc.(Physics)	Chulalongkorn University	2005

Scholarship Awards during Enrolment

The 8th Royal Golden Jubilee Ph.D. Program, Thailand Research Fund, 2006-2008

List of Publications and Proceedings

Publications

1. **Ruangchalermwong C.**, Li J.-F., Zhu Z.-X. and Muensit S., **(2008).** Phase transition and electrical properties of highly [111]-oriented and niobium modified $Pb(Zr_xTi_{1-x})O_3$ thin films with different Zr/Ti ratios, J. Phys. D: Appl. Phys., Vol. 41, p. 225302.
2. Zhu Z.-X., **Ruangchalermwong C.** and Li J.-F., **(2008).** Thickness and Nb-doping effects on ferro- and piezoelectric properties of highly *a*-axis-oriented Nb-doped $Pb(Zr_{0.3}Ti_{0.7})O_3$ films, J. Appl. Phys., Vol. 104, p. 54107.
3. **Ruangchalermwong** C. and Muensit S., **(2008).** Effect of carbon nanotubes incorporation on characteristics of sol-gel derived PZT film, CMU. J. Nat. Sci. Special issue on nanotechnology, Vol. 7, p. 1.

Proceedings

1. **Charnwit Ruangchalermwong** and Supasarote Muensit, **(2009).** Combined effect of niobium doping and crystal orientation on properties of $PbZr_{0.52}Ti_{0.48}O_3$ films prepared by sol-gel method, Pure and Applied Chemistry International Conference 2009, 14-16 January 2009, Naresuan University, Phitsanulok, Thailand.

2. **梁汉坤**, 祝志祥, 李敬锋 and S. Muensit, **(2008).** 组成对[100]-织构 PNZT 薄膜相结构及性能的影响, 第十二届全国电介质物理， 材料与应用学术会议, 18-21 April 2008, Xi'an Jiaotong University, Xi'an, Shanxi, P.R. China.
3. **Charnwit Ruangchalermwong** and Supasarote Muensit, **(2007).** Influence of incorporating of carbon nanotubes with sol-gel derived PZT films, The First Thailand National Nanotechnology Conference: Pharmaceutical, Nanomaterials, Devices and Applications, 14-16 August 2007, Chiangmai University, Chiangmai, Thailand.